ANALYSIS OF MULTICELL BOX GIRDERS WITH DIAPHRAGMS

BY

SANA RACHRACH ABDEL-SAMAD
B.Eng., American University of Beirut, 1961
S.M.C.E , Massachusetts Institute of Technology, 1963

THESIS

Submitted in partial fulfillment of the requirements
for the degree of Doctor of Philosophy in Civil Engineering
in the Graduate College of the
University of Illinois, 1967

Urbana, Illinois

UNIVERSITY OF ILLINOIS

THE GRADUATE COLLEGE

October 31, 1966

I HEREBY RECOMMEND THAT THE THESIS PREPARED UNDER MY SUPERVISION BY SANA RACHRACH ABDEL-SAMAD

ENTITLED ANALYSIS OF MULTICELL BOX GIRDERS WITH DIAPHRAGMS

BE ACCEPTED IN PARTIAL FULFILLMENT OF THE REQUIREMENTS FOR THE DEGREE OF Doctor of Philosophy in Civil Engineering

A R Robinson
In Charge of Thesis

N M Newmark
Head of Department

Recommendation concurred in†

J E. Stallmeyer
W. L. Langhaar
K N Reid
Harold M. Inst
C. Tsai

Committee on Final Examination†

† Required for doctor's degree but not for master's

D517

ACKNOWLEDGEMENT

The author wishes to express his gratitude to his adviser, Dr. A. R. Robinson, Professor of Civil Engineering, for his guidance and many suggestions. He also wishes to express his appreciation to Dr. R. N. Wright, Associate Professor of Civil Engineering for the help he gave and time he devoted to this investigation.

The author wishes to acknowledge Dr. C. P. Siess, Professor of Civil Engineering, for his comments, and Dr. J. W. Melin, Assistant Professor of Civil Engineering, for his suggestions related to the development of the computer program.

The numerical results were obtained using the IBM 7094-1401 computer system of the Department of Computer Science of the University of Illinois which is partially supported by National Science Foundation Grant NSF-GP700.

This investigation was partially supported by the American Iron and Steel Institute.

TABLE OF CONTENTS

LIST OF TABLES

LIST OF FIGURES

I. INTRODUCTION

1.1 Object

The use of box girders in bridge construction is common. Because of their high torsional stiffness, box girder bridges may give better lateral distribution of loads than the usual type of slab-stringer bridges. Besides, reinforced concrete box girders lend themselves to the maximum use of precasting and minimum amount of in-situ work.

To date, very little theoretical work has been done on box girder bridges. The analysis and design of such structures require a deeper understanding of the underlying structural behavior. The object of this investigation is to develop an analysis technique that applies to multicell box girders made of several materials and having stiffeners and diaphragms. The analysis method will consider all the factors that play an important role in the behavior of the box girder such as the distortion of the cross-section in its own plane and the warping of the cross-section.

Another object of this investigation is to study the behavior of multicell box girders making use of the analysis technique. The study of the effects of diaphragms on stresses and deflections is the major point of this behavioral study. Based upon this study, design recommendations are suggested whenever possible.

1.2 Scope

The box girders studied are straight and of constant cross-section. They are single span girders, simply supported or fixed

at each end. Single-cell girders as well as multicell girders are considered. The shape of a cell is either rectangular or trapezoidal. Cross-sections of the girders studied are shown in Figure 1. Steel, reinforced concrete and composite steel and concrete box girders are considered

The loads are assumed to be applied vertically at the nodes, i.e., the intersection line of two plate elements. Loads may be either concentrated or line loads. The study considers only the elastic behavior of the box girders.

The variational method which was proposed by Vlasov (1) for the study of girders of closed section is used in this work. Vlasov's method makes use of a set of generalized coordinates in a stiffness analysis. It is used here because it readily permits consideration of the deformations which are characteristic of the action of box girders but which need not be considered in other types of bridge systems. It allows consideration of the distortion of the cross-section in its plane, the warping of the cross-section, and the shear deformations in the plane of the plate elements. Vlasov's generalized coordinates method is extended in this investigation to consider composite sections, longitudinally and transversely stiffened sections, and sections stiffened with diaphragms.

The number, location, spacing and stiffness of intermediate diaphragms is varied to study the effect of the diaphragms on the behavior of the box girders.

The solution was programmed in FORTRAN language for use on an IBM-7094 digital computer.

No attempt is made to give an exhaustive study of the influence of parameters which affect the behavior of multicell box girders. However, the present work does provide the analytical tools needed for such a study as well as some insight into the general effect of certain important parameters.

This dissertation is divided into six chapters. Chapter 1 is an introductory Chapter; Chapters 2 and 3 present the method of analysis; Chapters 4 and 5 give the analysis results and recommendations for the design of box girder bridges; Chapter 6 concludes this presentation.

1.3 Historical Background

Most of the theoretical work applicable to box girders has been done in connection with aircraft structures and folded plate roofs. This has led to two distinct design methods. Box girders used in aircraft structures are heavily stiffened and their design considers the cross-section of the girder to be infinitely stiff in its own plane. On the other hand, folded plate roofs have only end diaphragms and their design considers the distortion of the cross-section in its own plane. This thesis studies a type of structure that is not well represented by either extreme.

The torsional behavior of thin-walled closed beams of rigid cross-section has been described by many authors. The solution for pure torsion of multicell closed sections is found in Timoshenko (2). The solution of torsion with variable twist and restrained warping has been presented by von Kármán et. al. (3)(4), Benscoter (5) and Dabrowsky (6). A solution also exists for multibeam bridges with beam

elements of box section and is given by Pool et. al.(7). The beam elements consist of a thick-walled single cell with a rigid cross-section. The beam elements are connected to each other longitudinally by shear keys.

The methods available for the solution of folded plates taking into account the deformation of the cross-section can be classified into "ordinary" methods and "elasticity" methods.

The ordinary methods assume that the longitudinal action of each plate is governed by beam theory and its transverse action is that of a continuous one way slab. This means that the following quantities are neglected: the longitudinal bending moment, the torsional moment in the plate elements, the transverse axial elongation and the in-plane shearing deformations of the plate elements. The difference between the ordinary methods is only in their formulation and not in the model itself. The methods belonging to this group are Gruber's (8)(9), Vlasov's folded plate method (10), Girkmann's (11), Gaafar's (12), Grüning's (13), and Yitzhaki's (14).

The elasticity methods consider both plane-stress elasticity theory and two-way slab theory. This means that all the quantities neglected in ordinary methods are considered. The first such method was proposed by Goldberg and Leve (15). Loads and node displacements are expressed as Fourier series, equilibrium equations are written at each node. The system is solved for the node displacements for each Fourier term. This method is suitable for cases where component plates are short with respect to length. However, it is restricted to a one span simply supported folded flat isotropic plates. Scordelis et. al. (16) programmed the same method using a stiffness matrix formulation.

Along similar lines, Wright (17) developed an analytical method that is a modified elasticity method. The assumptions of thin-walled beam theory are used considering transverse axial strain and shearing deformation in the plane of the plate elements and allowing for two-way bending action of component plates in the fixed node condition. The author helped in the programming of this method and makes use of it in this thesis for comparison purposes under the name of alternative method.

All the folded plate methods discussed are applicable to the study of box girders but they have certain limitations. Ordinary methods do not consider shear deformations, elasticity methods are restricted to a single span simply supported girder, and none of them is readily adaptable to the consideration of intermediate diaphragms.

Ordinary and elasticity methods deal with the properties of the individual plate elements in formulating the analysis. A solution is presented by Vlasov (1) that treats the girder as a unit. It considers thin-walled box girders specifically. This method is used in this investigation as explained in Section 1.2. It is suitable for the consideration of intermediate diaphragms. Longitudinal bending moment, torsional moment, transverse axial elongation are neglected. This model leads to a constant shear stress in the transverse direction of a plate element.

Besides the theoretical work available, some tests of multi-cell box girders have been reported by Rowe (18), Davis et. al. (19) and Sparkes et. al. (20). They are of limited use for purpose of comparison in this investigation.

Design methods are also available from AASHO (21) and PCA (22) for reinforced concrete multicell bridges. The AASHO design method basically reduces the bridge to a slab-stringer bridge allowing a better lateral load distribution to account for the torsionally stiffer closed section. The transverse moments resulting from the distortion of the cross-section are, however, neglected. Diaphragm spacing is suggested not to exceed 40 feet.

1.4 Nomenclature

Each symbol is defined when it is introduced in the text. The following is presented for the convenience of the reader. A few symbols which occur only in one place are not included.

a_{ji}	matrix of coefficients defined in Equations(2.12)
A_i	cross-sectional area of brace i
A_s	cross-sectional area of a longitudinal stiffener
b	width of a plate diaphragm shown in Figure 10
b_{ji}	matrix of coefficients defined in Equations(2.12)
B_i	vector occurring in expressions for boundary conditions
c	distribution factor defined in Equation (5.4)
c_{jk}	matrix of coefficients defined in Equations(2.12)
$C_{j,k}$	matrix of the linear sets of specified conditions at a point of suppression
d	depth of a plate diaphragm shown in Figure 10, or depth of a box girder*
d_{hi}	matrix of coefficients defined in Equations(2.12)

*No confusion is possible between these meanings.

D	flexural plate rigidity, or differential operator d/dz *
$D_{j,i}$	matrix of boundary values of Equations(3.10), or matrix of the values of suppressed functions at a point of suppression from Equations(3.21)*
e	number of plate elements
E	modulus of elasticity for the reference material, or modulus of elasticity for a plate diaphragm.*
E_b	modulus of elasticity for a brace
E_p	modulus of elasticity of plate element p
F	sectional area
F_e	equivalent sectional area for a longitudinally stiffened plate element
F_i	force in brace i
F_{i1}, F_{i2}	components of the force of brace i along members 1 and 2
G	shear modulus of the reference material, or shear modulus of a plate diaphragm*
G_p	shear modulus of plate element p
h	diaphragm thickness, or step length for the numerical integration*
H_c	parameter equal to d^3/L^2t used in Section 4.5
I	moment of inertia of a plate element per transverse unit length. The plate element is not stiffened transversely
I_e	equivalent moment of inertia of a transversely stiffened plate element per transverse unit length

I_{xx}, I_{yy}	moments of inertia of the girder cross-section about x-axis and y-axis respectively
I_w	"sectorial moment of inertia" of the girder cross-section defined by Equations(2.21)
L	length of box girder
L_i	longitudinal concentrated load applied at node i, also length of brace i*
m	number of transverse degrees of greedom
M(z,s)	point in the middle surface of a plate element of the girder given by its coordinates z and s
$M_T(z,s)$	transverse bending moment per unit transverse length
$M_x(z), M_y(z)$	moments in a girder about the x and y axes respectively
M_{xy}	torsional moment per unit length in a plate
n	number of nodes
N_c	number of compartments
p(z,s)	surface shear load per unit area in the longitudinal direction of the girder
P	longitudinal force at the four corners of a diaphragm, or applied vertical load on girder*
$P_j(z)$	the j<u>th</u> internal longitudinal generalized force
q(z,s)	surface shear load per unit area in the transverse direction of the girder
$Q_j(z)$	the j<u>th</u> internal transverse generalized force
$Q_T(z)$	transverse bimoment of a single cell box
r_{hk}	matrix of coefficients defined in Equations(2.12)
s	arc length along cross-section
s_{hk}	matrix of coefficients defined by Equations(2.12)

t	thickness of a plate element
T	net torsional moment in the cross-section of a girder, or transformation matrix defined by Equation (3.1)*
T^T	transpose of T
T_k	transverse concentrated load applied along member k
$u(z,s)$	longitudinal displacement
$u_{sj}(z)$	longitudinal displacement of node j
$u_{i,j}(z,s)$	the $j^{\underline{th}}$ longitudinal generalized displacement from the $i^{\underline{th}}$ initial-value problem
$U_i(z)$	the $i^{\underline{th}}$ longitudinal generalized displacement
$U_{io}(z)$	the $i^{\underline{th}}$ longitudinal generalized displacement before orthogonalization
$\Delta U_i'$	sudden change in the first derivative of the $i^{\underline{th}}$ longitudinal generalized displacement
$v(z,s)$	transverse displacement
$v_{i,j}(z,s)$	the $j^{\underline{th}}$ transverse generalized displacement from the $i^{\underline{th}}$ initial-value problem.
$V_j(z)$	the $j^{\underline{th}}$ transverse generalized displacement
$\Delta V_j'$	sudden change in the first derivative of the $j^{\underline{th}}$ transverse generalized displacement
$w(x,y)$	warping displacement of a rectangular box girder and of a diaphragm.
x,y	coordinate axes of a cross-section as shown in Figure 6
z	longitudinal coordinate
z_d	longitudinal coordinate of a concentrated load
$\alpha_l,\beta_l,\gamma_l$	angles defined for brace l in Figure 13
β	coefficient used in β method of numerical integration

γ	ratio of Young's modulus and shear modulus of the reference material
δ_T	vertical deflection caused by a torque
δ_{BC}, δ_{BU}	normalizing vertical deflections defined in Sections 4.1, 5.2
$\lambda_i(z)$	longitudinal distributed load along member i
λ_i	coefficient vector in Equations (3.10)
$\Lambda_h(z)$	the $h^{\underline{th}}$ external transverse generalized force or load
$\mu_k(s)$	transverse moment in the elementary frame when $V_k = 1$
ν	Poisson's ratio
$\pi_j(z)$	the $j^{\underline{th}}$ external longitudinal generalized force or load
$\pi_{jo}(z)$	the $j^{\underline{th}}$ external longitudinal generalized force before orthogonalization
$\rho_{i,k}$	matrix of coefficients used in Equations (3.21)
σ_{BC}, σ_{BU}	normalizing axial stresses defined in Sections 4.1, 5.2
$\sigma_L(z,s)$	longitudinal axial stress
$\sigma_T(z,s)$	transverse axial stress at the extreme fibers
$\tau(z,s)$	shear stress in the plane of the plate elements
τ_h, τ_v	shear stress in horizontal and vertical plate elements
τ_{BC}, τ_{BU}	normalizing shear stresses defined in Sections 4.1, 5.2
$\Phi_i(s)$	the $i^{\underline{th}}$ longitudinal generalized coordinate
Φ_{ji}	the value of the $i^{\underline{th}}$ longitudinal generalized coordinate at the $j^{\underline{th}}$ node
Φ_{jio}	the value of the $i^{\underline{th}}$ longitudinal generaliced coordinate at the $j^{\underline{th}}$ node before orthogonalization
$\Psi_j(s)$	the $j^{\underline{th}}$ transverse generalized coordinate

2. METHOD OF GENERALIZED COORDINATES

The object of this chapter is to present the generalized coordinates method developed by Vlasov. This method is extended to include diaphragms, stiffened plate elements and composite sections. In addition, a brief discussion is presented on various methods of integration of the final equations.

2.1 Assumptions

Consider the single span thin-walled beam shown in Figure 2. The position of any point M on the undeformed middle surface is determined by two coordinates: coordinate z which is the distance along the span from the plane z = 0, and coordinate s which is the arc length from an initial generator s = 0.

2.1.1 Properties of Plate Elements

The box girder is assumed to consist of flat plate elements connected rigidly at the nodes. Each plate is rectangular and of uniform thickness with or without longitudinal or transverse stiffeners. The plate material is assumed to be isotropic and linearly elastic. Any plate element and its stiffeners are of the same material although this restriction is not necessary.

The plates are thin and long, that is their width-to-thickness ratios and their length-to-width ratios are large, i.e., greater than or equal to ten.

In any plate element the axial longitudinal stress and the shear stress are assumed to be constant throughout the thickness; this amounts to neglect of longitudinal and torsional moments in the

individual plate. For plate elements with large length-to-width ratio, the longitudinal and torsional moments are small. This may be seen by taking a simply supported plate with a length-to-width ratio of 10 and with a Poisson's ratio of zero. A transverse sinusoidal moment applied on the long edge of the plate induces maximum longitudinal and maximum torsional moments that are respectively 0.006 and 0.103 of the maximum transverse moment (see Newmark (23)).

2.1.2 Loads

The loads considered are applied statically along the nodes as concentrated or distributed loads (Figure 3). However, in the derivation presented in this chapter only surface shear forces are considered. The simple extension to concentrated and distributed node loads is deferred to Section 3.5.

Loads applied perpendicular to plate elements between node points require some slight change in the procedure. They can be accounted for by superimposing the stresses in the fixed edge condition obtained using plate theory on the stresses produced when the fixed edge forces are applied as node loadings. This is clearly analogous to the procedure used in stiffness analysis of frames, e.g., slope deflection.

2.1.3 Displacements

The displacements are considered to be small. This assumption and the assumed linear elasticity of the materials permit use of the principle of superposition.

It is also assumed that the longitudinal strains vary linearly in a plate element. This means that any cross-section will

deform linearly between nodes in the longitudinal direction. This is in effect assuming that a plane section remains plane for each plate element. In some cases it may be desirable to introduce nodes in a plate between intersections with other plates. In this way it would be possible to study shear lag in a single plate of the girder.

It is assumed for transverse displacements that plate elements do not change in width. This is realistic since the width-to-thickness ratio is large and most of the energy of transverse deformation is bending energy. It is the same assumption that is used for frames when neglecting axial distortion of members. This assumption of inextensible plate elements does not mean that transverse normal forces are zero. These forces can be computed from equilibrium but are not required in the formulation of the analysis.

2.2 Generalized Coordinates

Consider again the box girder of Figure 2. An elementary strip of length dz is isolated at location z (Figure 4). When dz is unity this strip is called the "elementary frame" of the box girder.

The assumption of linear variation of the longitudinal displacement between node points of the elementary strip means that the nodal out-of-plane displacements determine the longitudinal deformation of the strip. The number of longitudinal degrees of freedom for the elementary strip is equal to the number of nodes, n. The longitudinal displacement u(z,s) of a point M on the surface can be written as a finite sum:

$$u(z,s) = \sum_{i=1}^{n} U_i(z)\, \Phi_i(s) \qquad (2.1)$$

where

$\Phi_i(s)$ is the $i^{\underline{th}}$ longitudinal generalized coordinate

$U_i(z)$ is the $i^{\underline{th}}$ longitudinal generalized displacement.

The choice of the longitudinal coordinates is limited only by the restriction that these coordinates be linearly independent. One obvious set of longitudinal coordinates is determined by a unit displacement of node i while displacements of the other n - 1 nodes are zero as shown in Figure 5a.

Two possible sets of longitudinal coordinates are shown in Figure 6 for a rectangular box. The set in Figure 6a is obtained as explained above, the second set has more immediate physical significance: the shape Φ_1 is an axial extension, Φ_2 and Φ_3 are bending deformations about the x and y axes, respectively, while Φ_4 is a warping deformation. In general, the longitudinal deformation of the cross-section can be broken into an axial extension, bending about two principal axes and n - 3 warping deformations.

The assumption of inextensible plate elements in the transverse direction imposes constraints on the transverse or in-plane deformation of the elementary strip. The inextensibility of each plate element imposes one condition on the displacements of the nodes at its ends and reduces the number of degrees of freedom by one for every plate element. Therefore the total number m of independent transverse coordinates is given by:

$$m = 2n - e \qquad (2.2)$$

where e is the number of plate elements.

The transverse displacement $v(z,s)$ of a point M of the middle surface can also be written as a finite sum:

$$v(z,s) = \sum_{j=1}^{m} V_j(z)\, \psi_j(s) \qquad (2.3)$$

where:

$\psi_j(s)$ is the $j^{\underline{th}}$ transverse generalized coordinate

$V_j(z)$ is the $j^{\underline{th}}$ transverse generalized displacement.

The choice of the transverse generalized coordinates is again limited only by the restriction that these coordinates be linearly independent.

As before, one set of transverse generalized coordinates is obtained as follows: member j of the elementary frame is given a unit displacement, j varying from 1 to e, while displacements along the remaining members are determined by assuming the elementary frame to act as a linkage (Figure 5b). Only m of these displacement patterns are linearly independent and the remaining e - m patterns are dropped.

Two possible sets of transverse coordinates are shown in Figure 7 for a rectangular box. The set of Figure 7a is obtained as described above. The set of Figure 7b has more direct physical meaning: the shape ψ_1 is a rigid body rotation, ψ_2 and ψ_3 are rigid body translation along the x and y axes respectively, and ψ_4 is a distortion pattern. In general, the transverse deformation can be broken into three rigid body motions and m - 3 distortion patterns.

The choice of the generalized coordinates in accordance with the basic assumptions reduces the two-dimensional problem involving the displacement functions $u(z,s)$ and $v(z,s)$ to a one-dimensional problem involving the generalized displacement functions $U_i(z)$ $i = 1, \ldots n$ and $V_j(z)$ $j = 1, \ldots m$.

2.3 Relations Between Stresses and Generalized Displacements

An element with sides equal to ds and dz and a thickness of t is isolated at point M(z,s) as shown in Figure 8. The external forces acting on the element are the surface forces p(z,s) in the longitudinal z-direction and q(z,s) in the transverse s-direction. Forces are present which correspond to the longitudinal axial stress $\sigma_L(z,s)$ and to the shearing stress $\tau(z,s)$ both stresses being constant through the thickness, and to the transverse bending stress that varies linearly through the depth being a maximum denoted by $\sigma_T(z,s)$ at the extreme fibers. The resultant of the transverse bending stresses is a transverse bending moment $M_T(z,s)$.

From the theory of elasticity for small deformation the stress-displacement relations yield:

$$\begin{aligned} \sigma_L(z,s) &= E\frac{\partial u}{\partial z} \\ \tau(z,s) &= G\left(\frac{\partial u}{\partial s} + \frac{\partial v}{\partial z}\right) \end{aligned} \tag{2.4}$$

where E is Young's modulus and G the shear modulus.

After u and v are replaced by their expressions from Equations (2.1) and (2.3), Equations(2.4) give:

$$\begin{aligned} \sigma_L(z,s) &= E\sum_{i=1}^{n} U_i'(z)\,\phi_i(s) \\ \tau(z,s) &= G\left(\sum_{i=1}^{n} U_i(z)\,\phi_i'(s) + \sum_{k=1}^{m} V_k'(z)\,\psi_k(s)\right) \end{aligned} \tag{2.5}$$

where the prime denotes differentiation with respect to the argument of the function.

The transverse moment per unit length is given by:

$$M_T(z,s) = \sum_{k=1}^{m} V_k(z)\ \mu_k(s) \qquad (2.6)$$

where $\mu_k(s)$ is the bending moment induced in the elementary frame deformed into the shape $\psi_k(s)$.

The extreme transverse bending stress is obtained by dividing $M_T(z,s)$ by the section modulus S_m of the corresponding member of the elementary frame:

$$\sigma_T(z,s) = \frac{\sum_{k=1}^{m} V_k(z)\ \mu_k(s)}{S_m} \qquad (2.7)$$

Equations (2.5) and (2.7) express the relations between stresses and generalized displacements.

Equations (2.5) and (2.7) with the choice of the generalized coordinates lead to a specific stress variation in the cross-section. The longitudinal axial stress and maximum transverse bending stress vary linearly between node points. The shear stress is constant in a plate element. Equation (2.6) shows that the transverse bending moment varies linearly between node points.

2.4 Virtual Work Equations

The virtual work equations are derived for the general case of a composite girder with all plate elements stiffened transversely and longitudinally.

For ease of formulation, a reference material is chosen with E and G as the modulus of elasticity and shear modulus. The constants E_p and G_p denote the moduli of the $p^{\underline{th}}$ plate element. The parameter t denotes the thickness of the plate without its stiffeners, d_L the longitudinal stiffeners spacing, A_s the area of a longitudinal stiffener,

and d_t the transverse stiffeners spacing as shown in Figure 9. The following assumptions are made for stiffened plate elements:

(a) The plate element and its stiffeners are of the same material.

(b) The plate alone carries the shear in its plane.

(c) Longitudinal stiffeners are shallow, closely spaced, and therefore are assumed to be equivalent to an added plate thickness in the longitudinal direction given by A_s/d_L; the total equivalent thickness is given by

$$t_e = t + A_s/d_L \tag{2.8}$$

(d) The transverse stiffeners increase the moment of inertia of the plate elements in the transverse direction. An effective moment of inertia I_e per unit transverse length is determined from an effective plate width that acts with the stiffener (Appendix A). The moment of inertia of the effective plate and stiffener is found about their neutral axis, and then divided by the transverse stiffeners spacing to give I_e.

If the plate element is not stiffened $t_e = t$ and $I_e = t^3/12$.

Attention is now turned to the equilibrium conditions. The elementary transverse strip of Figure 4 has $(m + n)$ independent degrees of freedom. The equilibrium of the strip can be formulated using the principle of virtual work. The work done by all forces on the elementary strip vanishes for any virtual displacement. To arrive at a consistent theory, the restriction on the displacements will restrict the virtual

displacements as well. Therefore only variations of the generalized coordinates are required for virtual displacements.

The equations of virtual work take the form:

$$\int_F \frac{\partial \sigma}{\partial z} \phi_j dF_e - \int_F \tau \phi_j' dF + \int_L p \phi_j ds = 0 \qquad j = 1, \ldots n$$

$$\int_F \frac{\partial \tau}{\partial z} \psi_h dF - \sum_{k=1}^{m} V_k \int_L \frac{\mu_k \mu_h}{E_p I_e} ds + \int_L q \psi_h ds = 0 \quad h = 1, \ldots m \tag{2.9}$$

where $dF_e = t_e ds$ and $dF = t ds$. The symbol F denotes integration over the whole cross-sectional area and L denotes integration over the whole arc length of the cross-section.

The first n equations express the work of all the forces in the n longitudinal displacement patterns. The first term in these equations expresses the external work of the axial longitudinal stresses, the second term the internal work of the shearing stresses, and the last term the external work of the applied longitudinal forces.

The second set of m equations expresses the transverse work of all forces in the m transverse displacement patterns. In these equations the first term expresses the external work of the shearing stresses. The third term expresses the external work of the transverse applied forces. The second term expresses the internal work done by the transverse moment and is explained below.

The moments $\mu_h(s)$ are induced in the elementary frame when deformed into the shapes $\psi_h(s)$. The parameter I_e is the moment of inertia of the members of the elementary frame including the effect of the transverse stiffeners. The internal work done by the transverse bending

moment M_T, when the elementary transverse strip goes through a virtual displacement $\psi_h(s)$, is equal to $\int_L \frac{\mu_h(s)}{E_p I_e} M_T ds$. This expression leads to the second term of the second set of m equations when M_T is replaced by its value from Equation (2.6).

The stresses from Equations (2.5) are substituted in Equations (2.9) to give:

$$\gamma \sum_{i=1}^{n} a_{ji} U_i'' - \sum_{i=1}^{n} b_{ji} U_i - \sum_{k=1}^{m} c_{jk} V_k' + \frac{1}{G} \pi_j = 0 \qquad j = 1, \ldots n$$

$$\sum_{i=1}^{n} d_{hi} U_i' + \sum_{k=1}^{m} r_{hk} V_k'' - \gamma \sum_{k=1}^{m} s_{hk} V_k + \frac{1}{G} \Lambda_h = 0 \qquad h = 1, \ldots m \tag{2.10}$$

Primes denote derivatives with respect to z. The terms π_j and Λ_h are given by:

$$\pi_j(z) = \int_L p(z,s)\, \phi_j(s)\, ds \qquad \Lambda_h(z) = \int_L q(z,s)\, \psi_h(s)\, ds \tag{2.11}$$

They are the generalized external forces or loads.

The coefficients of Equations (2.10) are given by the following expressions:

$$\begin{aligned}
\gamma &= E/G \\
a_{ji} &= \int_F \phi_j(s)\, \phi_i(s)\, (E_p/E)\, dF_e \\
b_{ji} &= \int_F \phi_j'(s)\, \phi_i'(s)\, (G_p/G)\, dF \\
c_{jk} &= \int_F \phi_j'(s)\, \psi_k(s)\, (G_p/G)\, dF \\
d_{hi} &= \int_F \psi_h(s)\, \phi_i'(s)\, (G_p/G)\, dF \\
r_{hk} &= \int_F \psi_h(s)\, \psi_k(s)\, (G_p/G)\, dF
\end{aligned} \tag{2.12}$$

$$s_{hk} = \frac{1}{E} \int_L \frac{\mu_h(s)\mu_k(s)}{E_p I_e} ds \qquad (2.12)$$

For plates with no longitudinal stiffeners dF_e reduces to dF. For plates with no transverse stiffeners I_e reduces to $t^3/12$. For a girder made out of a single material, the ratios E_p/E and G_p/G are unity.

Inspection of Equations(2.12) reveals certain relations between the various coefficients which are the expressions of Betti's law for the structure:

$$\begin{aligned} a_{ji} &= a_{ij} \\ b_{ji} &= b_{ij} \\ r_{hk} &= r_{kh} \\ s_{hk} &= s_{kh} \\ c_{jk} &= d_{hi}, \text{ when } j = i \text{ and } k = h \end{aligned} \qquad (2.13)$$

The system of equilibrium equations, Equations(2.10), consists of (m + n) simultaneous linear differential equations of the second-order with constant coefficients in terms of the (m + n) generalized displacements.

Equations(2.10) can be written in matrix form as:

$$\begin{aligned} \left[\gamma D^2 [a_{ji}] - [b_{ji}]\right] \{U_i\} - D[c_{jk}]\{V_k\} &= -\frac{1}{G}\{m_j\} \\ D[d_{hi}]\{U_i\} + \left[D^2[r_{hk}] - \gamma [s_{hk}]\right]\{V_k\} &= -\frac{1}{G}\{\Lambda_h\} \end{aligned} \qquad (2.14)$$

where D is the differential operator d/dz.

2.5 Orthogonal Coordinates

The choice of the generalized coordinates is limited only by the requirement of linear independence. They can be chosen such that they satisfy the following relations:

$$\begin{aligned} &\int_F \phi_i(s)\,\phi_j(s)\,\frac{E_\rho}{E}\,dF_e = 0 \qquad \text{for } i \neq j \\ &\int_F \psi_h(s)\,\psi_k(s)\,\frac{G_\rho}{G}\,dF = 0 \qquad \text{for } h \neq k \end{aligned} \tag{2.15}$$

The longitudinal coordinates are then orthogonal over the cross-section with respect to the weighting function E_ρ/E and similarly the transverse coordinates are orthogonal over the cross-section with respect to the weighting function G_ρ/G. With the orthogonal coordinates, Equations (2.10) take the simpler form:

$$\begin{aligned} &\gamma\, a_{jj}U_j'' - \sum_{i=1}^{n} b_{ji}U_i - \sum_{k=1}^{m} c_{jk}V_k' + \frac{1}{G}\,\pi_j = 0 \qquad j = 1, \ldots n \\ &\sum_{i=1}^{n} d_{hi}U_i' + r_{hh}V_h'' - \gamma \sum_{k=1}^{m} S_{hk}V_k + \frac{1}{G}\,\Lambda_h = 0 \qquad h = 1, \ldots m \end{aligned} \tag{2.16}$$

As a result, the second derivative of each generalized displacement appears in only one equation of the set and is the only second derivative in that equation. This facilitates the numerical integration of the system and the study of concentrated loads.

The method used to obtain an orthogonal set defined by Equations (2.15) is described in Chapter 3.

2.6 Internal Generalized Forces

The internal generalized forces are defined by the following expressions:

$$P_j(z) = \int_F \sigma_L(z,s)\, \phi_j(s)\, dF_e \qquad j = 1, \ldots n$$

$$Q_j(z) = \int_F \tau(z,s)\, \psi_j(s)\, dF \qquad j = 1, \ldots m \tag{2.17}$$

where P_j is the $j^{\underline{th}}$ longitudinal generalized force and Q_j is the $j^{\underline{th}}$ transverse generalized force. The integrals are taken over the cross-sectional area.

For a single cell box girder with the set of generalized coordinates of Figure 6b and Figure 7b the generalized forces have a definite meaning:

P_1 is the net axial force N

P_2 is the bending moment about x axis M_x

P_3 is the bending moment about y axis M_y

P_4 is defined to be the longitudinal bimoment B

Q_1 is the net torsional moment T

Q_2 is the total horizontal shear V_x

Q_3 is the total vertical shear V_y

Q_4 is defined to be the transverse bimoment Q_T.

These generalized forces can be expressed in terms of the generalized displacements using Equations(2.5) as:

$$P_j(z) = E \sum_{i=1}^{n} a_{ij} U_i'(z) \qquad j = 1, \ldots n$$

$$Q_j(z) = G\left(\sum_{i=1}^{n} c_{ij} U_i(z) + \sum_{k=1}^{m} r_{kj} V_k'(z) \right) \qquad j = 1, \ldots m \tag{2.18}$$

For orthogonal coordinates Equations(2.18) become:

$$P_j(z) = E\, a_{jj} U_j'(z) \qquad j = 1, \ldots n$$
$$Q_j(z) = G\left(\sum_{i=1}^{n} c_{ij} U_i(z) + r_{jj} V_j'(z) \right) \qquad j = 1, \ldots m \tag{2.19}$$

The longitudinal axial stress σ_L can be written in terms of the internal generalized forces for the case of orthogonal coordinates. This axial stress, using Equations (2.5) and (2.19), is equal to:

$$\sigma_L(z,s) = \sum_{j=1}^{n} \frac{P_j}{a_{jj}} \phi_j(s) \tag{2.20}$$

The meaning of Equation (2.20) may be clarified by examining the case of a single box having the generalized coordinates of Figures 6b and 7b. The generalized coordinates yields the following expressions for a_{jj} $j = 1, \ldots 4$:

$$\begin{aligned} a_{11} &= \int_F 1 \cdot dF = A \\ a_{22} &= \int_F y^2\, dF = I_{xx} \\ a_{33} &= \int_F x^2\, dF = I_{yy} \\ a_{44} &= \int_F w^2\, dF = I_w \end{aligned} \tag{2.21}$$

where w is the generalized coordinate ϕ_4, or the warping shape, A is the area, I_{xx} the moment of inertia about the x axis, I_{yy} the moment of inertia about the y axis and I_w the sectorial moment of inertia of the cross-section.

Equation (2.20) becomes, after substituting for P_j and a_{jj} their values determined above:

$$\sigma_L(z,s) = \frac{N(z)}{A} + \frac{M_x(z)}{I_{xx}} y + \frac{M_y(z)}{I_{yy}} x + \frac{B(z)}{I_w} w \qquad (2.22)$$

This expression is a generalization of the usual one for determining stresses in beams from the stress resultants.

2.7 Boundary Conditions

The system of differential equations, Equations (2.10), contains $(m + n)$ ordinary linear equations of the second order having constant coefficients. It follows that the required generalized displacement functions contain $2(m + n)$ arbitrary constants. This equals twice the number of spatial degrees of freedom, and agrees with the number of independent boundary conditions which may be given at the end sections. The problem has a unique solution when $2(m + n)$ suitable boundary conditions are specified.

Three types of end conditions are considered and are described below. The simply supported end and the fixed end are used in this investigation; the free end condition is presented for generality.

2.7.1 Simply Supported End

A simply supported boundary exists at an end when the support is unyielding. In addition, a diaphragm which is free to warp and rigid in shear is located at that end.

The virtual work of the end forces must vanish for all possible displacement patterns compatible with the boundary conditions when the boundary configuration stores no energy. For a simply supported end, n longitudinal displacements are possible and are chosen to be proportional to the generalized longitudinal coordinates. The

virtual work is given by the generalized forces. The work expressions lead to:

$$P_i(z)_{@\ end} = 0 \qquad i = 1, \ldots n \tag{2.23}$$

or using Equations(2.18)

$$U_i'(z)_{@\ end} = 0 \qquad i = 1, \ldots n \tag{2.24}$$

In addition to Equations(2.24) the transverse generalized displacements vanish at that end:

$$V_j(z)_{@\ end} = 0 \qquad j = 1, \ldots m \tag{2.25}$$

In a box girder with both ends simply supported, a longitudinal generalized displacement must vanish or be specified at one end for uniqueness of displacements. If this generalized displacement is taken to be U_1 the conditions at such an end may be expressed as:

$$\begin{aligned} U_1(z)_{@\ end} &= 0 \\ U_i'(z)_{@\ end} &= 0 \qquad i = 2, \ldots n \\ V_j(z)_{@\ end} &= 0 \qquad j = 1, \ldots m \end{aligned} \tag{2.26}$$

2.7.2 Fixed End

A fixed end exists when all the generalized displacements vanish at that end. The conditions can be written as:

$$\begin{aligned} U_i(z)_{@\ end} &= 0 \qquad i = 1, \ldots n \\ V_j(z)_{@\ end} &= 0 \qquad j = 1, \ldots m \end{aligned} \tag{2.27}$$

2.7.3 Free End

A free end is defined to be an end where displacements are not restrained. Supports and diaphragms are absent.

The virtual work of the end forces must vanish for all the possible displacements patterns that are compatible with the boundary conditions. For a free end, $(m + n)$ displacements are possible and are chosen to be proportional to the longitudinal and transverse generalized coordinates. The virtual work is given by the generalized forces and the work expressions lead to:

$$\begin{aligned} P_i(z)_{@\ end} &= 0 \qquad i = 1, \ldots n \\ Q_j(z)_{@\ end} &= 0 \qquad j = 1, \ldots m \end{aligned} \tag{2.28}$$

Equations (2.19) and (2.28) yield:

$$\begin{aligned} U_i'(z)_{@\ end} &= 0 \qquad i = 1, \ldots n \\ r_{jj}V_j'(z) + \sum_{i=1}^{n} c_{ij}U_i(z)_{@\ end} &= 0 \qquad j = 1, \ldots m \end{aligned} \tag{2.29}$$

2.8 Action of Intermediate Diaphragms

Diaphragms are placed at intermediate points to stiffen the box girder. They can be of two types, plates or cross-bracing. In analysis, a diaphragm is considered deformable and linearly elastic. It exerts a system of self equilibrating forces on the girder which depend only on the box girder displacements.

2.8.1 Rectangular Plate Diaphragms

Plate diaphragms possess an in-plane stiffness and an out-of-plane stiffness. Therefore they resist both the relative transverse and relative longitudinal displacements of a section of the box girder. The thickness of the diaphragm is denoted by h, its depth by d, its width by b, its Young's modulus by E, and its shear modulus by G.

2.8.1.1 In-Plane Action

The diaphragm is assumed to act in pure shear. Under deformation, the edges of the plate diaphragm are assumed to remain straight and therefore do not conform to the bent configuration of the elementary frame. Compatibility of the deformation of the diaphragm and the girder is attained only at the node points.

For a deformation $\Psi_h V_h = 1$ (Figure 10), the shear forces induced in the plate diaphragm are given by:

$$S_1 = Ghd/b$$
$$S_2 = Gh \qquad (2.30)$$

2.8.1.2 Out-of-Plane Action

The plate diaphragm exerts concentrated longitudinal forces directed along the nodes of the box girder. These corner forces are determined from the theory of bending of plates.

A deformation of the plate diaphragm given by $\Psi_i U_i = 1$ (Figure 11), is the sum of four displacement patterns. The four displacements are a longitudinal displacement of the whole diaphragm, a rotation about the x axis, a rotation about the y axis and a warping

displacement pattern. It can be shown easily that the warping displacement at each of the four nodes is equal in absolute value to:

$$S_0 = (S_1 + S_4 - S_2 - S_3)/4 \tag{2.31}$$

where S_1, S_2, S_3, S_4 are the algebraic values taken by ϕ_i at the four corners of the diaphragm.

Only the warping deformation of the diaphragm produces corner forces and attention is now directed to this warping (Figure 12). The warping deformation of the diaphragm is given by:

$$w = cxy \tag{2.32}$$

where w is the longitudinal displacement of a point defined by its coordinates x and y in the middle surface of the diaphragm. The constant c is given by:

$$c = \frac{4S_0}{bd} \tag{2.33}$$

From plate theory, the corner forces are equal to $2M_{xy}$. The torsional moment M_{xy} is given by:

$$M_{xy} = D(1 - \nu) \frac{\partial^2 w}{\partial x \partial y} \tag{2.34}$$

where $D = Eh^3/12(1 - \nu^2)$ and ν is Poisson's ratio. Therefore, the corner force P is obtained from M_{xy} by replacing w from Equation (2.32) and by multiplying the result by 2:

$$P = Eh^3 S_0/3bd(1 + \nu) \tag{2.35}$$

A comparison between in-plane and out-of-plane stiffness of a plate diaphragm of practical proportions indicates that out-of-plane stiffness is small compared to in-plane stiffness. The ratio of in-plane

stiffness to out-of-plane stiffness is proportional to h^2/bd. This ratio is a maximum of 0.01 for practical box girder proportions. Moreover, a box girder is much stiffer in the longitudinal direction than in the transverse direction. Neglect of the longitudinal corner warping forces seems warranted.

For a box girder with several cells, the forces induced in all the separate rectangular diaphragms are computed for all the generalized coordinates.

2.8.2 Cross-Bracing

An X-brace does not possess substantial warping or flexural stiffness. It acts to restrain the transverse deformation of the box girder through direct tension or compression. It is assumed that the compression in any brace is well below the buckling load.

For a transverse displacement given by $\psi_h V_h = 1$ (Figure 13), the axial deformation in a brace i is given by:

$$\Delta L_i = + \sin \beta_i / \cos \gamma_i \tag{2.36}$$

where β_i and γ_i are the angles shown on Figure 13 for the specified ψ_h.

The force in the brace is given by:

$$F_i = E_b A_i \Delta L_i / L_i \tag{2.37}$$

where E_b is Young's modulus, A_i the cross-sectional area and L_i the length of brace i.

The force F_i is resolved into components along the two adjacent members at node 1 as follows:

$$F_{i1} = F_i \sin \beta_i / \sin(\pi - \alpha_i - \beta_i)$$
$$F_{i2} = F_i \sin \alpha_i / \sin(\pi - \alpha_i - \beta_i) \qquad (2.38)$$

where α_i is defined in Figure 13.

For every $\psi_h V_h = 1$ (h = 1, ...m), the cross-bracing is replaced by systems of forces (at each end of a brace) given by equations of the same type as Equations (2.36), (2.37) and (2.38).

2.8.3 Trapezoidal Plate Diaphragms

The analysis of trapezoidal box girders with intermediate plate diaphragms uses the concept of equivalent bracing system. More exact analysis of a trapezoidal plate diaphragm is possible, Gustafson (24), but is more complex than required here.

A rectangular plate diaphragm is equivalent to cross-bracing consisting of two diagonal braces having each a cross-sectional area given by:

$$A_i = \frac{h.L_i}{(E_b/G) \sin 2\beta_i} = \frac{h.L_i}{(E_b/G) \sin 2\alpha_i} \qquad (2.39)$$

where h is the thickness of the plate diaphragm, L_i the length of a brace, E_b Young's modulus of the bracing, G shear modulus of the plate diaphragm and α_i and β_i the angles defined in Figure 14a.

By extension, a trapezoidal plate diaphragm is considered equivalent to two diagonal braces having each an area given by Equation (2.39) with angles α_i and β_i as defined in Figure 14b.

2.9 Methods of Solution

The system of differential equations, Equations (2.10), must be solved for the generalized displacements. The stresses and node

displacements are then determined by substituting the values of the generalized displacements in Equations (2.1), (2.3), (2.5) and (2.7). Several methods of solving the system are available. They are discussed below.

2.9.1 Closed Form Solution

Equations (2.10) can be solved in a closed form making use of the boundary conditions at both ends. The method of initial parameters provides such a solution. The boundary-value problem is solved as an initial-value problem in terms of unknown initial parameters. After integration along the span, the initial parameters are found from the boundary conditions at the far end. Diaphragm effects are evaluated readily.

This solution is developed by Vlasov (1) for the case of a rectangular single cell box girder. However this method becomes impractical as the number of degrees of freedom increases.

2.9.2 Fourier Expansion

In this method, loads and generalized transverse displacements are expanded into sine series and the generalized longitudinal displacements are expanded into cosine series. This expansion corresponds to the case of simply supported ends.

The system, Equations (2.10), is reduced to a system of algebraic equations for each term of the Fourier expansion. The unknowns are the amplitudes of the generalized displacements. The final solution is given by the sum of all the Fourier components of each generalized displacement.

This solution is convenient but has certain obvious disadvantages. It can be applied only to very special type of end conditions. Diaphragms are difficult to consider and convergence of the solution may present some problems.

2.9.3 Numerical Integration

This work uses numerical integration to solve Equations (2.10). This method of solution was chosen because of its generality, and its adaptability to programming on a digital computer with a minimum of hand computations.

The boundary-value problem is solved as a sequence of initial-value problems by numerical integration. The final solution is the linear combination of the initial-value problems that satisfies the boundary conditions at the far end. The procedure is essentially an initial parameter method in numerical form.

3. METHOD OF SOLUTION

The solution of the system of linear differential equations, Equations (2.10), can be obtained by any of the several methods mentioned briefly at the end of the previous chapter. The method of numerical integration is used in this work because of its generality. The special features of the solution method form the subject matter of this chapter.

3.1 Orthogonalization of the Generalized Coordinates

The system of differential equations, Equations (2.10), takes a simpler form when the generalized coordinates are orthogonal as defined in Section 2.5. The integration of the system also becomes easier because of the decoupling of the second derivatives of the generalized displacements. As will be seen, the treatment of concentrated loads also becomes simpler after orthogonalization. A method is presented here for obtaining a system of orthogonal generalized coordinates from an arbitrarily chosen set of coordinates that are independent but not necessarily orthogonal. This method will yield a set of orthogonal coordinates but this set is not a unique set for the box girder.

3.1.1 Original Set of Generalized Coordinates

The longitudinal coordinates $\phi_{i0}(s)$ for i = 1, ...n are chosen to be a unit longitudinal displacement of node i while other nodes are restrained in the longitudinal direction. This set of coordinates is definitely not orthogonal.

The transverse coordinates $\psi_h(s)$ for h = 1, ...m are chosen to be a unit transverse displacement along a given member j, j varying from 1 to e; displacements along the remaining members are determined by assuming the elementary frame to act as a linkage. Only the m independent coordinates are kept. This set of coordinates is orthogonal.

3.1.2 Change of Displacement Variables

A change of variables is then performed for the longitudinal generalized displacements only. No change of variable is made for the transverse generalized displacements. The change of variables is defined by:

$$\{U_{io}\} = [T] \cdot \{U_i\} \tag{3.1}$$

where U_{io} is the original longitudinal displacement vector corresponding to the original set of coordinates; the vector U_i is the new longitudinal displacement vector corresponding to the new orthogonal set of coordinates that will be determined later.

T is the transformation matrix.

As in the matrix theory of frames (25), the principle of virtual work leads to the contragredient transformation for the generalized longitudinal load vector:

$$\{\pi_j\} = [T]^T \cdot \{\pi_{jo}\} \tag{3.2}$$

where π_{jo} is the original longitudinal load vector corresponding to the original set of coordinates, π_j is the new longitudinal load vector corresponding to the new orthogonal coordinates to be determined.

Equations (2.10) are written for the original displacement functions U_{io} as:

$$\begin{aligned} &\gamma D^2[a_{ji}]\{U_{io}\} - [b_{ji}]\{U_{io}\} - D[c_{jk}]\{V_k\} + \frac{1}{G}\{\pi_{jo}\} = 0 \\ &D[d_{hi}]\{U_{io}\} + D^2[r_{hk}]\{V_k\} - \gamma[s_{hk}]\{V_k\} + \frac{1}{G}\{\Lambda_h\} = 0 \end{aligned} \tag{3.3}$$

After substituting for U_{io} using Equation (3.1) and premultiplying the first equation by $[T]^T$, Equations (3.3) become:

$$\begin{aligned} &\gamma D^2[T]^T[a_{ji}][T]\{U_i\} - [T]^T[b_{ji}][T]\{U_i\} - D[T]^T[c_{jk}]\{V_k\} + \frac{1}{G}\{\pi_j\} = 0 \\ &D[d_{hi}][T]\{U_i\} + D^2[r_{hk}]\{V_k\} - \gamma[s_{hk}]\{V_k\} + \frac{1}{G}\{\Lambda_h\} = 0 \end{aligned} \tag{3.4}$$

The new coordinates corresponding to the new generalized displacements are orthogonal if the matrix product $[T]^T[a_{ji}][T]$ is a diagonal matrix. This follows if $[T]$ is the matrix of the eigen vectors of $[a_{ji}]$, Hildebrand(26).

3.1.3 Determination of the Orthogonal Coordinates

The longitudinal displacement of all the node points is given in terms of the initial set of generalized longitudinal coordinates Φ_{io} and displacements U_{io} as:

$$u(z,s_j) = \sum_{i=1}^{n} U_{io}(z)\, \Phi_{io}(s_j) \qquad j = 1, \ldots n \tag{3.5}$$

where s_j is the transverse coordinate of node j.

Equations (3.5) are written as a matrix equation:

$$\{u_{sj}\} = [\Phi_{jio}]\{U_{io}\} \tag{3.6}$$

The matrix Φ_{jio} is a unit matrix by the original choice of the coordinates. Substituting for U_{io} its value from Equation (3.1), Equation (3.6) becomes:

$$\{v_{sj}\} = [T_{ji}]\{U_i\} \tag{3.7}$$

The longitudinal node displacements are also given by an equation similar to Equation (3.7) in terms of the new set of generalized displacements U_i and orthogonal coordinates Φ_{ji}:

$$\{v_{sj}\} = [\Phi_{ji}]\{U_i\} \tag{3.8}$$

Equations (3.7) and (3.8) show that $\Phi_{ji} = T_{ji}$. This means that the magnitude of the $i^{\underline{th}}$ new orthogonal longitudinal coordinate at the $j^{\underline{th}}$ node, i.e., the displacement of the $j^{\underline{th}}$ node when $U_i = 1$ and $U_j = 0$ for $j \neq i$, is equal to the $j^{\underline{th}}$ component of the $i^{\underline{th}}$ eigenvector of matrix a_{ji}.

The problem of finding the new set of orthogonal coordinates is an eigenvalue problem. This investigation uses a standard computer subroutine to find the eigenvalues of a given matrix.

3.2 Evaluation of the Matrix s_{hk}

The general term of matrix s_{hk} is given by the equation:

$$s_{hk} = \frac{1}{E}\int_L \frac{\mu_h(s)\ \mu_k(s)}{E_p I_e}\, ds \tag{3.9}$$

where $\mu_h(s)$ and $\mu_k(s)$ are again the moments induced in the elementary frame for $V_h = 1$ and $V_k = 1$ respectively. It is possible to evaluate $\mu_h(s)$ and $\mu_k(s)$ using the theory of indeterminate frames, and to determine s_{hk} by integration as in Equation (3.9). An easier approach is used in this work. The expression under the integral sign is the internal work done through a displacement $V_h = 1$ by the bending moment $\mu_k(s)$ that is induced in the elementary frame by $V_k = 1$. This is the

total internal work; for the transverse axial distortions and shearing distortions are both zero in the elementary frame, and consequently the transverse axial forces and shearing forces do not perform any work.

The internal work equals the external work in absolute magnitude. The term s_{hk} is equal to the work of the reactions induced at the supports of the elementary frame by $V_k = 1$, when undergoing a displacement $V_h = 1$. The elementary frame is assumed to be supported by hinge supports at all nodes. The work of the reactions induced by different displacement patterns given by $\psi_h V_h$ with $V_h = 1$ will generate the matrix s_{hk}. In this investigation the "STRESS" program, Fenves et. al. (27), is used to determine both $\mu_{(h)}$ and s_{hk} with h, k = 1, ...m.

3.3 Solution of the Boundary-Value Problem as a Set of Initial-Value Problems.

The analysis of a box girder leads to a linear boundary-value problem, as shown in Section 2.7. This boundary-value problem is completely defined by 2(m + n) boundary conditions, (m + n) at each end. This boundary-value problem is solved as a set of (m + n + 1) initial-value problems. The first (m + n) problems consider the effect of the initial boundary and the last problem the effect of the loads.

For each of the (m + n + 1) problems, 2(m + n) boundary values are specified at the initial end, i.e., all the generalized displacements and their first derivatives. A total of (m + n) of these values are the actual initial boundary values, the remaining (m + n) boundary values are assumed. For the first (m + n) problems, the sets of assumed (m + n) boundary values are taken to be linearly independent. For the last problem, i.e. the load solution, the (m + n) assumed boundary values are set equal to zero for convenience.

Each of the (m + n + 1) problems is solved starting from the initial end. The first (m + n) problems are combined linearly and added to the load solution to satisfy the boundary conditions at the far end. This process can be expressed algebraically:

$$\sum_{i=1}^{m+n} D_{j,i} \lambda_i + D_{j,\, m+n+1} = B_j \qquad j = 1, \ldots m+n \qquad (3.10)$$

where B_j is the value of the $j^{\underline{th}}$ specified boundary function at the far end, $D_{j,i}$ is the value of the $j^{\underline{th}}$ specified boundary function at the far end that is obtained from the solution of the $i^{\underline{th}}$ initial-value problem and λ_i is a coefficient of proportionality.

The system of equations (3.10) is solved for λ_i (i=1, ...m+n). The final solution is given by:

$$\begin{aligned} U_j &= \sum_{i=1}^{m+n} U_{j,i} \lambda_i + U_{j,m+n+1} \qquad j = 1, \ldots m \\ V_h &= \sum_{i=1}^{m+n} V_{h,i} \lambda_i + V_{h,m+n+1} \qquad h = 1, \ldots n \end{aligned} \qquad (3.11)$$

where $U_{j,i}$, $V_{h,i}$ are the generalized displacements for the $i^{\underline{th}}$ initial-value problem, i running from 1 to m + n, and where $U_{j,m+n+1}$, $V_{h,m+n+1}$ are the generalized displacements for the load solution.

3.4 Numerical Integration

Each of the (m + n + 1) initial-value problems is integrated numerically using a step-by-step method of integration. The integration is discussed for one initial-value problem.

3.4.1 Initialization

All the (m + n) generalized displacements are specified at the initial end as well as their first derivatives, giving the 2(m + n) necessary initial conditions. The second derivatives of the generalized displacements can be found at the initial end by substituting for the generalized displacements and their first derivatives in Equations (2.10) or (2.16). Equations (2.10) are used when the coordinates are not orthogonal. Equations (2.16) are used when the coordinates are orthogonal. Because of the orthogonalization, the determination of the second derivatives is direct and does not involve the solution of simultaneous equations.

3.4.2 Numerical Integration in One Interval

The generalized displacements, their first and second derivatives are assumed to be known at station t along the span. The generalized displacements, their first and second derivatives are determined at the next station t + 1 by using the numerical integration described by Newmark (28) and the equilibrium equations as explained below.

The equations for the numerical integration scheme used here are written as:

$$U_{j,t+1} = U_{j,t} + U'_{j,t}\,h + (\tfrac{1}{2} - \beta)U''_{j,t}h^2 + \beta U''_{j,t+1}h^2$$

$$U'_{j,t+1} = U'_{j,t} + \frac{h}{2}\,(U''_{j,t} + U''_{j,t+1}) \qquad j = 1, \ldots n \qquad (3.12)$$

$$V_{h,t+1} = V_{h,t} + V'_{h,t}h + (\tfrac{1}{2} - \beta)V''_{h,t}h^2 + \beta V''_{h,t+1}h^2$$

$$V'_{h,t+1} = V'_{h,t} + \frac{h}{2}\,(V''_{h,t} + V''_{h,t+1}) \qquad h = 1, \ldots m \qquad (3.13)$$

where h is the step length between stations t and t + 1, $U_{j,t}$, $U'_{j,t}$, $U''_{j,t}$, $V_{h,t}$, $V'_{h,t}$, $V''_{h,t}$ are the generalized displacements and their

derivatives at t, and $U_{j,t+1}$, $U'_{j,t+1}$, $U''_{j,t+1}$, $V_{h,t+1}$, $V'_{h,t+1}$, $V''_{h,t+1}$ are the generalized displacements and their derivatives at t + 1. The coefficient β ranges normally from 0 to 0.50.

The equilibrium equations are written at t + 1 for the generalized orthogonal coordinates as:

$$\gamma a_{jj} U''_{j,t+1} - \sum_{i=1}^{n} b_{ji} U_{i,t+1} - \sum_{k=1}^{m} c_{jk} V'_{k,t+1} + \frac{1}{G} \pi_{j,t+1} = 0 \qquad j = 1, \ldots n$$

$$\sum_{i=1}^{n} d_{hi} U'_{i,t+1} + r_{hh} V''_{h,t+1} - \gamma \sum_{k=1}^{m} s_{hk} V_{k,t+1} + \frac{1}{G} \Lambda_{h,t+1} = 0 \qquad h = 1, \ldots m \qquad (3.14)$$

Equations (3.12), (3.13) and (3.14) are solved for the generalized displacements and their first and second derivatives at t + 1 using the following iteration procedure:

1. The second derivatives are assumed at t + 1, e.g., equal to the second derivatives at t.
2. The generalized displacements and their first derivatives are found at t + 1 by the numerical integration process of Equations (3.12) and (3.13).
3. The generalized displacements and their first derivatives obtained in step 2 are used in Equations (3.14) to yield a new set of second derivatives at t + 1.
4. The assumed and computed values of the second derivatives are compared. If they differ appreciably the process is repeated, beginning at step 2 but now using the latest set of computed values as the new set of assumed second derivatives.

This process continues until the assumed and computed values of the second derivatives agree within a satisfactory limit.

3.4.3 Integration From the Initial to the Far End of the Box Girder

The numerical integration starts at the initial end where all the generalized displacements and their first and second derivatives are obtained as described in Section 3.4.1. The integration proceeds to the far end of the girder, step-by-step, using the interation procedure described in Section 3.4.2. Thus the generalized displacements and their first and second derivatives are determined throughout the box girder.

3.4.4 Convergence and Stability

The numerical solution of the system of differential equations, Equations (2.16), can differ from the true solution in two ways. First, the numerical solution may not converge in a single step, that is the new values of second derivatives may not approach any definite values. Second, the numerical solution may converge to definite values in each interval, but the computed solution may have a totally different character from the true one. The first type of difficulty is a failure of convergence and the second type is termed an instability.

The convergence and stability of the numerical solution depends upon the value used for β. For a system with exponential type solutions, the criteria for stability and convergence coincide. This can be shown by considerations similar to those used in Reference (28).

The numerical solution converges for all the problems that are analyzed using a β of 1/6. Therefore, all the numerical results obtained correspond to stable solutions.

3.5 Effect of Node Loads

Only surface forces are considered in the derivation of the equations of equilibrium, Equations (2.16). This section introduces in the equations of equilibrium the effect of line loads and concentrated loads at the nodes. These loads are either applied externally or are exerted by the diaphragms. Transverse moments applied linearly along the nodes are not considered. These moments arise from loads applied between nodes. They can be easily accounted for by introducing their work into Equations (2.16). The work done by a transverse moment applied at node i, when the elementary frame undergoes a distortion pattern given by $\psi_h(s)$, is given by the value of the transverse moment times the rotation of node i. The rotation of node i can be determined from elementary frame analysis using the "STRESS" computer program.

A load applied at a node in any given direction can be decomposed into 3 components: one longitudinal component along the node line and two transverse components along two different directions given by the directions of the members meeting at this node. In what follows only one transverse or longitudinal load is considered at a time.

3.5.1 Distributed Node Loads

Only the generalized load terms are modified in Equations (2.16) for a distributed node load.

For a transverse line load of intensity $\theta_k(z)$ acting along member k, the $h^{\underline{th}}$ transverse generalized load is equal to the work done by the load when the elementary frame undergoes a displacement $V_h = 1$, that is:

$$\Lambda_h(z) = \theta_k(z) \cdot (\psi_h)_k \qquad h = 1, \ldots m \qquad (3.15)$$

where $(\psi_h)_k$ is the value of the $h^{\underline{th}}$ transverse generalized coordinate along member k.

Similarly, for a longitudinal line load of intensity $\lambda_i(z)$ acting along node i, the longitudinal generalized loads are given by:

$$\pi_j(z) = \lambda_i(z) \cdot (\phi_j)_i \qquad j = 1, \ldots n \qquad (3.16)$$

where $(\phi_j)_i$ is the value of the $j^{\underline{th}}$ longitudinal generalized coordinate at node i.

3.5.2 Concentrated Node Loads

A concentrated transverse load T_k applied along member k at $z = z_d$ can be thought of as the limit of a line load of intensity $\theta_k(z)$ extending between $z_d - \epsilon$ and $z_d + \epsilon$, ϵ being arbitrarily small:

$$T_k = \int_{z_d-\epsilon}^{z_d+\epsilon} \theta_k(z)\, dz \qquad \text{for all } \epsilon > 0 \qquad (3.17)$$

The transverse generalized loads $\Lambda_h(z)$ h = 1, ...m corresponding to the line load θ_k are given by Equations (3.15)

Substitution of the generalized loads from Equations (3.15) into the second set of Equations (2.16) gives:

$$\sum_{i=1}^{n} d_{hi}U_i' + r_{hh}V_h'' - \gamma \sum_{k=1}^{m} s_{hk}V_k + \frac{1}{G}\,\theta_k(z)\,(\psi_h)_k = 0 \qquad (3.18)$$

$$h = 1, \ldots m$$

Integrating Equations (3.18) from $z_d - \epsilon$ and $z_d + \epsilon$, taking the limits as ϵ goes to zero, using the fact that the generalized displacements are continuous and using Equation (3.17) give:

$$\Delta V_h' \ @ \ z_d = - T_k (\psi_h)_k \ / \ G \ r_{hh} \qquad h = 1, \ldots m \qquad (3.19)$$

Similarly for a longitudinal concentrated load L_i applied along node i, the following expression holds:

$$\Delta U_j' = - L_i (\psi_j)_i \ / \ E \ a_{jj} \qquad j = 1, \ldots n \qquad (3.20)$$

where $\Delta V_h'$ and $\Delta U_j'$ are sudden changes in V_h' and U_j' at z_d. Therefore, concentrated loads cause at their point of application a sudden change of the first derivatives of the appropriate generalized displacements.

Equations (3.19) and (3.20) are valid for orthogonal coordinates. For non-orthogonal coordinates the expressions will be more complicated and the solution of simultaneous equations will be needed to determine the discontinuities.

The derivatives of the generalized displacements are discontinuous under the concentrated loads. Similar discontinuities occur in the slope of a solid beam under a point load when shear deformations are considered, and in the axial strain of a column loaded by an intermediate axial load.

In the numerical integration the effect of a concentrated load is to change the corresponding first derivatives abruptly. The numerical integration is performed up to the location of the load. After convergence, the increment in the first derivative is introduced. From the known values of the generalized displacements and the first derivatives a new set of second derivatives is determined and the numerical integration is continued.

3.5.3 Concentrated Loads Exerted by Intermediate Diaphragms

A diaphragm induces longitudinal and transverse generalized forces that are proportional to the generalized displacements as shown in Section 2.8. These forces are concentrated and given by Equations (2.30), (2.35) and (2.38) for unit generalized displacements.

In the numerical integration, the iteration of the last step is performed until convergence. The concentrated forces of the diaphragms are computed from the values of the generalized displacements obtained from the last iteration. The increment of the appropriate first derivative is applied, a new set of second derivatives is computed and the integration continues.

3.6 Suppression of the Exponentially Growing Solutions

The closed form solution of the system of differential equations (2.10) or (2.16) yields generalized displacement functions of the exponential type. For every initial-value problem, some of the boundary conditions at the initial end are arbitrarily chosen to be linearly independent. Therefore the propagated solution possesses the two types of exponential functions, the exponentially growing as well as the exponentially decaying ones. The former lead to larger and larger values for the displacements and their derivatives as the numerical integration proceeds from the initial to the far end. Consequently, Equations (3.10) become a set of ill-conditioned simultaneous equations that yield absurd results because of inherent round-off problems.

A method described in Reference (29) is used to eliminate the exponentially growing solutions. It involves the following steps:

1. The numerical integration is carried out for the $(m + n + 1)$ initial-value problems as explained previously. Integration is stopped at a point where any generalized displacement or its first derivative is deemed too large compared to the maximum boundary value at the initial end.

2. At this point, called a point of suppression, the $(m + n + 1)$ partial solutions are combined to satisfy $(m + n + 1)$ sets of arbitrary conditions, one set at a time.

The arbitrary conditions are imposed on a set of chosen $(m + n)$ displacement functions which may be displacements or their first derivatives. These functions are called suppressed functions. These sets of arbitrary conditions are chosen to be linearly independent. Each set assigns values to the suppressed functions at the point of suppression of the same order of magnitude as the initial boundary conditions.

The combination of the partial solutions is linear for each set of imposed conditions at the point of suppression. The suppression can be represented algebraically by:

$$\sum_{i=1}^{m+n} D_{j,i}\, \rho_{i,k} = C_{j,k} \qquad j,k = 1, \ldots m + n$$

$$\sum_{i=1}^{m+n} D_{j,i}\, \rho_{i,m+n+1} + D_{j,m+n+1} = C_{j,m+n+1} \qquad j = 1, \ldots m + n \tag{3.21}$$

where $D_{j,i}$ is the value of the $j^{\underline{th}}$ suppressed function at the point of suppression obtained from the $i^{\underline{th}}$ initial-value problem, $C_{j,k}$ is the value assigned to the $j^{\underline{th}}$ suppressed function in the $k^{\underline{th}}$ set and $\rho_{i,k}$ is a

proportionality factor. The $(m + n + 1)^{\underline{th}}$ solution is the load solution for which $C_{j,m+n+1}$ may be taken as a zero vector.

Equations (3.21) are solved for the factors $\rho_{i,k}$ and a new set of $(m + n + 1)$ initial-value problems are obtained that contain much less of the growing part of the solution; they are given by:

$$(U_{j,k})_{new} = \sum_{i=1}^{m+n} (U_{j,i})_{old}\, \rho_{i,k}$$

$$(U_{j,m+n+1})_{new} = \sum_{i=1}^{m+n} (U_{j,i})_{old}\, \rho_{i,m+n+1} + (U_{j,m+n+1})_{old} \qquad (3.22)$$

$$j = 1, \ldots m$$

$$k = 1, \ldots m+n$$

Here, $U_{j,k}$ is the $j^{\underline{th}}$ longitudinal generalized displacement of the $k^{\underline{th}}$ initial-value problem and the $(m + n + 1)^{\underline{th}}$ solution is the load solution. Similar expressions hold for U', V and V'.

3. The new $(m + n + 1)$ solutions are carried through another suppression interval, usually a large number of steps of integration, and step 2 is applied wherever suppression is necessary.

4. The final solution is obtained by combining the $(m + n + 1)$ solutions of the last suppression to satisfy the boundary conditions at the far end as explained in Section 3.3.

4. BEHAVIOR OF SINGLE CELL BOX GIRDERS

4.1 General

The study of single cell box girders can be helpful in understanding the behavior of multicell box girders. This chapter presents analytical results for different types of single cell girders for different end conditions and loadings.

The girders studied are either simply supported at both ends or fixed at both ends. The loads considered are applied vertically at one node as shown in Figure 15. They are either concentrated or distributed loads. The effect of varying the location of a concentrated load is investigated. The distributed loads studied are either uniform extending over the whole span, or vary as a half sine wave.

A load of total magnitude P applied at one node, whether concentrated or distributed, may be resolved into a bending load and a torsional load as shown in Figure 16. The solution for the bending load is given by ordinary beam theory, neglecting shear lag effects. The solution for the torsional load involves the deformation of the cross-section in its own plane according to the model of Chapters 2 and 3. To obtain the total effect of a single node load P, the bending solution is added to the torsional solution that is presented in this chapter.

Diaphragms may be introduced at both ends and at intermediate points along the span of the girder. The number and location of the diaphragms is varied to assess the influence of diaphragms on the behavior of the girder. A compartment is defined as the segment of a girder enclosed between two consecutive diaphragms. The number of

compartments N_c is zero when there are no diaphragms, one when only end diaphragms are present, two when end and one midspan diaphragms are present, and so on.

The quantities studied are longitudinal axial stress, transverse bending stress, shear stress and deflection. These quantities are presented for the torsional load of Fibure 16b in a normalized fashion. The normalizing quantities are obtained from one of two reference bending loads, Figure 16a.

The first bending load is a uniformly distributed loading of magnitude P/2L applied vertically at each top node and extending over the whole simply supported span. The terms σ_{BU}, τ_{BU}, and δ_{BU} are the maximum bending stress, the maximum shear stress, and the maximum vertical deflection produced by the uniform reference bending loading.

The second bending load consists of two midspan concentrated loads of magnitude P/2 acting on the two top nodes of the simply supported girder. The terms σ_{BC}, τ_{BC}, and δ_{BC} are the maximum axial stress, the maximum shear stress and the maximum vertical deflection produced by this loading.

The longitudinal axial stresses and the transverse bending stresses induced by the torsional load of Figure 16b are normalized with respect to σ_{BU} if the load is uniform, and with respect to σ_{BC} if the load is concentrated. The shear stresses induced by the torsional load of Figure 16b are normalized with respect to τ_{BU} if the load is uniform, and with respect to τ_{BC} if the load is concentrated. The deflections induced by the torsional load of Figure 16b are normalized with respect to δ_{BU} if the load is uniform and with respect to δ_{BC} if the load is concentrated.

Several cross-section shapes are studied. A rectangular reinforced concrete box girder is analyzed in Section 4.2, a trapezoidal reinforced concrete box in Section 4.3, a rectangular steel box with stiffeners in Section 4.4. A parameter study of a square box is presented in Section 4.5.

The sign convention used in this investigation for the reported quantities follows.

Vertical deflection is positive downward.

Longitudinal axial stress and transverse bending stress are positive when they are tensile stresses.

Shear stress is positive in a plate element when it acts in the positive direction in the plate element on a front face. The positive direction in a plate element is to the right for horizontal plate elements and downward for vertical or inclined plate elements.

4.2 Behavior of a Rectangular Reinforced Concrete Box Girder

This section presents the variation along the span of stresses and deflections induced in the single cell box girder shown in Figure 17a. The girder, denoted by IRC, has a rectangular cross-section, a depth of 8 ft., and a width of 10 ft. The thickness is 6 in. for all plate elements. The girder is 100 ft. long. This single cell box girder is representative of a typical cell of a reinforced concrete multicell box girder bridge. The modulus of elasticity is taken as 3,000,000 psi and Poisson's ratio as 0.10.

Stresses and deflections are studied for different torsional loads, end conditions, and diaphragm configurations. They are normalized as described in Section 4.1.

Rigid end diaphragms are always present. The thickness of the flexible intermediate diaphragms is 6 in. if not specified otherwise.

Effects of the diaphragm stiffness on girder behavior and the forces in the diaphragms are considered.

4.2.1 Longitudinal Axial Stress σ_L

The variation of this stress is linear across any wall of the cross-section, and for a torsional load has the same maximum at all four corners, with opposite signs at adjacent corners. No net horizontal thrust or bending moment is produced by this stress, i.e., it is self-equilibrating, Figure 18a. In what follows σ_L denotes the maximum stress at the corner. The variation of σ_L at node 1 or 4 along the span is shown in Figures 19 to 26 for torsional loads. The stress σ_L is normalized with respect to σ_{BU} for uniform torsional loads and with respect to σ_{BC} for concentrated torsional loads (Section 4.1).

For simply supported girder under uniform torsional load, Figure 19, σ_L is negative, builds up from zero at one end to a maximum of $0.109\,\sigma_{BU}$ then drops to a relative minimum at midspan when there are only end diaphragms. When an intermediate diaphragm is introduced a positive peak stress always occurs at the location of the diaphragm. For a midspan diaphragm the positive peak stress at the location of the diaphragm is the maximum stress along the span and is larger than the maximum σ_L for no intermediate diaphragms. Several intermediate diaphragms must be used to reduce the maximum σ_L to the no intermediate diaphragm stress level.

For a girder loaded by a uniform load at one node, a midspan diaphragm reduces the stress at the loaded node but increases the stress at the unloaded node. For the girder considered here with a midspan diaphragm, the stress at the unloaded node is larger than the stress at the loaded node when no intermediate diaphragms are present. This is important in design because midspan stress controls design for a simply supported girder.

For fixed end girder under uniform torsional load, Figure 20, longitudinal axial stresses are induced at both ends because of the constraints on the longitudinal displacements. If there are no intermediate diaphragms the stress σ_L is maximum at the ends, equal to 0.347 σ_{BU} with a positive sign, becomes negative at L/6 and reaches a relative negative maximum at midspan. The introduction of a midspan diaphragm reduces the positive stress at the ends. But, as in the simply supported case, it induces a high positive stress at midspan. However, the midspan stress is not so critical because it is less than the end stress and does not occur at the critical end section. If more intermediate diaphragms are present, the maximum value of σ_L is reduced.

The variation of σ_L along the span is shown for a simply supported girder with concentrated loads at L/2, L/3 and L/6 in Figures 21 to 23. For no intermediate diaphragms σ_L is maximum directly below the load and drops sharply on both sides of the loads to zero at both ends. This maximum increases slightly as the load approaches one end, but drops to zero for the load directly at one end. The introduction of intermediate diaphragms decreases the maximum stress under the load only when the nearest diaphragm is within a distance of about L/6 from the load; the closer this diaphragm the more the peak σ_L is decreased. If the diaphragm is directly below the load, the longitudinal axial stress becomes negligible. Table I shows the variation of the peak σ_L under a midspan concentrated load as two symmetrically placed diaphragms come closer to the load, it also shows the peak σ_L for a midspan diaphragm and the peak σ_L for a rigid cross-section.

For a girder with fixed ends and no intermediate diaphragms which is subjected to torsional loads applied at L/2, L/3 or L/6, Figure

24, σ_L again peaks directly below the load. This stress is the maximum σ_L for the loads applied at L/2 or L/3 and is almost equal to the maximum stress if the ends were simply supported. End fixity, as for uniform loads, induces longitudinal axial stresses at the ends. The peak stress at the end becomes larger than the peak stress under the load for a concentrated load applied near the support, e.g., at L/6. For such a load, the peak stress under the load is significantly smaller than the stress that would have existed if the ends were simply supported. The introduction of diaphragms, Figures 25 and 26, starts to reduce peak stresses under the loads when the nearest diaphragm is within a distance of L/6 from the load. The effect on the end axial stresses is important when the diaphragm is near the end or is close to the loads. For the concentrated load applied at L/6 with a diaphragm located at 2L/9 the end stress becomes less than the peak stress under the load, Figure 26..

Table 2 shows the maximum longitudinal axial stress in the girder with only end diaphragms for different loading and end conditions. The important results concerning the longitudinal axial stresses induced by torsional loadings are summarized below.

4.2.1.1 End Diaphragms Only

(a) For a uniform torsional load the maximum σ_L occurs near the quarter point of the span for simply supported end conditions, Figure 19, and at the ends for fixed end conditions, Figure 20. The fixed end girder has a much larger maximum σ_L as shown in Table 2.

(b) For concentrated torsional loads maximum σ_L occurs directly below the load as shown in Figures 21 to 25, except for a load close to a fixed end which produce a maximum σ_L at the fixed end as

shown in Figure 26. However, end fixity does not seem to affect the maximum σ_L much as shown in Figure 24 and Table 2.

(c) The peak stress under concentrated torsional loads, as the load moves towards the end, increases for simply supported ends and decreases for fixed ends as shown in Figure 24 and Table 2. However, the peak stress is nearly constant when the load is in the middle half of the girder for both simply supported girder and fixed girder. The peak stress is zero for load at the end.

4.2.1.2 End and Intermediate Diaphragms

(a) For a simply supported girder with uniform torsional load, a single midspan diaphragm increases the maximum σ_L; several intermediate diaphragms are required to reduce σ_L below the stress level obtained for no intermediate diaphragms as shown in Figure 19.

(b) For a fixed girder with uniform torsional load, the introduction of intermediate diaphragms consistently decreases the peak stress at the end as shown in Figure 20.

(c) For torsional concentrated loads, intermediate diaphragms are effective in reducing σ_L when the nearest diaphragm is within a distance of L/6 from the load. This is valid for both simply supported and fixed girders as shown in Table 1 and Figures 21 to 23 and Figures 25 to 26.

4.2.2 Transverse Bending Stress σ_T

The torsional load of Figure 16b induces transverse moments which vary linearly between nodes as shown in Figure 18b. The stresses induced by the moments vary linearly through the thickness of the wall. In the following discussion the transverse bending stress σ_T denotes the

maximum stress that occurs in the extreme fiber at a corner point. The stress σ_T is normalized with respect to σ_{BU} for uniform torsional loads and with respect to σ_{BC} for concentrated torsional loads (Section 4.1). The variation of σ_T along the span is studied for different loading and end conditions as well as diaphragm spacings.

For a simply supported or fixed girder under uniform torsional loads (see Figures 27 and 28), with end diaphragms only, σ_T builds up from zero at both ends to a maximum at midspan. The introduction of diaphragms reduces σ_T to negligible amounts at the location of the diaphragms and decreases the maximum value of σ_T along the span. The reduction of the maximum σ_T is progressive as more intermediate diaphragms are introduced. End fixity decreases σ_T appreciably near the support, but causes little change at midspan.

For a simply supported or fixed girder under concentrated torsional load (see Figures 29 to 34), with end diaphragms only, σ_T builds up from zero at both ends to a maximum at or very near to the load location. The maximum σ_T seems nearly independent of the location of the load and of the end conditions for loads applied at a distance greater than L/4 from the ends as shown in Figure 32. For a load applied close to the end, i.e., L/6 away from the end, the maximum σ_T is slightly reduced for a simply supported girder and markedly reduced for a fixed end girder as shown in Figure 32 and Table 4. Figures 29 to 31 and Figures 33 and 34 show that intermediate diaphragms always reduce σ_T; the reduction becomes greater as a load approaches a diaphragm. Diaphragms are more effective in reducing the transverse bending stresses than the longitudinal axial stresses. Reference to Tables 1 and 3 shows that σ_T is appreciably reduced when two diaphragms, symmetrically placed

with respect to a midspan concentrated load, are L/6 away from the load; in this case σ_L is essentially unchanged.

Table 4 presents a summary of the results obtained for σ_T, for no intermediate diaphragms, and for different loading and end conditions. The important results concerning the transverse bending stress induced by torsional loadings are summarized below.

4.2.2.1 End Diaphragms Only

(a) For a uniform load, σ_T is zero at both ends and is maximum at midspan. End fixity decreases slightly the maximum σ_T as shown in Figures 27 and 28.

(b) For concentrated loads σ_T is zero at both ends and is maximum at or near the load as shown in Figures 29 to 34. This maximum stress, for the simply supported girder, first increases slightly then decreases as the load approaches the end. For a fixed girder the stress always decreases as shown in Table 4.

4.2.2.2 Effect of Intermediate Diaphragms

(a) Diaphragms are effective in reducing σ_T, the more intermediate diaphragms the more the reduction, as shown in Figures 27 to 31 and Figures 33 and 34.

(b) Diaphragms are more effective in reducing transverse bending stress than in reducing longitudinal axial stress as shown in Tables 1 and 3.

4.2.3 Shear Stresses τ_h and τ_v

The shear stresses discussed here are caused by the torsional load. Shear stresses are constant through the width of each plate element. Parallel plates have the same shear stress with opposite signs.

Therefore, two shear stresses shown in Figure 18c are studied: τ_h the shear stress in horizontal plates and τ_v the shear stress in vertical plates. Both of these stresses are normalized with respect to τ_{BU} for uniform torsional loads and with respect to τ_{BC} for concentrated torsional loads (Section 4.1). The shear stress caused by the bending load of Figure 16a is shared equally by the vertical plate elements and is assumed constant through their depth. The variation of τ_{BU}, τ_{BC} along the length of the girder is given by elementary beam theory.

The stresses τ_h and τ_v are plotted with length in Figures 35 to 39 for different loading and end conditions with and without intermediate diaphragms. Comparison is made with shear stresses of the rigid section determined from the Saint-Venant theory of torsion.

For a uniform torsional load, Figure 35, the Saint-Venant shear stresses τ_h and τ_v are equal and they vary linearly from 0 at midspan to a value of $0.5\ \tau_{BU}$ at the ends. The end conditions have no effect. For the same load on a deformable cross-section the shear stresses are affected near the ends: τ_v increases while τ_h decreases. The increase in τ_v is equal to the decrease in τ_h as required for external equilibrium. The introduction of an intermediate diaphragm affects the shear stress distribution at the location of the diaphragm and this effect dies out away from the diaphragm. The maximum shear stress τ_v still occurs at the end. The maximum shear stress τ_v that occurs at the end increases with a midspan diaphragm, then slowly approaches the Saint-Venant shear stress as more intermediate diaphragms are added. End conditions have little effect; a fixed end girder has slightly larger shear stress τ_v at the end.

The discontinuities in the shear stress at the location of a diaphragm define the diaphragm stresses (Section 4.2.5)

For concentrated torsional loads, an abrupt change in shear occurs at the load location in the loaded vertical plate element. This change is equal to the load applied (Section 3.5). For a torsional load applied at midspan, Figure 36, τ_v drops from 1.0 τ_{BC} at midspan to 0.45 τ_{BC} at the ends and τ_h builds up from 0 to 0.55 τ_{BC}. The sum $(\tau_v + \tau_h)$ is equal to τ_{BC} at any point along the span as required for equilibrium. Thus, the torsional shear distribution approaches the Saint-Venant shear stress of 0.5 τ_{BC} near the ends. The end conditions have very little effect. As shown in Figure 38a for a torsional load applied at L/6, τ_v and τ_h become practically equal to the Saint-Venant shear stress at the far end. The stresses τ_v and τ_h remain quite different from each other and from Saint-Venant torsional shear stress at the near end. End fixity, as shown in Figure 39 for a load applied at L/6, increases τ_v and decreases τ_h. The maximum shear stress still occurs directly below the load in the vertical plates.

From Figure 36 and 38b it is seen that intermediate diaphragms are very effective in distributing the shear stresses equally between vertical and horizontal plate elements in the unloaded compartments. In the compartment loaded with a midspan load no shear transfer seems to occur from the vertical plates to the horizontal plates as shown in Figure 36. However, a certain amount of shear transfer takes place in the loaded compartment for a load at L/6 and thus the maximum shear stress is reduced, Figure 38b. A diaphragm located under the load gives good distribution of shear stresses -- everywhere nearly equal to Saint-Venant shear stresses as shown in Figures 36, 37, 38a, and 38b. A diaphragm always has a beneficial effect in reducing shear stresses induced by concentrated loads.

Table 5 summarizes the results obtained for the maximum shear stresses in a girder with only end diaphragms. The important results concerning the maximum shear stresses induced by torsional loads are summarized below:

4.2.3.1 End Diaphragms Only

(a) The maximum shear stress always occurs in the vertical plates. It occurs at the ends for uniform load and directly under the load for concentrated loads as shown in Figures 34 to 39.

(b) End fixity slightly increases the maximum shear stress as shown in Table 5.

(c) For a concentrated load anywhere along the span, the maximum shear stress always occurs below the load. This maximum stress is equal to τ_{BC} when the load is at midspan, increases to a maximum as the load is nearer to the end, then drops to τ_{BC} again for the load directly over the end support. This is shown in Table 5 and is a major design point for girders subjected to high concentrated loads. The shear stress can be 50% higher than that determined from elementary theory.

4.2.3.2 Effect of Intermediate Diaphragms

(a) For a uniform load, a midspan diaphragm increases the shear stress at the support. Several equally spaced diaphragms are necessary to decrease the maximum τ_v below the maximum τ_v for only end diaphragms, Figure 35.

(b) For a concentrated load diaphragms are always effective in reducing the shear stresses especially in the unloaded compartments, Figures 36 and 38b.

(c) For effective shear control, diaphragms should be spaced more closely in the vicinity of the supports to avoid the high shear stresses induced by concentrated loads applied near the ends.

4.2.4 Deflection δ_T

The vertical deflection of the vertical plate elements is considered here. The box girder is loaded with a torsional load and the two vertical plates have the same deflection with opposite signs. The deflection as shown in Figure 18d is denoted by δ_T. The deflection is normalized with respect to δ_{BU} for uniform torsional loading and with respect to δ_{BC} for concentrated torsional loading (Section 4.1).

In Figures 40 and 41 the variation of the deflection along the span is shown for a simply supported girder under uniform and midspan concentrated torsional loads. Table 6 presents the maximum deflections for different end conditions and for uniform and concentrated torsional loads. It also has entries for the bending deflection for the load of Figure 16a with and without consideration of the effect of shear deformation, and for the torsional deflection when the section is rigid.

For a girder under torsional loading and for only end diaphragms, the deflections in a fixed ended girder is slightly smaller than the deflection in a simply supported girder.

As shown in Figures 40 and 41, intermediate diaphragms are effective in reducing the deflections. For a simply supported girder under uniform torsional load, two diaphragms at the third points reduce the deflection almost to the rigid Saint-Venant torsional deflection and are more effective than a single midspan diaphragm. However, for a midspan concentrated torsional load, the maximum deflection is much smaller

for a single midspan diaphragm than for two diaphragms at the third points. For a midspan diaphragm under a concentrated midspan torsional load, the torsional deflection equals the rigid Saint-Venant deflection, Table 6. End fixity does not reduce the torsional deflection appreciably; it does however decrease the bending deflection, Table 6.

4.2.5 Stresses in Intermediate Diaphragms

It is shown above that intermediate diaphragms significantly affect the behavior of box girders. The diaphragms act mainly in pure shear as explained in Section 2.8. The warping stiffness of the diaphragm has been neglected throughout this study after it was found to affect only the third significant figure of the results.

The shear stress in the diaphragm is determined below. It is normalized with respect to τ_{BU} for a uniform torsional load on the girder and with respect to τ_{BC} for concentrated torsional load (Section 4.1).

For a uniform torsional load, the abrupt change in τ_v at the location of a diaphragm defines the shear in the diaphragm. For a plate diaphragm having the same thickness as the plate elements, the change in τ_v is equal to the shear stress in the diaphragm. This stress is about $0.5\ \tau_{BU}$ for the simply supported girder as shown in Figure 35. End fixity does not alter this value much.

For a concentrated torsional load, the shear stress in the diaphragm is also equal to the change in τ_v at the location of the diaphragm when the load is not over the diaphragm. The shear stress in a diaphragm is maximum when the load is applied at the diaphragm and is essentially equal to τ_{BC} as is apparent from Figures 36 to 39.

4.2.6 Effect of Intermediate Diaphragm Stiffness

The box IRC is studied with a midspan diaphragm 1 in. thick. The purpose is to show the effect of the diaphragm stiffness on the stresses. The box is simply supported and loaded by concentrated loads.

Figures 42 and 43 show that for a torsional load at L/6, σ_L and σ_T are almost unchanged. This is because the diaphragm is far from the load. For a load directly over the 1 inch thick diaphragm at midspan, the stresses σ_L and σ_T are larger than for a 6 in. thick diaphragm, but still insignificant compared to the stresses in the absence of an intermediate diaphragm. For a load at L/2, the shear stress is affected slightly as shown in Figure 44. However the flexible diaphragm is still quite effective in distributing the shear to the girder plate elements.

Table 7 summarizes the results for σ_L, σ_T, τ_h and τ_v. It can be concluded that the diaphragms stiffening action is insensitive to variations in the stiffness of the diaphragms for the range of stiffness values considered here. In practice, concrete diaphragms cannot be made less than 3 inches thick and consequently these diaphragms can be considered as rigid for all practical purposes.

4.3 Behavior of a Trapezoidal Reinforced Concrete Box Girder

In this section, the effect of the shape of the cross-section is studied. For this purpose a trapezoidal box girder denoted by ITC is studied and compared to the rectangular box of Section 4.2. The box girder is 100 ft. long, with a depth of 8 ft., a top flange of 10 ft. and a bottom flange of 6 ft. The plate elements are 6 in. thick, Figure 17b. It is made out of reinforced concrete with E = 3,000,000 and ν = 0.1.

The variation of stresses and deflections along the span is similar to IRC; only the relative magnitudes vary. A comparison between the two boxes is made in Table 8 for the longitudinal axial stresses and transverse bending stresses for simply supported end conditions. Only torsional loads are considered. The thickness of the diaphragms is 6 inches.

It is clear from Table 8 that the trapezoidal box girder behaves more rigidly than the rectangular girder, i.e., the transverse bending stresses are smaller as well as the longitudinal axial stresses. The normalizing stresses are obtained for the trapezoidal girder using the bending response of the trapezoidal girder as in Section 4.1; and they are obtained for the rectangular girder using the bending response of the rectangular girder as in Section 4.1.

4.4 Behavior of a Rectangular Steel Box Girder

A steel box girder denoted by IRS, of proportions reasonable for bridges is analyzed in this section. The steel has a Young modulus of 30,000,000 psi and a Poisson's ratio of 0.30. The girder, shown in Figure 17c, is rectangular in shape, 8 ft. deep and 10 ft. wide, has a length of 140 ft. The plate elements are 3/8 in. thick. Stiffeners are provided to prevent buckling of the plate elements and to increase the overall stiffness of the box. The vertical plate elements are stiffened transversely every 6 ft. The top flange is stiffened transversely by a floor beam every 15 ft., and has longitudinal stiffeners at 2 ft. spacing. The bottom flange is unstiffened. Detailed description of the stiffeners is presented in Figure 17d. Rigid plate diaphragms are provided at both ends and the ends are simply supported. The effect of intermediate plate diaphragms and cross-bracing is studied.

The method of Chapter 2 is compared to the alternative method used by Wright (17) for the girder without intermediate diaphragms. The behavior of the box is also investigated for intermediate plate diaphragms and bracing. The stresses in the braces are discussed.

4.4.1 Comparison to Alternative Solution

Comparison is made for a concentrated load of 10 kips applied at midspan at node 1. In the alternative solution the load is spread over a length of 10 inches. The girder has only end diaphragms which are assumed to be rigid.

For purpose of comparison, the first Fourier term of the 10 K. concentrated load is used. Table 9 shows the results. The solution according to Chapter 2 agrees well with the alternative solution for the midspan longitudinal axial stresses, the transverse bending stresses and the deflections. The transverse bending stresses are slightly different because of the transverse shortening of the plate elements considered in the alternative solution. The alternative solution considers a parabolic distribution of shear stress across the width of a plate element. The average shear stress obtained from the parabolic distribution is very close to the author's constant shear value.

This agreement between the two solutions shows that the torsional moment and the axial elongation of the plate elements can be neglected and that the shear stress can be taken as constant in a plate element. The simplified model proposed by the author is as adequate as the model of Reference (17) for closed section girders.

The alternative solution uses much less computer time than the author's for the first Fourier term. However, the author's solution requires no more time for concentrated loads and may be more efficient

when a large number of Fourier terms would be required to describe the response.

4.4.2 Approximation of a Concentrated Load by its First Fourier Term

The example of Section 4.4.1 is used to study the effect of approximating a concentrated load by its first Fourier term.

Table 9 shows the stresses and deflections for the total load and for its first Fourier term, both obtained using the author's method. Comparing the two sets of response quantities shows that:

1. Deflections and transverse bending stresses are slightly underestimated by using only the first Fourier term.

2. Longitudinal axial stresses are greatly underestimated by using only the first Fourier term.

3. Shear stresses are not well predicted by using only one term in the Fourier analysis.

4.4.3 Effect of Intermediate Diaphragms

This section considers the effect of intermediate diaphragms on the behavior of the steel girder under a concentrated load applied at midspan at node 1. The load is broken into bending and torsional components as shown in Figure 16. Only the torsional component is considered here; the bending component is not affected by the diaphragms. The stresses and deflections caused by the torsional load are normalized with respect to the corresponding stresses and deflections induced by the bending load as for the rectangular reinforced concrete box IRC(Section 4.2).

Several configurations of intermediate diaphragms are considered. Two systems of 3/8 in. steel plate diaphragms are studied. The first

has 2 diaphragms at the third points and the second has 2 diaphragms at 7L/18 and 11L/18. Three systems of steel X-braces are studied. Each bracing system consists of pairs of braces, each brace being a 4" x 3" x 5/16" angle with an area of 2.09 inches^2. The X-brace is equivalent to a .0347 in. thick plate diaphragm, Equation (2.39). Therefore an X-brace is 10.8 times more flexible than the plate diaphragm. Bracing system A consists of pairs of braces located at the third points, bracing system B consists of pairs of braces located at the sixth points and bracing system C consists of pairs of braces located at the ninth points of the span.

The variation along the span of the result quantities is similar to IRC and is not presented. Only the maximum values of these quantities are shown in Table 10. These all occur at midspan.

1. The longitudinal axial stress is maximum in the bottom flange. Intermediate diaphragms affect the longitudinal axial stress when the nearest diaphragm is within a distance of L/6 from the load, and then the closer the nearest diaphragm the more the reduction. The reduction is slightly affected by the stiffness or number of intermediate diaphragms.

2. The transverse bending stresses for only end diaphragms are large. The maximum σ_T occurs in the top node of the webs, occurs in the stiffeners, and is equal to 4.27 σ_{BC}. The same transverse bending moment occurs in both top flange and webs but the webs have a smaller section modulus. These stresses are computed for "smeared" stiffeners. It is expected that with close stiffener spacing, the resultant curvatures are approximately correct. Actual stresses would be computed taking account of the actual form of the structure.

Intermediate diaphragms greatly reduce the transverse bending stresses. Even the very flexible bracing at the third points reduces σ_T from $4.27\ \sigma_{BC}$ to $1.272\ \sigma_{BC}$. The closer the diaphragms to the load the more the reduction. Both bracing systems B and C reduce maximum σ_T to almost the same value although C has more X-braces. This is because system B has an X-brace directly below the load at midspan.

3. The shear stress τ_v has a maximum of τ_{BC} directly below the load at midspan. Intermediate diaphragms do not decrease the maximum shear stress τ_v unless the diaphragm is under the load. The stiffness of the diaphragm does affect the shear stress. For bracing B the maximum τ_v is $0.63\ \tau_{BC}$ while for a plate diaphragm it would have been much closer to $0.50\ \tau_{BC}$.

4. The deflection δ_T is reduced by intermediate diaphragms. The stiffness of the diaphragms slightly affects the deflection. The closer the nearest diaphragm is to the load, the smaller is the deflection.

4.4.4 Stresses in Braces

Table II shows the stresses in the braces for the cross-bracing systems A, B and C. The stress in a brace can be high compared to the buckling stress and this stress increases the closer the load is to the brace. The X-brace closest to a load takes the largest proportion of the stresses while the other X-braces are slightly stressed.

4.5 Parameter Study for a Square Box

A parameter study is presented for square box girders with uniform plate thickness and ends simply supported. The structure has a length L, a depth d, and a uniform plate thickness t. The girder is loaded by a uniform torsional load of Figure 16b. The box girder is studied with and without end and equally spaced intermediate diaphragms.

Young's modulus is 30,000,000 psi and shear modulus is 11,000,000 psi, i.e., $\nu = 0.36$.

The study uses the closed form solution mentioned in Section 2.8.1 because of its simplicity for a square single cell box girder. A detailed development is not presented herein as it follows directly from Reference (1) pp. 231-244. The initial unknown parameters are determined from the far end boundary conditions, and the generalized displacements are determined throughout the girder. All diaphragms are assumed completely rigid and the transverse bimoments exerted by the diaphragms are found by assuming the transverse distortion of the cross-section equal to zero at the location of the diaphragms. This assumption is in agreement with the fact that the transverse bending stresses are negligible at the location of a diaphragm as shown in Figure 27.

The solution of the initial unknown parameters is determined from a system of simultaneous equations that express the boundary conditions at the far end. This system becomes very ill-conditioned for $\frac{d^3}{L^2 t} \leq .0125$, which means physically that there is little interaction between the two ends as in a "long" beam on an elastic foundation. The solution is modified by neglecting the far end boundary conditions as done in a long beam on elastic foundations and in the bending solution of cylinders. This corresponds to the use of the suppression technique in the numerical solution.

The result quantities presented include the longitudinal axial stress, the transverse bending stress, the shear stress and the deflection. The longitudinal axial stress and the transverse bending stress are normalized with respect to σ_{BU}, the shear stress with respect to τ_{BU}

and the deflection with respect to δ_{BU} (Section 4.1). The variation of these quantities along the span is similar to the variation presented for the rectangular concrete box (Section 4.2) and is not presented here. However, summary plots are given that show the maximum values attained by the response quantities for different beam proportions and numbers of compartments N_c.

From dimensional analysis, single cell girders with the same L/d and d/t ratios give the same normalized result quantities. The parameter study is made for different L/d and d/t ratios, but it is presented for different $H_c = d^3/L^2t$ ratios in Figures 46 to 49. The response quantities of any two girders with the same H_c parameter but with different L/d and d/t ratios are the same for all practical purposes. This is shown in Figure 45 for the longitudinal axial stresses for $H_c = 0.2$. The average curve is used for a given H_c in Figures 46 to 49.

4.5.1 No End or Intermediate Diaphragm

For a girder without diaphragms, the longitudinal axial stress σ_L is zero throughout the span, Figure 46. The transverse bending stress σ_T is constant throughout the girder and is proportional to H_c, Figure 47. The stress σ_T can be quite large for large H_c. The shear stress is equal to the Saint-Venant shear stress of $0.5\ \tau_{BU}$ and is independent of H_c, Figure 48. The deflection δ_T increases with H_c and can become quite large, Figure 49.

4.5.2 End Diaphragms Only

End diaphragms are used to reduce the transverse bending stress and deflection. However, longitudinal axial stresses are induced which

shows the coupling of warping and transverse distortion of the cross-section. At the same time the shear stress τ_v is increased.

For $H_c \geq 0.4$ the maximum longitudinal axial stress always occurs at midspan. As H_c becomes smaller the maximum stress location moves closer and closer to the ends. The maximum longitudinal axial stress increases with H_c and can become quite large as shown in Figure 46.

From Figure 47, the transverse bending stress is reduced appreciably for $H_c \geq 0.4$, but is practically unchanged for $H_c < 0.4$. End diaphragms are more effective for flexible sections where they are needed most, i.e., the higher range of H_c.

The shear stress τ_v is increased and this increase is larger the larger is H_c, as shown in Figure 48.

End diaphragms reduce the deflections markedly as shown in Figure 49.

4.5.3 End and Midspan Diaphragms

The addition of a midspan diaphragm to a girder with end diaphragms is now analyzed.

The longitudinal axial stress σ_L has its maximum always at midspan. The maximum longitudinal axial stress is decreased for $H_c > 0.4$, is constant for $H_c = 0.4$ and is increased for $H_c < 0.4$ as shown in Figure 46. A midspan diaphragm is effective where needed the most, i.e., in the large H_c range. However, σ_L seems never to exceed $0.5\,\sigma_{BU}$.

The maximum transverse bending stress is reduced further by introducing a midspan diaphragm and seems never to exceed $0.3\,\sigma_{BU}$ as shown in Figure 47.

The maximum shear stress decreases for $H_c \geq .4$, and increases for $H_c < 0.4$ as shown in Figure 48 after introducing a midspan diaphragm.

The deflection becomes much smaller for all proportions when a midspan diaphragm is used as shown in Figure 49.

4.5.4 End and More Than One Intermediate Diaphragms.

The effect of introducing two intermediate diaphragms is to reduce σ_L, σ_T, and δ_T for all values of H_c as shown in Figures 46 to 49. The stresses σ_L and σ_T are less than $0.2\,\sigma_{BU}$, and the deflection δ_T is practically the rigid section deflection. The maximum shear stress is not changed appreciably, and remains practically constant for H_c less than 0.4. The stress τ_v does not exceed $0.64\,\tau_{BU}$ as shown in Figure 48.

Further introduction of diaphragms reduces the stresses and deflections progressively but insignificantly. Two equally spaced intermediate diaphragms besides the end diaphragms is the optimum diaphragm configuration for uniformly distributed loading.

4.5.5. Effect of Poisson's Ratio

The parameter study presented here applies for $\nu = 0.36$ and is valid for steel box girders. By changing ν to 0.10 for a girder with $L/d = 10$ and $d/t = 20$ the normalized stresses are affected in the third significant figure while the normalized deflections are not decreased more than 20%. Consequently, the effect of ν is negligible. Therefore the results can be used for girders with reinforced concrete girders proportions, i.e., for $H_c' \leq .20$.

5. BEHAVIOR OF MULTICELL BOX GIRDERS UNDER CONCENTRATED LOADS AT MIDSPAN

5.1 General

This chapter presents the analytical results for multicell box girders. The girders are simply supported at both ends and possess rigid end diaphragms. They are loaded by vertical concentrated node loads located at midspan. Concentrated loads are representative of wheel load effects on a highway bridge.

The effect of introducing intermediate diaphragms is investigated.

No attempt is made to present the resultant quantities as functions of parameters, although the method developed in this work is appropriate for such a parameter study. The purpose of this chapter is to present the behavior of several multicell box girder bridges, mainly those of proportions consistent with reinforced concrete construction, and to assess current design methods. Section 5.2 presents response quantities for several multicell box girders loaded by concentrated node loads at midspan. Comparison of the author's method with the alternative method (17) is also presented for a composite bridge. Section 5.3 studies the longitudinal bending moment distribution of axle loads. In this section the importance of the transverse bending stresses for design purposes is also assessed. In addition, a design method is proposed.

5.2 Behavior of Multicell Box Girders under Concentrated Node Loads at Midspan

5.2.1 Multicell Reinforced Concrete Girders

5. BEHAVIOR OF MULTICELL BOX GIRDERS UNDER CONCENTRATED LOADS AT MIDSPAN

5.1 General

This chapter presents the analytical results for multicell box girders. The girders are simply supported at both ends and possess rigid end diaphragms. They are loaded by vertical concentrated node loads located at midspan. Concentrated loads are representative of wheel load effects on a highway bridge.

The effect of introducing intermediate diaphragms is investigated.

No attempt is made to present the resultant quantities as functions of parameters, although the method developed in this work is appropriate for such a parameter study. The purpose of this chapter is to present the behavior of several multicell box girder bridges, mainly those of proportions consistent with reinforced concrete construction, and to assess current design methods. Section 5.2 presents response quantities for several multicell box girders loaded by concentrated node loads at midspan. Comparison of the author's method with the alternative method (17) is also presented for a composite bridge. Section 5.3 studies the longitudinal bending moment distribution of axle loads. In this section the importance of the transverse bending stresses for design purposes is also assessed. In addition, a design method is proposed.

5.2 Behavior of Multicell Box Girders under Concentrated Node Loads at Midspan

5.2.1 Multicell Reinforced Concrete Girders

Three reinforced concrete girders are studied here under mid-span concentrated node loads. The girders are shown in Figure 50a, b, c. They are 100 ft. long and 8 ft. deep. Their plate elements are 6 in. thick. The girder 2RC consists of two similar cells with a total width of 20 ft. The girder 3RC consists of three similar cells with a total width of 30 ft. The girder 2RPC is similar to 3RC except that the middle plate element of the bottom flange is deleted to give a hybrid open-closed section. The three girders discussed here would ordinarily have deck overhangs on both sides, but these are not considered here. Girder 2RC is suitable for 2 lanes of traffic while 3RC and 3RPC are suitable for 3 lanes of traffic.

Flexible reinforced concrete plate diaphragms are introduced at intermediate points along the span. The plate disphragms are 6 in. thick. The analytic treatment of the plate diaphragms follows Section 2.8. For the open-closed girder 2RPC the 6 in. plate diaphragm is replaced by six braces, each brace with a cross-sectional area determined from Equation 2.39. This approximation seems justified because variations in the stiffness of the diaphragms does not affect the results strongly (cf. Sections 4.2.6 and 4.4.3).

Girders and diaphragms are made of the same reinforced concrete with $E = 3{,}000{,}000$ psi and $\nu = 0.1$.

The orthogonal coordinates used in the analysis are shown for 2RC in Figure 51. The generalized transverse coordinates were chosen at the outset while the generalized longitudinal coordinates were obtained by orthogonalization as described in Section 3.1. The similar orthogonal coordinates for 3RC and 2RPC are not shown.

For each box girder two midspan loadings are considered: a concentrated vertical load over an exterior web and a concentrated vertical load over an interior web. From the two loadings, the response of the box girder can be determined easily for any midspan vertical node loading. This section presents the response of the girder for the total node load, i.e., the load is not broken into torsional and bending components as done in Chapter 4. The response quantities considered are the longitudinal axial stress, the transverse bending stress, the shear stress and the vertical deflection. Their variation along the span is considered. The lateral distribution of loads is also discussed.

1. The longitudinal axial stress σ_L is normalized with respect to the average maximum bending stress at midspan. The average bending stress at midspan σ_{BC} is given by the total longitudinal bending moment at midspan divided by the section modulus of the bridge.

The variation along the span for the longitudinal axial stress in girder 2RC, loaded by a vertical midspan concentrated load a the exterior node and stiffened only by end diaphragms, is shown in Figure 52. The stress in both ends of a vertical web is the same but with opposite sign. The stress in the various flanges is practically the same for sections in the end thirds of the span, which implies complete distribution. The stress at the loaded node increases rapidly in the middle third of the span to a peak of $1.97\,\sigma_{BC}$ while the stresses in the unloaded nodes increase much less.

Similar graphs can be plotted for the second load and for the other girders. Instead, Tables 12 to 14 are presented giving the node stresses at midspan for the three girders and for the two loading cases. The effect of introducing diaphragms is also shown. In the same Tables an entry denoted "rigid" gives the longitudinal axial stresses assuming

the cross-section to be rigid in its own plane. The rigid section stresses are computed using Reference (6).

Several points can be made by studying Tables 12 to 14:

(a) When there are no intermediate diaphragms, the maximum stress occurs in the loaded web.

(b) When there are no intermediate diaphragms, higher stresses are induced in 3RC and 2RPC than in 2RC. The girders 3RC and 2RPC have practically the same maximum stresses.

(c) The maximum stress in any girder occurs in the exterior web except for 2RPC where the maximum stress occurs in the interior web but is still very close to the maximum exterior web stress.

(d) The introduction of diaphragms is more effective in reducing the stresses the closer they are to the load. A midspan diaphragm below the load reduces the stresses almost to the rigid section stresses.

2. The transverse bending stress σ_T is normalized with respect to the average maximum bending stress at midspan. The variation along the span is shown in Figure 53 for 2RC loaded at the exterior web for the girder with no intermediate diaphragms. Five curves are shown for the different member end stresses. The stresses increase from zero at one end to a maximum at midspan. The maximum transverse bending stress occurs in the ends of the interior web.

Similar graphs can be plotted for the second load and for the other girders. Instead Tables 15 to 17 are presented giving the maximum stresses at the ends of the members at midspan for the three girders and for the two loading cases. The effect of introducing diaphragms is also shown. The rigid section transverse bending stresses are zero and are shown under the entry "rigid" for completeness.

Several points can be made concerning transverse bending stresses:

(a) For no intermediate diaphragms the maximum stress occurs at the top of an interior web when the exterior web is loaded, and in the top flange of the box girder when an interior web is loaded.

(b) Higher maximum transverse bending stresses are induced in the girders for loads applied over the exterior webs.

(c) Higher maximum transverse bending stresses are induced in wider multicell girders because more eccentric loads can be applied.

(d) The introduction of diaphragms is quite effective in reducing the transverse bending stresses. The closer the two diaphragms are to the load the greater is the reduction. Diaphragms are more effective in reducing the transverse bending stress than the longitudinal axial stress. A midspan diaphragm under the load reduces the transverse bending stresses practically to zero.

3. The shear stresses are normalized with respect to the average shear stress at the end. The average shear stress τ_{BC} at the end is given by dividing the total longitudinal vertical shear at the end equally between the webs and assuming uniform distribution of shear stress.

For a concentrated load at midspan, the shear stress is maximum in the loaded web at midspan, and directly below the load the total shear in the loaded web changes by an amount equal to the load. The introduction of an intermediate diaphragm is very effective in distributing the load to the other elements of the girder in the unloaded compartments. This will be shown for 3RC under an edge load. For better understanding of the behavior, the load is divided into two components as shown in Figure 54. Load (a) is essentially a bending load and Load (b) is a torsional load.

The shear stresses caused by the bending load 54a are plotted in Figure 55. Only the webs have shear stress in them. The exterior webs that are loaded carry most of the shear, but in a sufficient distance they do transfer some of their load to the interior webs. The introduction of two diaphragms symmetrical with respect to midspan is very effective in transmitting shear stress from the exterior webs to the interior webs which become slightly more loaded than the exterior webs. This is valid only in the unloaded compartment. Not much change occurs in the loaded compartment however. For a midspan diaphragm the shear stress is almost taken equally between all webs and equals τ_{BC}.

The shear stresses caused by the torsional load 54b are plotted in Figure 56. Vertical and horizontal plate elements take the torsional load in shear. The shear stress is maximum at midspan in the loaded webs but decreases gradually towards the ends as the shear stress is distributed to the other elements. The shear stress distribution at the end becomes close to the Saint-Venant shear distribution shown in Figure 57. The introduction of two diaphragms placed symmetrically with respect to midspan produces almost the Saint-Venant shear distribution over the whole unloaded compartments. Again, not much distribution occurs in the loaded compartment.

The shear stress distribution is similar in 2RC and 2RPC. Figure 57 shows that the shear stress distribution at the end with two intermediate diaphragms becomes close to the Saint-Venant shear stress distribution for 2RC, 2RPC and 3RC.

4. The vertical deflections are normalized with respect to maximum pure bending deflections δ_{BC}. The deflection δ_{BC} is given by the usual expression $PL^3/48EI$ where P is the total concentrated load

applied at midspan and I the moment of inertia of the bridge. The vertical deflections of the nodes are shown in Figures 58 to 60 for different node loads, for only end diaphragms, for end and midspan diaphragms and for end and two intermediate diaphragms at 7L/18 and 11L/18.

Several conclusions can be drawn from Figures 58 to 60:

(a) For any girder, the deflections are larger for loads applied at the exterior webs.

(b) The deflection at the node is maximum when the node is directly loaded.

(c) The deflections are larger for 2RPC and 3RC than for 2RC.

(d) The introduction of two diaphragms at 7L/18 and 11L/18 reduces the maximum deflection almost as effectively as a single midspan diaphragm.

5. The lateral distribution of node loads to the beam elements that constitute the multicell box girder is studied here. Each beam element consists of a web with top and bottom flanges extending on both sides of the web to mid-distance between webs. Thus, 3RC is divided into two interior I-beams and two exterior [-beams. Each beam as defined above takes some fraction of the total longitudinal bending moment. The distribution of the longitudinal bending moment to the different beam elements is the criterion of the lateral distribution of loads.

The longitudinal bending moment in a beam element is determined about the center of gravity of the whole cross-section of the bridge, from the known longitudinal axial stresses. The longitudinal bending

moments are given in Tables 18 and 19 for exterior and interior beam elements of the three girders for different diaphragm configurations and for different midspan concentrated node load locations. The longitudinal bending moments are normalized with respect to the total moment at midspan in the multicell bridge, and consequently the values given in Tables 18 and 19 are also wheel load factors as used in AASHO Specifications(21).

Examination of Tables 18 and 19 leads to the following conclusions:

1. For only end diaphragms, the maximum moment occurs in the loaded beam elements. As the load moves away from the beam element the moment gradually decreases in that beam element.

2. The introduction of diaphragms is effective in improving the lateral load distribution. A midspan diaphragm is most effective as the lateral distribution of loads becomes almost complete.

5.2.2 Composite Girder - A Comparison With the Alternative Method

A composite girder with open-closed section is studied briefly. The purpose is to show the wide range of applicability of the author's solution as well as to present a comparison with the alternative solution.

The composite girder is shown in Figure 50d. It is denoted by 2TPCS and has length of 100 ft. It consists of two separate trapezoidal steel girders 61.5 in. deep supporting a reinforced concrete slab 7 in. thick and 25 ft. wide. Each trapezoidal steel girder has a bottom flange 80 in. wide by 9/16 in. thick, and a 3/8 in. thick web. Webs and bottom flange are stiffened every 50 in. with 3/8 in. x 6 in. plate stiffeners.

The materials properties are:

for steel	E = 30,000,000	ν = 0.3
for reinforced concrete	E = 3,000,000	ν = 0.1

The box girder is studied under a 10 k. midspan concentrated load located over the exterior web or the interior web. The first Fourier term of the load is used for comparison. The girder possesses only end diaphragms.

The comparison is presented in table form for the longitudinal axial stress, transverse bending stress and deflection at midspan in Tables 20 to 22.

The values compare very well for all quantities as apparent from Tables 20 to 22. The transverse bending stresses differ slightly because of the transverse extensibility of the alternative model. The alternative method by allowing transverse deformations gives a more flexible structure with slightly larger deflections than the author's method.

The difference in transverse bending stress at node 6, for locations 6a and 6b, is due to the difference in section moduli as determined from Appendix A.

5.3 Behavior of Multicell Reinforced Concrete Box Girders under Axle Loads at Midspan

In this section, the three reinforced concrete box girders are loaded by axle loads at midspan. The lateral distribution of loads is assessed. The transverse bending moments are compared to the slab moments proposed by AASHO Specifications (1961).

5.3.1 Axle Load Configuration

The axle load configuration of the AASHO Specifications (21) is used. One axle per lane is considered to be located at midspan. The bridges are designed for the number of lanes specified by AASHO Specifications: 2RC is designed for 2 lanes, 3RC and 2RPC for three lanes. In strict conformity to AASHO Specification 3RC and 2RPC must be designed for 2 lanes. But deck overhangs usually are present on both sides and the roadway width is larger so it is reasonable to study 3RC and 2RPC for three lanes. The transverse location of the wheel loads at midspan to give maximum moments in interior and exterior beams is shown in Figure 61. For 3RC and 2RPC, the two-lane configuration also is shown.

5.3.2 Lateral Distribution of Loads

The lateral distribution of loads is presented in Table 23 for both the exterior and interior beams of the three reinforced concrete multicell bridges for different diaphragm configurations. This table gives the maximum proportion of a wheel load that goes to the different beams, i.e., gives the wheel load factors. These factors are determined from Tables 18 and 19 and the truck load configurations of Figure 61. A wheel load between nodes is distributed to the two adjacent nodes as if the slab is simply supported at those two nodes. Its influence coefficient is obtained by interpolating linearly with distance the influence coefficients of the two adjacent nodes given by Tables 18 and 19. It is equivalent to assuming that the midspan moment influence line for a beam element is linear between nodes.

Table 23 also gives the wheel load factors for complete lateral distribution. The complete distribution of a wheel load occurs when each beam element takes a longitudinal moment proportional to its moment of

inertia, that is when the stress is uniform in the top plate elements and uniform in the bottom plate elements.

The study of the values presented in Table 23 shows that:

1. The interior beams are more heavily loaded than the exterior beams.

2. The load is quite uniform transversely, so the lateral distribution of loads is good, even for no intermediate diaphragms.

3. The more uniform the load, the better the lateral distribution. The distribution for 3 lanes is better than for 2 lanes.

4. The introduction of intermediate diaphragms improves the distribution in all cases. The distribution does not deteriorate by adding a midspan diaphragm as for results obtained for I-beam bridges (30).

5. Intermediate diaphragms are more effective when closer to the load. A midspan diaphragm does give the best distribution.

6. The wheel load factors for exterior and interior beams with only end diaphragms is no larger than 1.08 times the wheel load factor for complete distribution and for the number of lanes proposed by the AASHO Specifications (1961).

7. Although intermediate diaphragms improve the distribution, their introduction is not important as the lateral distribution in the multicell girders is quite good to start with.

5.3.3 Transverse Bending Stresses

The magnitude of the transverse bending stresses in 2RC created by loads at the nodes is compared to the magnitude of the stresses induced in the top slab under a wheel load halfway between nodes.

The maximum moment under the load is given by AASHO to be equal to:

$$(M_{ot})_{max} = 0.8 \frac{(S + 2)P}{32} \qquad (5.1)$$

where M_{ot} is the transverse moment in the slab under the wheel load P, and where S is the distance between nodes. The factor 0.8 is a continuity factor.

The maximum stress in the slab under the load is given by:

$$(\sigma_{ot})_{max} = 6M_{ot}/t^2 \qquad (5.2)$$

The maximum transverse bending stress induced in 2RC under axle loading can be estimated by the maximum stress in the ends of the interior web caused by an isolated load P vertically applied at the exterior top node

$$(\sigma_T)_{max} = 2.02 \frac{PL}{4Sm} \qquad (5.3)$$

where Sm is the section modulus of the whole bridge and 2.02 is obtained from Table 15.

The ratio $(\sigma_T)_{max} / (\sigma_{ot})_{max}$ obtained from Equations (5.1), (5.2), and (5.3) by replacing the specified quantities by their values for 2RC is only .073. The transverse bending stresses due to node loads are secondary compared to the slab stresses in bridges of the proportions studied here.

5.3.4 Design Recommendations

The design of multicell box girders needs considerable investigation. However, from the results of this brief study, Sections 5.3.2

The maximum moment under the load is given by AASHO to be equal to:

$$(M_{ot})_{max} = 0.8 \frac{(S + 2)P}{32} \qquad (5.1)$$

where M_{ot} is the transverse moment in the slab under the wheel load P, and where S is the distance between nodes. The factor 0.8 is a continuity factor.

The maximum stress in the slab under the load is given by:

$$(\sigma_{ot})_{max} = 6M_{ot}/t^2 \qquad (5.2)$$

The maximum transverse bending stress induced in 2RC under axle loading can be estimated by the maximum stress in the ends of the interior web caused by an isolated load P vertically applied at the exterior top node

$$(\sigma_T)_{max} = 2.02 \frac{PL}{4Sm} \qquad (5.3)$$

where Sm is the section modulus of the whole bridge and 2.02 is obtained from Table 15.

The ratio $(\sigma_T)_{max} / (\sigma_{ot})_{max}$ obtained from Equations (5.1), (5.2), and (5.3) by replacing the specified quantities by their values for 2RC is only .073. The transverse bending stresses due to node loads are secondary compared to the slab stresses in bridges of the proportions studied here.

5.3.4 Design Recommendations

The design of multicell box girders needs considerable investigation. However, from the results of this brief study, Sections 5.3.2

and 5.3.3, the following simple recommendations can be proposed for multicell box girders of reinforced concrete proportions;

1. The stress distribution caused by truck loads in all lanes of a multicell box girder is good without intermediate diaphragms. The addition of intermediate diaphragms would appear to be required only for less uniform design loading conditions.

2. The transverse bending stresses induced by node loads are relatively small. However, transverse bending stresses occur in the webs and bottom slab as well as the deck slab. The present AASHO Specifications does not provide for any transverse reinforcement in the webs. It is felt that the webs should be reinforced to possess about 10% of the transverse flexural capacity of the deck slab.

3. The AASHO distribution formulas need some improvement. Design of multicell box girders can be made using improved wheel distribution factors. The following scheme is proposed.

The design moment of a beam element is obtained from

$$M_B = c \frac{I_B}{\Sigma I_B} \cdot M \qquad (5.4)$$

where M is the total design moment in the bridge, I_B is the moment of inertia of the beam element, ΣI_B is the moment of inertia of the whole section and c is a distribution factor.

The factor c depends upon structural proportions, the design load configuration and whether the beam element is exterior or interior. A parameter study is necessary to determine the variation of c. For the multicell bridges studied here c is less than 1.10, for exterior and interior beams using the AASHO axle configuration, i.e., 2 lanes for 2RC and 3 lanes for 2RPC and 3RC.

6. SUMMARY AND CONCLUSIONS

6.1 Summary

Vlasov's generalized coordinates method is extended to consider multicell composite box girders with intermediate diaphragms and with transverse or longitudinal stiffeners. The resulting system of linear differential equations is solved numerically. Two features of the numerical solution in Chapter 3 are the orthogonalization of the generalized coordinates and the suppression of the exponentially growing solutions. Results are presented for different types of single cell box girders, and a parameter study is given in Chapter 4 for a single cell square box under uniform torsional load. Results also are presented for several multicell box girders under node and truck loads and design recommendations are discussed in Chapter 5.

The effect of introducing diaphragms is studied extensively. The number and location of diaphragms are varied and the effect of their stiffness is investigated in Chapters 4 and 5.

Comparison of the solution proposed here to an alternative solution (17) is made for a single cell steel box girder and for a multicell composite box girder in Chapters 4 and 5.

6.2 Conclusions

The method presented in this work is a powerful method for studying many types of multicell box girders. It is also a general method in that it considers all the important factors that play a role in the response of closed section structures, i.e., transverse distortion of the cross-section, warping of the cross-section and shear deformations.

The transverse distortion of the cross-section induces transverse bending stresses that affect the longitudinal axial stresses. Distortion leads to high axial warping stresses and transverse bending stresses. Diaphragms may be introduced to alleviate these problems. The analysis and design of box girders often should consider transverse bending stresses and its effect on longitudinal axial stresses. The transverse distortion is more important for structure with high ratio of live load to dead load, with more eccentric loads, and for structures that are thin and short. Detailed conclusions are made in Chapters 4 and 5. They are summarized below.

6.2.1 Single Cell Under Uniform Torsional Load

1. For a simply supported girder with end diaphragms only, the longitudinal axial stress σ_L, the transverse bending stress σ_T, and the deflection δ_T are maximum near or at midspan and the shear stress τ_V is maximum at the end.

2. If the ends are fixed, the longitudinal axial stress can become a maximum at the ends. The shear stress τ_V is increased at the ends, and the transverse bending stress is decreased.

3. For a simply supported square box girder with only end diaphragms all the maximum stresses and deflections increase with the parameter H_c in general.

4. Intermediate diaphragms generally are effective in reducing stresses and deflections. Two diaphragms at the third points reduce stresses and deflections to small values. The larger H_c the more effective are the diaphragms. For small H_c the introduction of a midspan diaphragm decreases σ_T and δ_T but increases σ_L and τ_V and therefore a midspan diaphragm is to be avoided for girder with small H_c values.

6.2.2 Single Cell Under Concentrated Torsional Load

1. For a simply supported girder with only end diaphragms the stresses and deflections all have their peak directly below the load or very close to it.

2. For a simply supported girder the longitudinal axial stresses and the maximum transverse bending stresses occur when the load is at midspan or very close to it. The shear stress is maximum when the load is close the the end but not at the end.

3. End fixity does influence the response quantities when the load is near the end. Longitudinal axial stresses are produced at the end and become higher as the load approaches the end. Eventually, the end stresses may exceed the peak under the load. The end stresses must, of course, drop to zero when the load is at the end. The transverse bending stresses are decreased for loads close to the ends. The shear stress τ_v is increased for loads close to the end.

4. The introduction of intermediate diaphragms is effective in reducing σ_T and δ_T. The longitudinal axial stress is decreased when the nearest diaphragm is close to the load. A diaphragm located below the load reduces the distortion of the cross-section almost to zero.

5. The stiffening action of diaphragms is insensitive to practical variations in the stiffness of the diaphragms.

6.2.3 Simply Supported Reinforced Concrete Multicell Box Girders Under Concentrated Node Loads at Midspan

1. The maximum stresses and deflections occur at midspan. The maximum normalized longitudinal and transverse stresses are larger for multicell girders than single cell girders.

2. The maximum longitudinal axial stress occurs in the exterior beam elements in general.

3. The introduction of intermediate diaphragms is effective in reducing the stresses and deflections. The closer the diaphragms to the load, the greater is the reduction.

6.2.4 Simply Supported Reinforced Concrete Multicell Box Girders Under Axle Loads at Midspan

1. Although substantial longitudinal axial stresses are caused by torsional loadings on multicell girders, these stresses are not critical in design. This is mainly due to the low ratio of live to dead load in bridges and to the small eccentricity of standard design loads.

2. Multicell girders under standard truck loads give good lateral distribution of loads even for only end diaphragms.

3. Transverse bending stresses are small compared to the slab transverse stresses. However, the webs should be transversely reinforced to give about 10% of the deck flexural resistance.

6.3 Recommendations for Further Studies

Although this investigation shows the transverse bending stresses to be of little significance and that good lateral distribution exists for standard loading, an economical and safe design method still should be developed for multicell reinforced concrete bridges. Therefore a parameter study is recommended to determine the variation of the distribution coefficient c of Section 5.3.4.

The present analysis can be used to perform a parameter study of a single box under a midspan concentrated torsional load similar to Section 4.5. It can also be extended to account for moments at the nodes. It easily can be extended to study multicell box girders continuous over several supports.

An interesting extension is the study of curved box girders. In curved box girders higher torsional loads are expected and the distortion of the cross-section will probably play a more important role. In such a case, the stiffening action of diaphragms could be of major importance.

TABLE 1

Effect of Diaphragm Location on σ_L at Midspan.
Simply Supported Girder IRC under Concentrated Torsional Load at Midspan.

Number of Intermediate Diaphragms	Zero	Two				One	Rigid Solution
Location	--	$\frac{4L}{18}$, $\frac{14L}{18}$	$\frac{6L}{18}$, $\frac{12L}{18}$	$\frac{7L}{18}$, $\frac{11L}{18}$	$\frac{8L}{18}$, $\frac{10L}{18}$	L/2	---
σ_L/σ_{BC}	-0.416	-0.467	-0.437	-0.340	-0.204	-0.010	-0.009

TABLE 2

Effect of Loading and End Conditions on Maximum σ_L.
Girder IRC with Only End Diaphragms.

Loading		Simply Supported Ends		Fixed Ends	
		Maximum Stress	Location	Maximum Stress	Location
Uniform Load		$-0.109\ \sigma_{BU}$	L/5	$+0.347\ \sigma_{BU}$	0 and L
Concentrated Load at	L/2	$-0.416\ \sigma_{BC}$	L/2	$-0.431\ \sigma_{BC}$	L/2
	L/3	$-0.448\ \sigma_{BC}$	L/3	$-0.399\ \sigma_{BC}$	L/3
	L/6	$-0.512\ \sigma_{BC}$	L/6	$-0.361\ \sigma_{BC}$*	L/6
				$+0.520\ \sigma_{BC}$	0

*Stress listed is not a maximum.

TABLE 3

Effect of Diaphragm Location on σ_T at Midspan.
Simply Supported Girder IRC under Concentrated
Torsional Load at Midspan.

Number of Intermediate Diaphragms	Zero	Two				One	Rigid Solution
Location	--	$\frac{4L}{18}$, $\frac{14L}{18}$	$\frac{6L}{18}$, $\frac{12L}{18}$	$\frac{7L}{18}$, $\frac{11L}{18}$	$\frac{8L}{18}$, $\frac{10L}{18}$	L/2	
σ_T/σ_{BC}	0.788	0.635	0.332	0.161	0.051	0.022	0.000

TABLE 4

Effect of Loading and End Conditions on Maximum σ_T.
Girder IRC with Only End Diaphragms.

Loading		Simply Supported Ends		Fixed Ends	
		Maximum Stress	Location	Maximum Stress	Location
Uniform Load		0.682 σ_{BU}	L/2	0.621 σ_{BU}	L/2
Concentrated Load at	L/2	0.788 σ_{BC}	L/2	0.770 σ_{BC}	L/2
	L/3	0.810 σ_{BC}	L/3	0.702 σ_{BC}	L/3
	L/6	0.650 σ_{BC}	L/6	0.387 σ_{BC}	$\simeq 2L/9$

TABLE 5

Effect of Loading and End Conditions on Maximum τ_v.
Girder IRC with Only End Diaphragms.

Loading		Simply Supported Ends		Fixed Ends	
		Maximum Stress	Location	Maximum Stress	Location
Uniform Load		0.605 τ_{BU}	0 - L	0.700 τ_{BU}	0 - L
Concentrated Load at	L/2	1.000 τ_{BC}	L/2	1.000 τ_{BC}	L/2
	L/3	1.145 τ_{BC}	L/3	1.178 τ_{BC}	L/3
	L/6	1.315 τ_{BC}	L/6	1.500 τ_{BC}	L/6
	0	1.000 τ_{BC}	0	1.000 τ_{BC}	0

TABLE 6

Maximum Deflection δ_T in Girder IRC

Loading		Number of Equally Spaced Intermediate Diaphragms	Simply Supported Ends	Fixed Ends
Uniform Load	Bending Solution without Shear Deformations	----	1.000 δ_{BU}	0.200 δ_{BU}
	Bending Solution with Shear Deformations	----	1.050 δ_{BU}	0.253 δ_{BU}
	Torsional Solution	0	0.109 δ_{BU}	0.100 δ_{BU}
		1	0.058 δ_{BU}	0.048 δ_{BU}
		2	0.035 δ_{BU}	0.036 δ_{BU}
		Rigid Section	0.030 δ_{BU}	0.030 δ_{BU}
Concentrated Load at L/2	Bending Solution without Shear Deformations	----	1.000 δ_{BC}	0.250 δ_{BC}
	Bending Solution with Shear Deformations	----	1.065 δ_{BC}	0.316 δ_{BC}
	Torsional Solution	0	0.151 δ_{BC}	0.148 δ_{BC}
		1	0.039 δ_{BC}	0.039 δ_{BC}
		2	0.084 δ_{BC}	0.084 δ_{BC}
		Rigid Section	0.038 δ_{BC}	0.038 δ_{BC}

TABLE 7

Effect of Midspan Diaphragm Stiffeness on Maximum Stresses. Simply Supported Girder IRC under Concentrated Torsional Loads.

Load Location	Stress	6 in. Midspan Diaphragm	1 in. Midspan Diaphragm
L/2	σ_L/σ_{BC}	-0.010	-0.067
	σ_T/σ_{BC}	0.022	0.133
	τ_v/τ_{BC}	0.520	0.570
	τ_h/τ_{BC}	0.480	0.430
L/3	σ_L/σ_{BC}	-0.448	-0.446
	σ_T/σ_{BC}	0.535	0.567
L/6	σ_L/σ_{BC}	-0.512	-0.526
	σ_T/σ_{BC}	0.620	0.624

TABLE 8

Comparison Between the Maximum Stresses* in Girders IRC and ITC for Simply Supported End Conditions.

Load	Box	Stress	No Intermediate Diaphragms	Midspan Diaphragm	Two Diaphragms at L/3, 2L/3
Uniform Load	IRC	σ_L/σ_{BU}	-0.11	-0.30	-0.16
		σ_T/σ_{BU}	0.68	0.33	0.12
	ITC	σ_L/σ_{BU}	-0.05	-0.15	-0.11
		σ_T/σ_{BU}	0.31	0.24	0.12
Concentrated Load at L/2	IRC	σ_L/σ_{BC}	-0.42	-0.01	-0.44
		σ_T/σ_{BC}	0.79	0.02	0.63
	ITC	σ_L/σ_{BC}	-0.29	-0.01	-0.32
		σ_T/σ_{BC}	0.54	0.02	0.36

*Maximum stresses occur at Node 4.

TABLE 9

Comparison of Methods of Analysis. Stresses and Deflections in Girder IRS for a Sinusoidal Load at Node 1. No Intermediate Diaphragms.

Stress or Deflection	Location	Alternative Solution	Author's Solution	
		First Fourier Term of 10 k. Midspan Load	First Fourier Term of 10 k. Midspan Load	Total Solution of 10 k. Midspan Load
Longitudinal Axial Stress in psi at Midspan	Node 1	-494.	-494.9	-811.1
	Node 2	-342.	-341.8	-221.3
	Node 3	679.	680.3	1083.4
	Node 4	494.	494.6	366.8
Transverse Bending Stress in psi at Midspan**	Sec. 1a-2a	846.	852.6	1021.4
	Sec. 1b-2b	2580.	2591.	3103.4
	Sec. 3b-4b	91.8	85.1	101.9
	Sec. 3a-4a	239.	225.0	269.4
Shear Stress in psi at Support	Member 1	- 40.7*	- 40.9	- 39.1
	Member 2	136.0*	136.7	100.8
	Member 3	41.2*	40.5	38.9
	Member 4	40.7*	40.9	39.1
Shear Stress in psi at Midspan	Member 1	0.	0.	- .1
	Member 2	0.	0.	139.1
	Member 3	0.	0.	.0
	Member 4	0.	0.	.1
Vertical Deflection at Midspan in in.	Nodes 1-3	.123	.123	.129
	Nodes 2-4	.085	.085	.083

*Average shear stress determined by using parabolic approximation.

**Stress in absolute value.

TABLE 10

Maximum Stresses and Deflections in Girder IRS.
Midspan Concentrated Torsional Load.

Diaphragm Configuration	σ_L/σ_{BC}		σ_T/σ_{BC}***				τ_h/τ_{BC}	τ_v/τ_{BC}	δ_T/δ_{BC}
	Node 1	Node 3	Sec. 1a	Sec. 3a	Sec. 1b-2b	Sec. 3b-4b			
No Intermediate Diaphragm	-.407	.493	1.409	.372	4.27	.141	0.00	1.00	.216
Two X-Braces at Third Points*	-.374	.455	.419	.112	1.272	.041	0.00	1.00	.071
Five X-Braces at Sixth Points*	-.095	.115	.101	.027	.307	.010	0.37	0.63	.034
Eight X-Braces at Ninth Points*	-.185	.225	.101	.027	.310	.010	0.00	1.00	.035
Two Plate Diaphragms at Third Points**	-.376	.454	.356	.094	1.080	.036	0.00	1.00	.073
Two Plate Diaphragms at $\frac{7L}{18}$, $\frac{11L}{18}$**	-.292	.345	.154	.041	0.467	.015	0.00	1.00	.047

* ** X-brace consists of two 4" x 3" x 5/16" angles.
Plate diaphragm is a 3/8" thick steel plate.

*** Stress in absolute value.

TABLE II

Cross-Bracing Stresses in Girder 1RS.
Midspan Concentrated Torsional Load.

Cross-Bracing	Two X-Braces at Third Points	Five X-Braces at Sixth Points			Eight X-Braces at Ninth Points			
Location of Brace	L/3	L/6	L/3	L/2	L/9	2L/9	L/3	4L/9
$\frac{\text{Stress in Brace}}{\sigma_{BC}}$	±0.35	±.02	±.14	±.97	±.01	±.02	±.10	±.56

TABLE 12

Normalized Longitudinal Axial Stresses at Midspan of Girder 2RC.
Midspan Concentrated Loads.

Loading	Node	No Intermediate Diaphragm	Two Intermediate Diaphragms at 7L/18 and 11L/18	Two Intermediate Diaphragms at 8L/18 and 10L/18	Midspan Diaphragm	Rigid Solution
Load at Node 1	1	-1.97	-1.66	-1.44	-1.13	-1.07
	2	-0.77	-0.78	-0.83	-0.94	-1.00
	3	-0.44	-0.72	-0.86	-0.98	- .93
Load at Node 2	1	-0.78	-0.79	-0.85	-1.01	-1.0
	2	-1.24	-1.23	-1.11	-0.99	-1.0
	3	-0.78	-0.79	-0.85	-1.01	-1.0

TABLE 13

Normalized Longitudinal Axial Stresses at Midspan of Girder 3RC.
Midspan Concentrated Loads.

Loading	Node	No Intermediate Diaphragm	Two Intermediate Diaphragms at 7L/18 and 11L/18	Two Intermediate Diaphragms at 8L/18 and 10L/18	Midspan Diaphragm	Rigid Solution
	1	-2.65	-1.98	-1.64	-1.25	-1.12
Load at	2	-0.97	-0.81	-0.85	-1.03	-1.04
Node 1	3	-0.57	-0.80	-0.86	-0.88	-0.96
	4	-0.17	-0.66	-0.78	-0.93	-0.88
	1	-0.99	-0.83	-0.87	-1.06	-1.04
Load at	2	-1.55	-1.44	-1.31	-1.05	-1.01
Node 2	3	-0.70	-0.78	-0.82	-0.93	-0.99
	4	-0.56	-0.82	-0.90	-0.98	-0.96

TABLE 14

Normalized Longitudinal Axial Stresses at Midspan of Girder 2RPC.
Midspan Concentrated Loads.

Loading	Node	No Intermediate Diaphragm	Two Intermediate Diaphragms at 7L/18 and 11L/18	Midspan Diaphragm	Rigid Solution
	1	-2.28	-1.60	- .87	-1.01
	2	-0.81	- .57	- .69	-0.80
	3	-0.39	- .67	-1.01	-0.77
Load at	4	0.10	- .52	- .48	-0.56
Node 1	5	2.52	1.87	1.16	1.09
	6	1.04	.65	.97	1.27
	7	.11	.72	.81	.73
	8	.37	.81	1.05	.91
	1	-1.10	- .65	-1.18	-0.86
	2	-1.32	-1.12	- .56	-0.79
	3	-0.45	- .60	- .63	-0.78
Load at	4	-0.10	- .66	-1.01	-0.71
Node 2	5	0.70	.55	.92	1.03
	6	2.62	1.83	1.19	1.09
	7	2.33	.81	1.06	0.91
	8	0.44	.79	.87	0.97

TABLE 15

Normalized Transverse Bending Stresses at Midspan of Girder 2RC.
Midspan Concentrated Loads.

Loading	Section or Node	No Intermediate Diaphragm	Two Intermediate Diaphragms at 7L/18 and 11L/18	Two Intermediate Diaphragms at 8L/18 and 10L/18	Midspan Diaphragm	Rigid Solution
Load at Node 1	1	1.59	.23	.11	.07	0.
	2a	1.47	.24	.11	.08	0.
	2b	.55	.03	.03	.02	0.
	2c	2.02	.21	.09	.06	0.
	3	.86	.03	.00	.00	0.
Load at Node 2	1	.57	.17	.09	.06	0.
	2a	.68	.21	.12	.07	0.
	2b	.68	.21	.12	.07	0.
	2c	.00	.00	.00	.00	0.
	3	.57	.17	.09	.06	0.

TABLE 16

Normalized Transverse Bending Stresses at Midspan of Girder 3RC.
Midspan Concentrated Loads

Loading	Section or Node	No Intermediate Diaphragm	Two Intermediate Diaphragms at 7L/18 and 11L/18	Two Intermediate Diaphragms at 8L/18 and 10L/18	Midspan Diaphragm	Rigid Solution
Load at Node 1	1	2.23	.33	.17	.13	.00
	2a	2.06	.34	.17	.12	.00
	2b	.79	.04	.02	.01	.00
	2c	2.85	.30	.15	.14	.00
	3a	1.06	.03	.02	.04	.00
	3b	.82	.04	.02	.02	.00
	3c	1.89	.06	.00	.02	.00
	4	1.05	.04	.00	.01	.00
Load at Node 2	1	.46	.25	.14	.08	.00
	2a	.78	.32	.18	.11	.00
	2b	1.52	.35	.19	.13	.00
	2c	.74	.03	.02	.02	.00
	3a	1.32	.30	.16	.11	.00
	3b	1.76	.08	.04	.00	.00
	3c	1.49	.22	.12	.10	.00
	4	.45	.01	.00	.02	.00

TABLE 17

Normalized Transverse Bending Stresses at Midspan of Girder 2RPC.
Midspan Concentrated Loads.

Loading	Section or Node	No Intermediate Diaphragm	Two intermediate Diaphragms at 7L/18 and 11L/18	Midspan Diaphragm	Rigid Solution
Load at Node 1	1	1.56	.34	.16	.00
	2a	1.06	.49	.30	.00
	2b	1.52	.45	.42	.00
	2c	2.58	.03	.12	.00
	3a	1.63	.46	.64	.00
	3b	0.44	.17	.16	.00
	3c	1.20	.29	.47	.00
	4	0.10	.02	.04	.00
	5	1.76	.28	.11	.00
	6	1.93	.22	.06	.00
	7	0.50	.09	.20	.00
	8	0.31	.04	.12	.00
Load at Node 2	1	1.41	.25	.09	.00
	2a	2.17	.26	.02	.00
	2b	2.31	.03	.24	.00
	2c	0.14	.24	.26	.00
	3a	2.23	.09	.07	.00
	3b	0.69	.02	.07	.00
	3c	1.54	.07	.15	.00
	4	.04	.01	.10	.00
	5	1.11	.25	.12	.00
	6	0.84	.24	.16	.00
	7	0.59	.03	.11	.00
	8	0.33	.02	.10	.00

TABLE 18

Influence Coefficients for the Moment in Exterior Beam* of Multicell Box Girders for Various Transverse Positions of Load at Midspan.

Box Girder	Midspan Load at Node No.	No Intermediate Diaphragm	Two Intermediate Diaphragms at 7L/18 and 11L/18	Midspan Diaphragm	Complete Distribution
2RC	1	.458	.393	.288	.263
	2	.230	.232	.265	.263
	3	.132	.193	.256	.263
3RC	1	.415	.325	.215	.180
	2	.196	.169	.188	.180
	3	.106	.145	.173	.180
	4	.045	.123	.164	.180
2RPC	1	.508	.366	.240	.217
	2	.261	.185	.239	.217
	3	.074	.175	.218	.217
	4	.045	.165	.198	.217

* Beam element at Node 1.

TABLE 19

Influence Coefficients for the Moment in Interior Beam* of Multicell Box Girders for Various Transverse Positions of Load at Midspan

Box Girder	Midspan Load at Node No.	No Intermediate Diaphragm	Two Intermediate Diaphragms at 7L/18 and 11L/18	Midspan Diaphragm	Complete Distribution
2RC	1	.411	.412	.456	.474
	2	.540	.534	.468	.474
	3	.411	.412	.456	.474
3RC	1	.356	.304	.330	.320
	2	.446	.415	.331	.320
	3	.250	.273	.304	.320
	4	.168	.251	.288	.320
2RPC	1	.353	.218	.275	.283
	2	.532	.406	.275	.283
	3	.131	.273	.264	.283
	4	.092	.251	.285	.283

* Beam element at Node 2.

TABLE 20

Comparison of Methods of Analysis. Longitudinal Axial Stresses in Girder 2TPCS for a Sinusoidal Node Load.*

	Node	Load at Node 1		Load at Node 2	
		Author's Solution	Alternative Solution	Author's Solution	Alternative Solution
Concrete Top Flange	1	-30.65	-31.30	-24.25	-24.70
	2	-20.83	-20.90	-20.43	-20.40
	3	-14.75	-14.45	-16.56	-16.30
	4	- 8.07	- 7.35	-11.92	-11.40
Steel Girders	1	-224.3	-229.0	-177.5	-180.0
	2	-152.4	-152.0	-149.5	-149.0
	3	-108.0	-106.0	-121.5	-119.5
	4	- 59.06	- 53.8	- 87.22	- 83.6
	5	454.6	438.0	379.0	372.0
	6	432.4	432.0	409.5	406.0
	7	198.9	202.0	254.9	255.0
	8	211.6	219.0	253.9	259.0

*First Fourier term of a 10 K. midspan load. Stresses are expressed in psi.

TABLE 21

Comparison of Methods of Analysis. Transverse Bending Stresses in Girder 2TPCS for a Sinusoidal Node Load.*

Location of Stress	Load at Node 1		Load at Node 2	
	Author's Solution	Alternative Solution	Author's Solution	Alternative Solution
1a	15.76	15.4	5.29	5.88
2a	4.21	6.04	40.89	41.40
2b	25.76	25.40	45.85	45.70
3a	38.46	38.70	33.93	33.90
3b	25.87	26.00	21.61	21.7
4a	3.94	4.23	4.68	4.89
1b	1487.0	1410.	499.1	539.
5b	1411.0	1290.	216.2	262.
2c	2033.0	1880.	473.0	413.
6b	1518.0	1410.	26.13	79.1
3c	1187.0	1200.	1161.0	1160.
7b	663.4	657.	683.9	669.
4b	372.0	375.	442.0	437.
8b	504.1	509.	543.3	540.
5a	1305.	1200.	200.	242.
6a	1404.	1290.	24.17	73.1
7a	613.7	607.	632.6	618.
8a	466.3	465.	502.6	494.

*First Fourier term of a 10 K. midspan load. Stresses are expressed in psi and in absolute value.

TABLE 22

Comparison of Methods of Analysis.
Vertical Deflections in Girder 2TPCS
for a Sinusoidal Node Load.*

Node	Load at Node 1		Load at Node 2	
	Author's Solution	Alternative Solution	Author's Solution	Alternative Solution
1	.0562	.0563	.0428	.0432
2	.0423	.0432	.0441	.0449
3	.0254	.0258	.0309	.0313
4	.0195	.0206	.0249	.0258

*First Fourier term of a 10 K. midspan load. Deflections are expressed in in.

TABLE 23

Wheel Load Distribution Factors for Exterior and Interior Beams.
Multicell Box Girders with Axle Loads at Midspan.

Box Girder	Beam*	No Intermediate Diaphragm	Two Intermediate Diaphragms at 7L/18 and 11L/18	Midspan Diaphragm	Complete Distribution
2RC	E	1.13	1.11	1.05	1.05
	I	1.90	1.90	1.90	1.90
3RC Designed for 2 lanes	E	.92	.85	.75	.72
	I	1.33	1.33	1.29	1.28
3RC Designed for 3 lanes	E	1.16	1.14	1.08	1.08
	I	1.94	1.93	1.93	1.92
2TPC Designed for 2 lanes	E	.98	.98	.92	.86
	I	1.24	1.21	1.13	1.13
2TPC Designed for 3 lanes	E	1.33	1.33	1.32	1.30
	I	1.78	1.74	1.70	1.70

*E for exterior beam, I for interior beam.

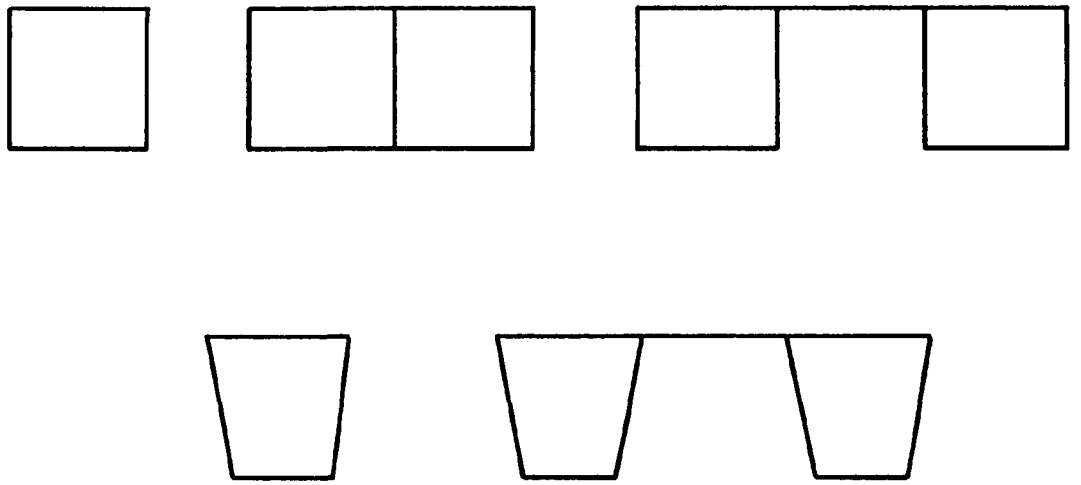

Figure 1. Typical Cross-Sections of Box Girders

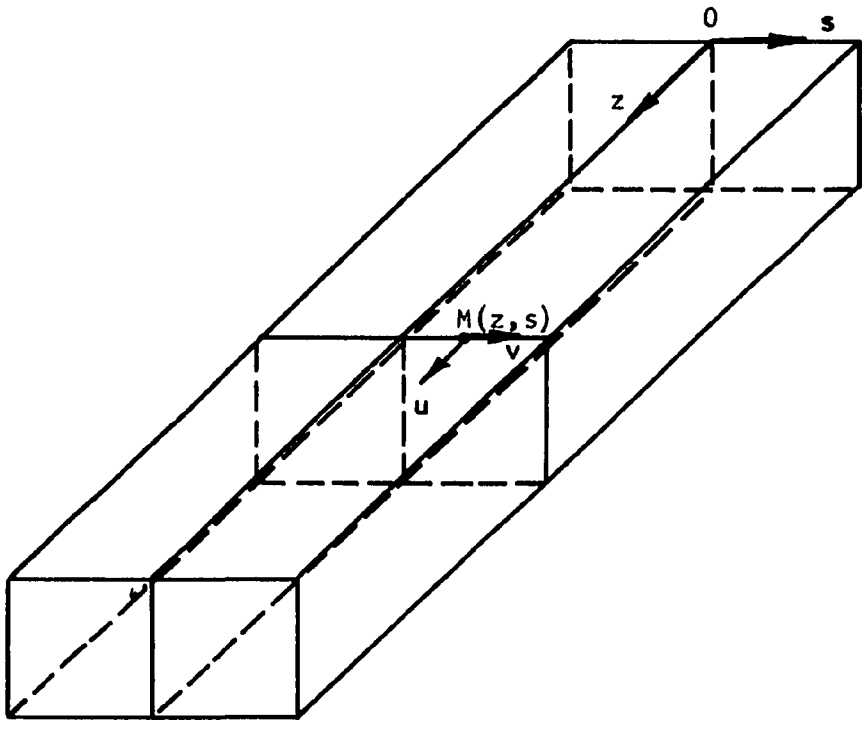

Figure 2. Coordinate System

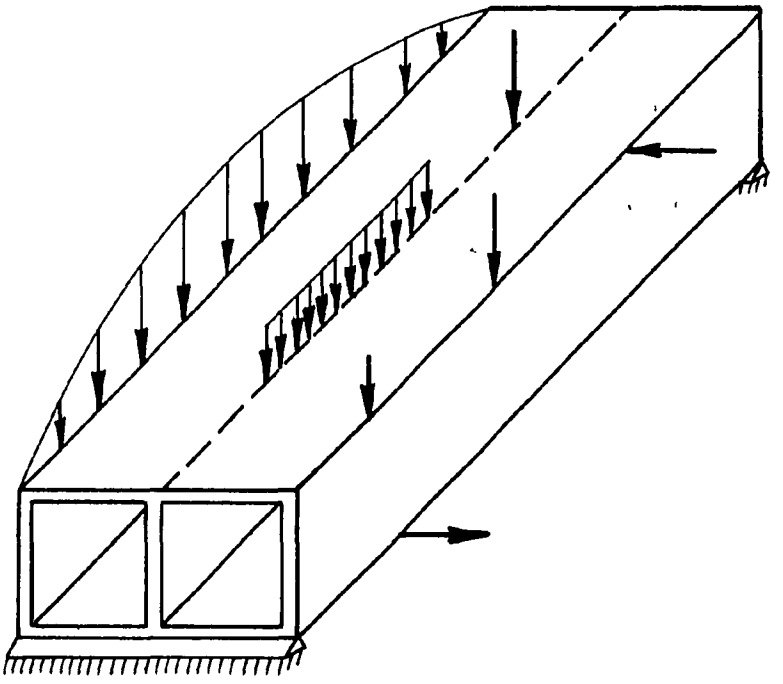

Figure 3. Types of Loads Considered

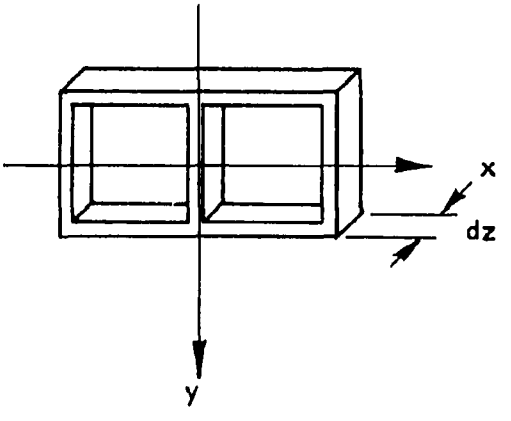

Figure 4. Elementary Strip

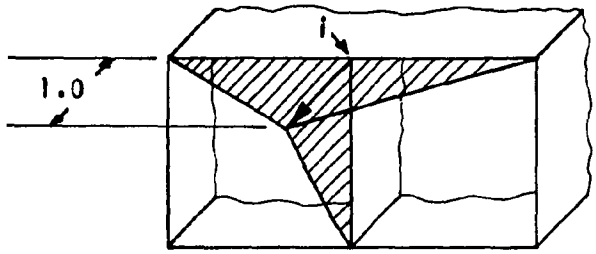

(a) Longitudinal Displacement of Node i - $\phi_i(s)$

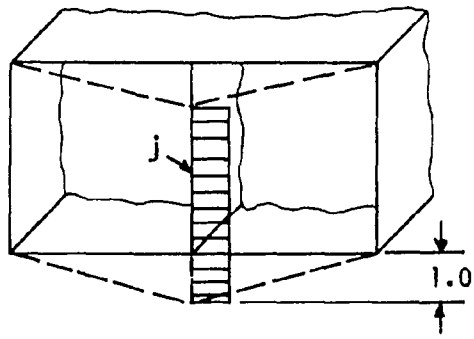

(b) Transverse Displacement of Member j - $\psi_k(s)$

Figure 5. Longitudinal and Transverse Displacement Patterns

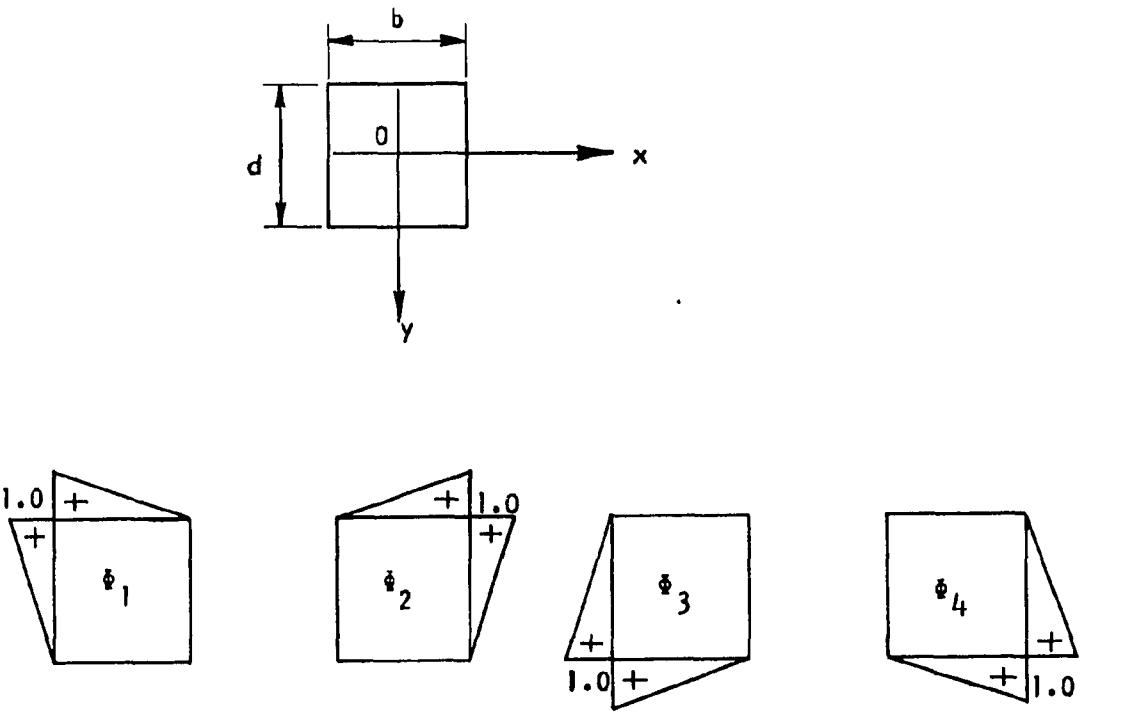

(a)

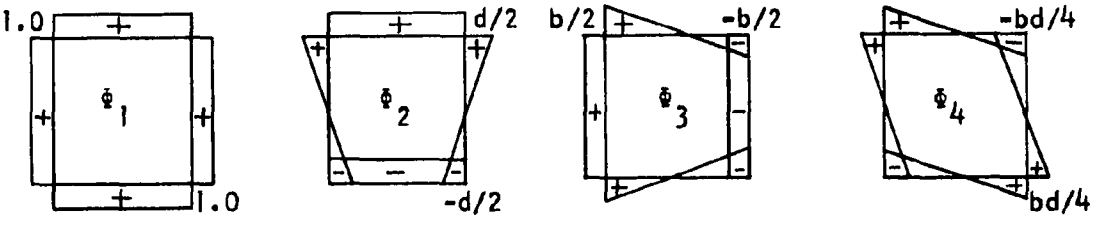

(b)

Figure 6. Longitudinal Generalized Coordinates of a Rectangular Box with Constant Thickness

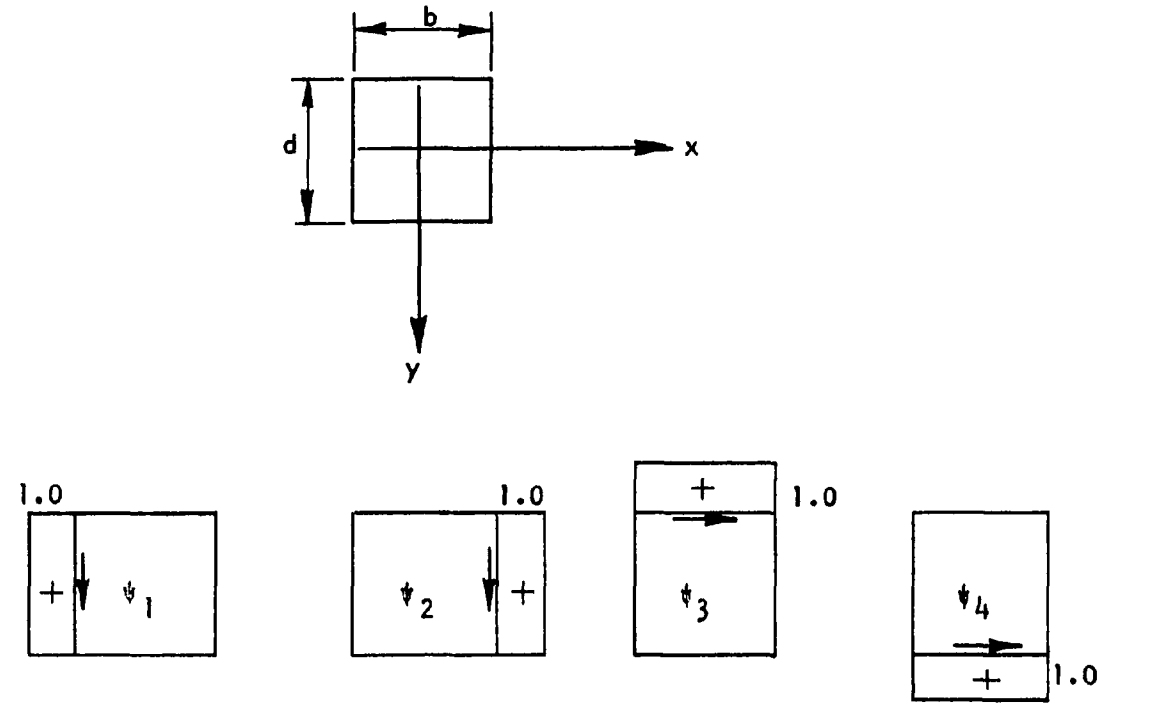

Figure 7. Transverse Generalized Coordinates of a Rectangular Box with Constant Thickness

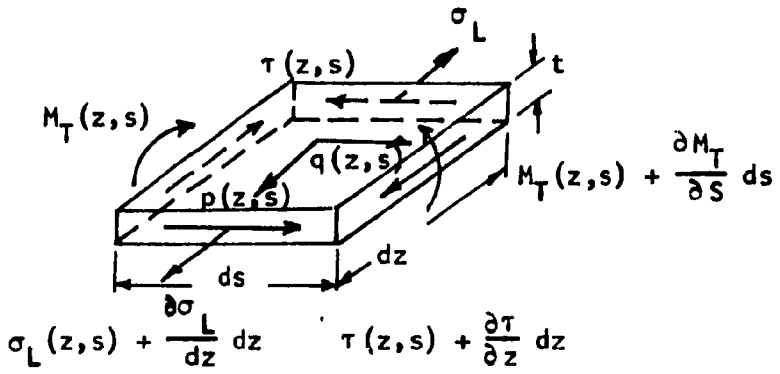

Figure 8. Forces Acting on an Element

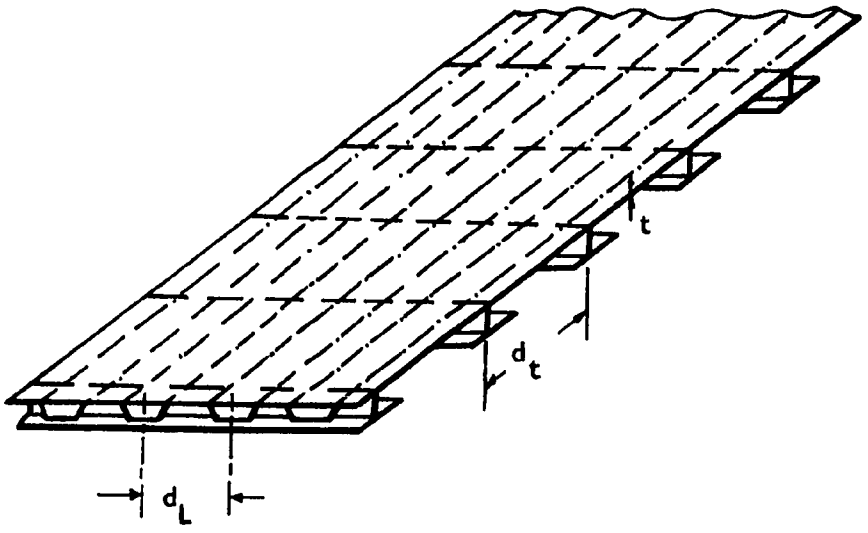

Figure 9. Stiffened Plate Element

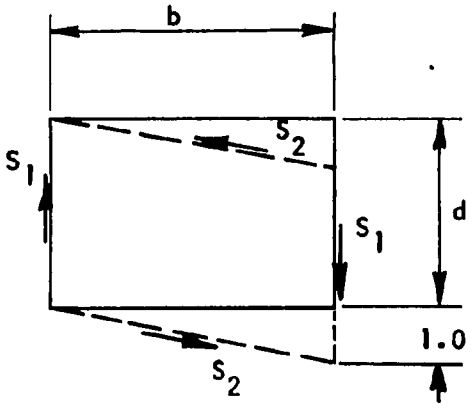

$$\Psi_h V_h = 1$$

Figure 10. Transverse Action of a Plate Diaphragm

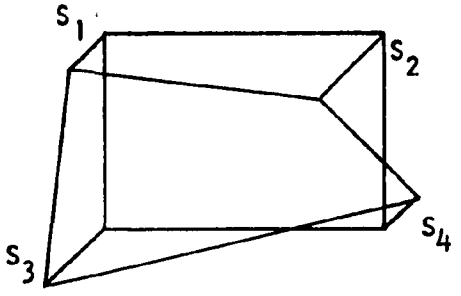

$$\Phi_i U_i = 1$$

Figure 11. Typical Longitudinal Deformation of a Plate Diaphragm

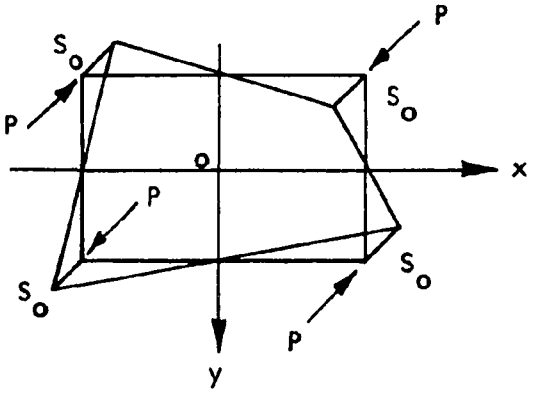

Figure 12. Longitudinal Action of a Plate Diaphragm

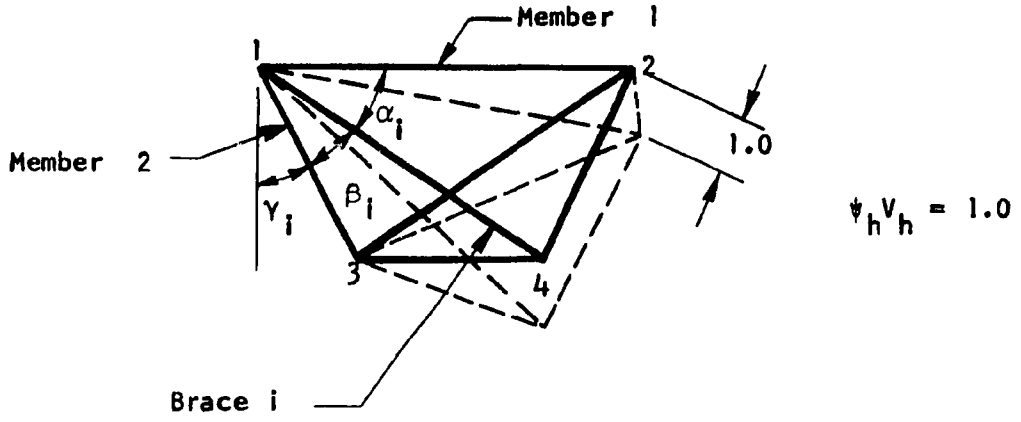

Figure 13. Transverse Action of an X-Brace

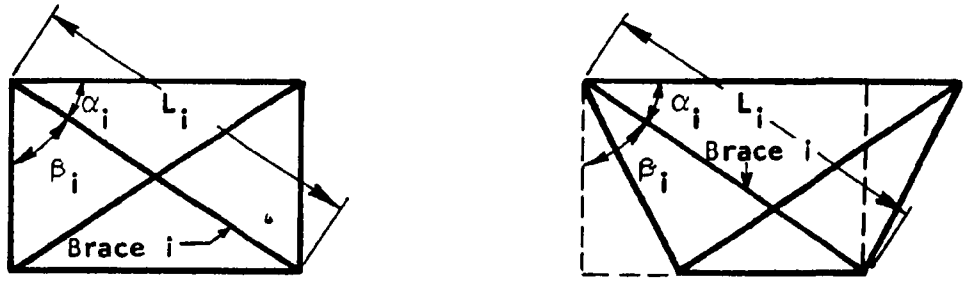

(a) Rectangular Plate

(b) Trapezoidal Plate

Figure 14. Equivalent X-Brace

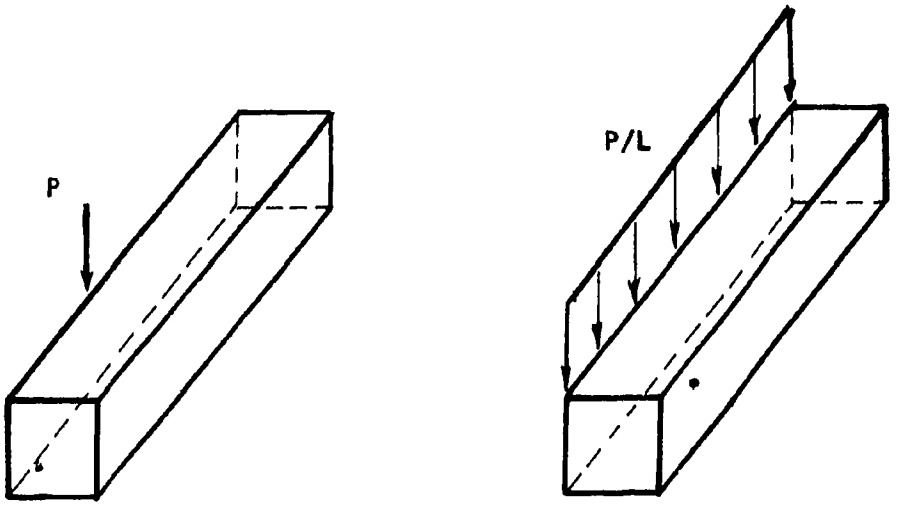

Figure 15. Loads Applied on Single Cell Girders

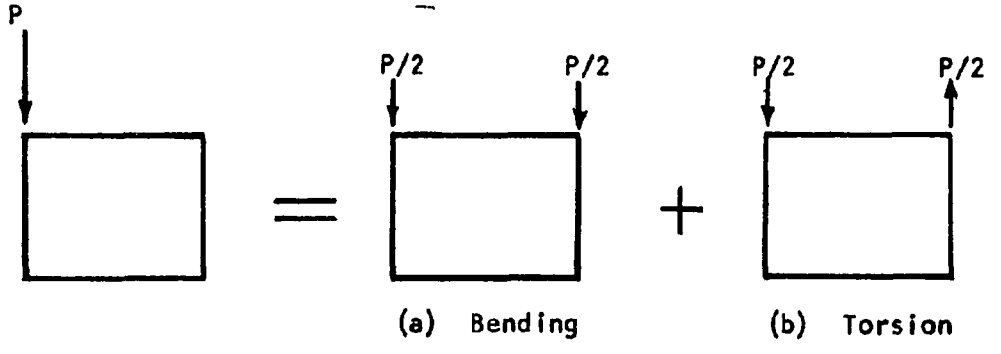

Figure 16. Resolution of a Node Load

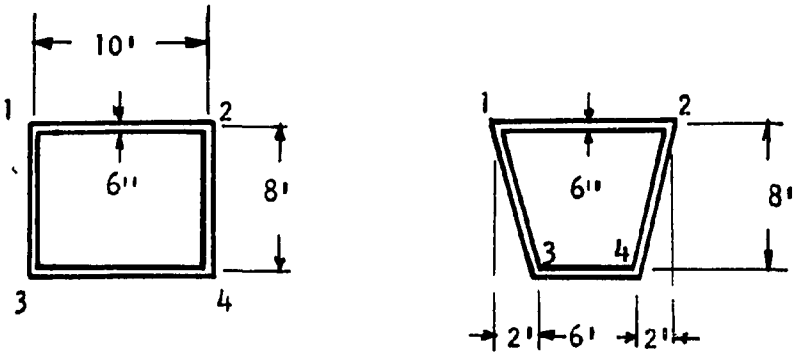

(a) IRC

(b) ITC

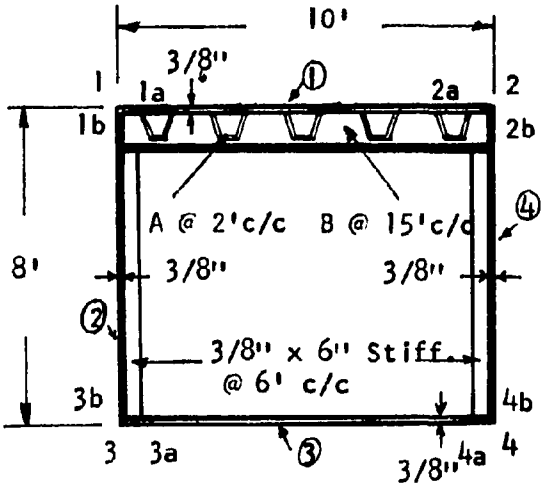

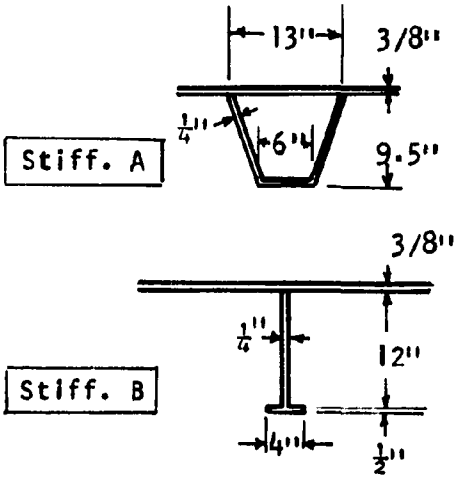

(c) IRS

(d) Stiffeners of IRS

Figure 17. Cross-Sections of Single Cell Box Girders

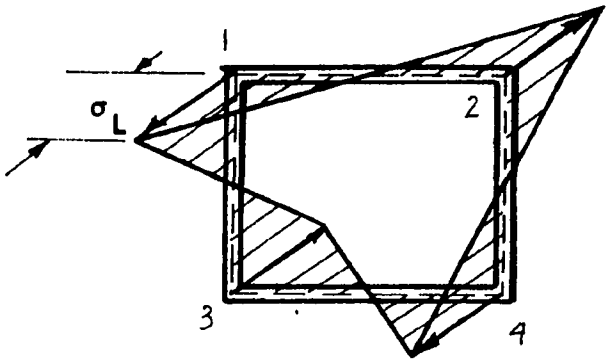

(a) Longitudinal Axial Stress

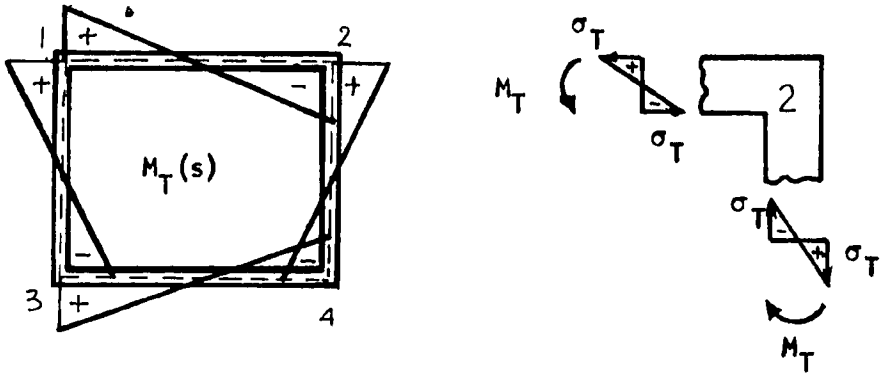

(b) Transverse Bending Moment and Stress

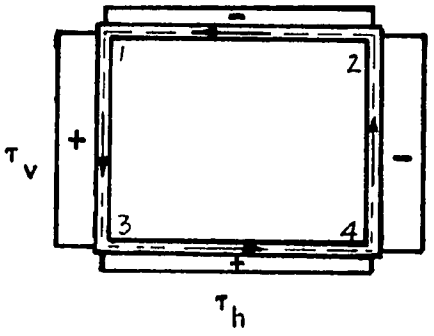

(c) Shear

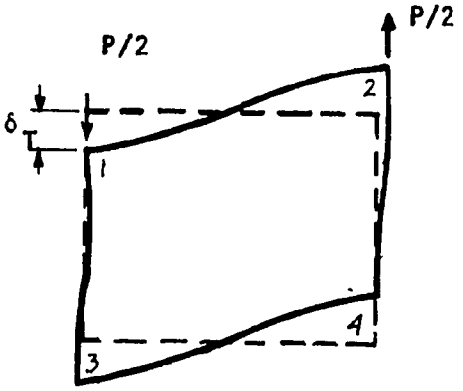

(d) Deflection

Figure 18. Stress and Deformation Patterns Induced in Girder 1RC by a Torsional Load

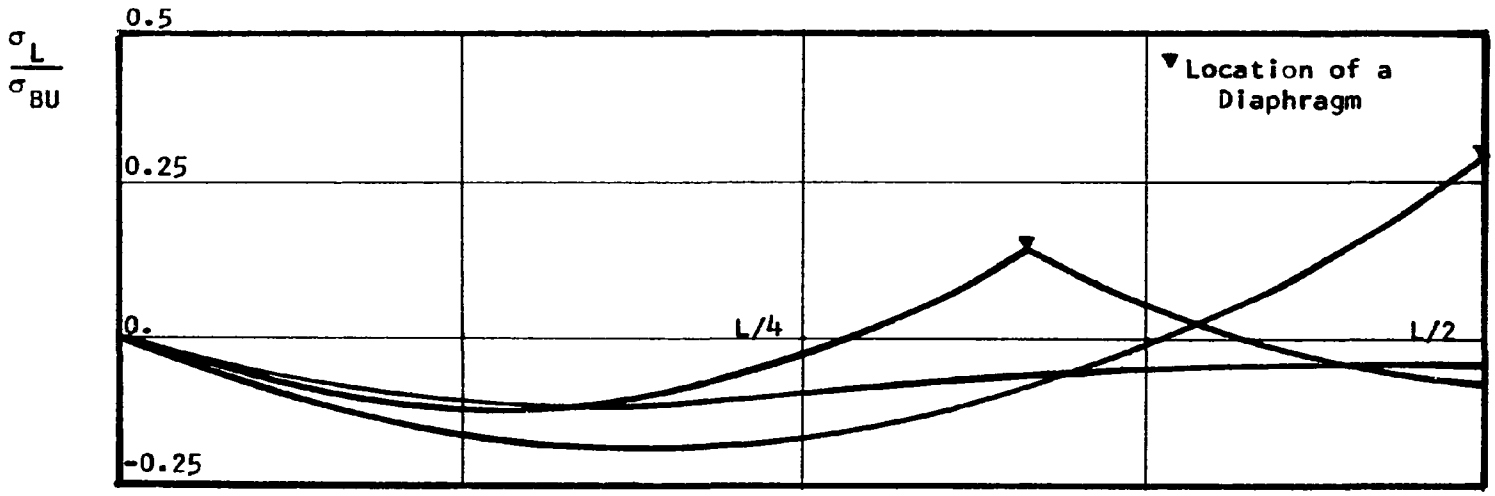

Figure 19. Variation of σ_L Along Girder 1RC. Simply Supported Ends. Uniform Torsional Load.

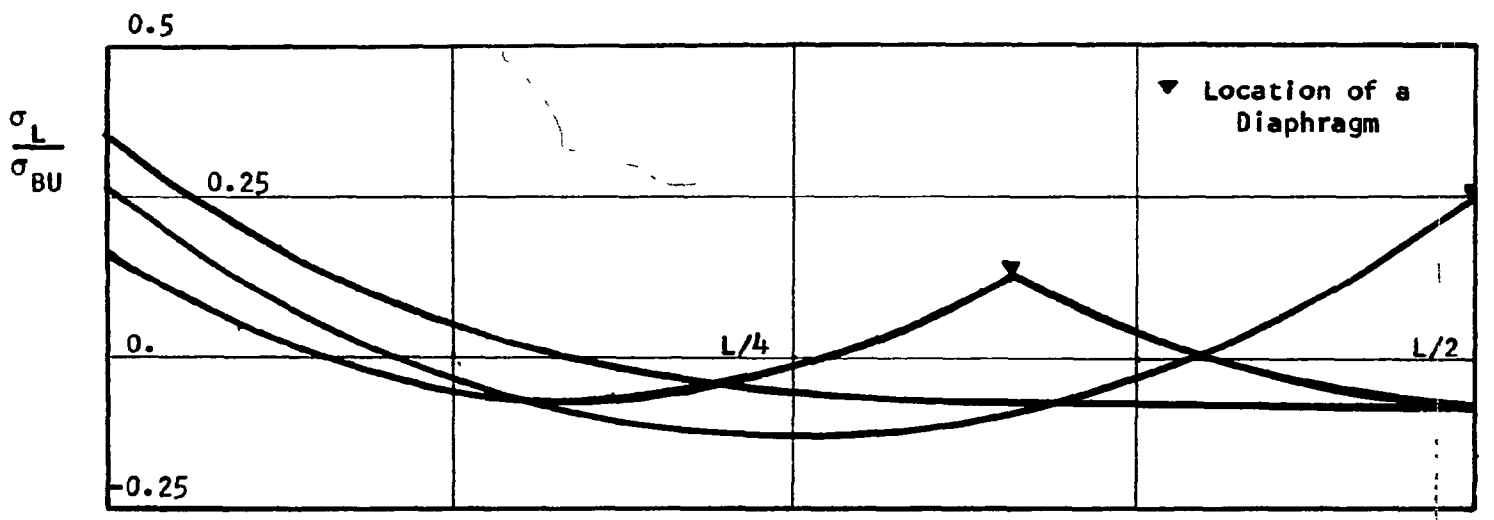

Figure 20. Variation of σ_L Along Girder 1RC. Fixed Ends. Uniform Torsional Load.

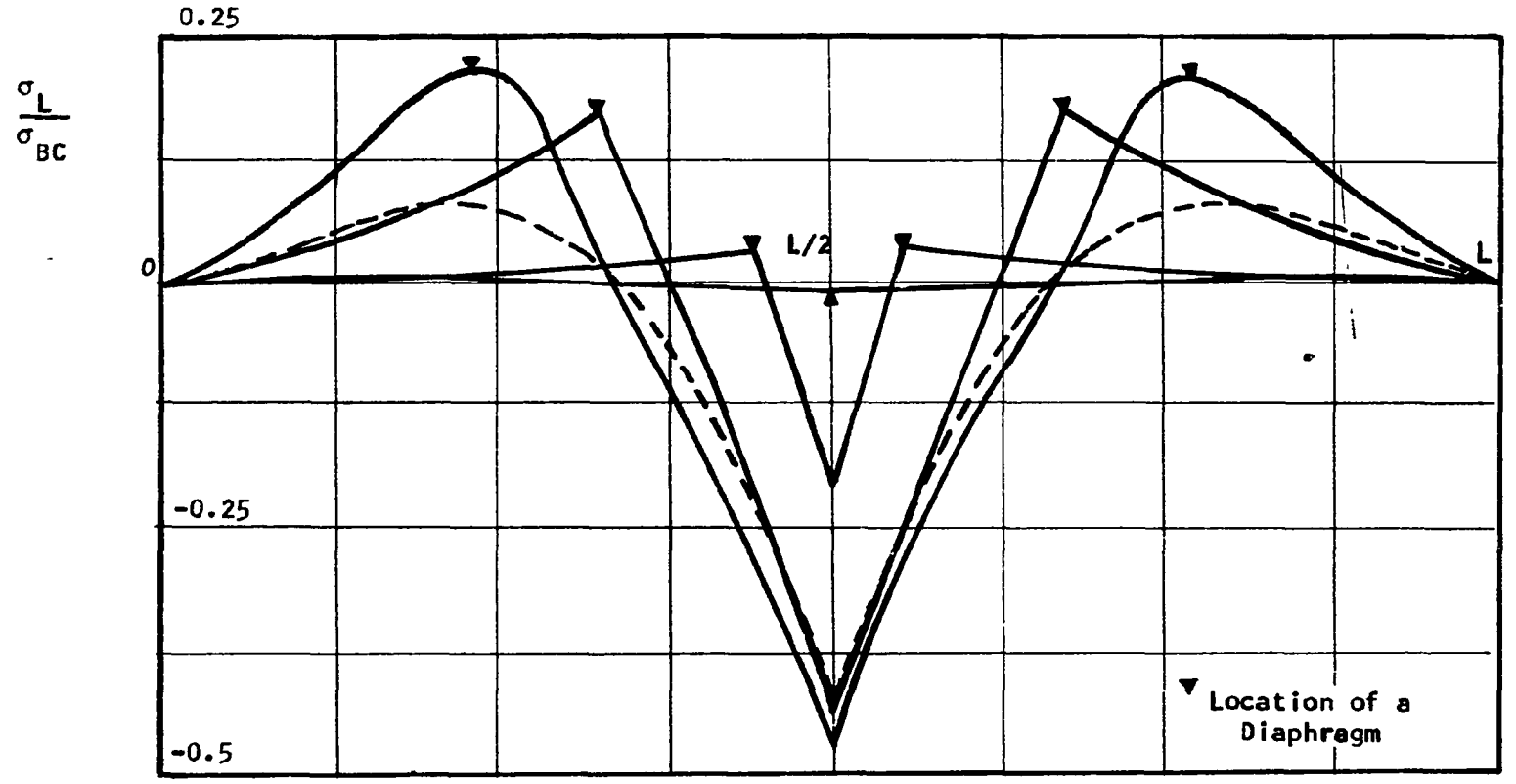

Figure 21. Variation of σ_L Along Girder 1RC. Simply Supported Ends. Concentrated Torsional Load at L/2.

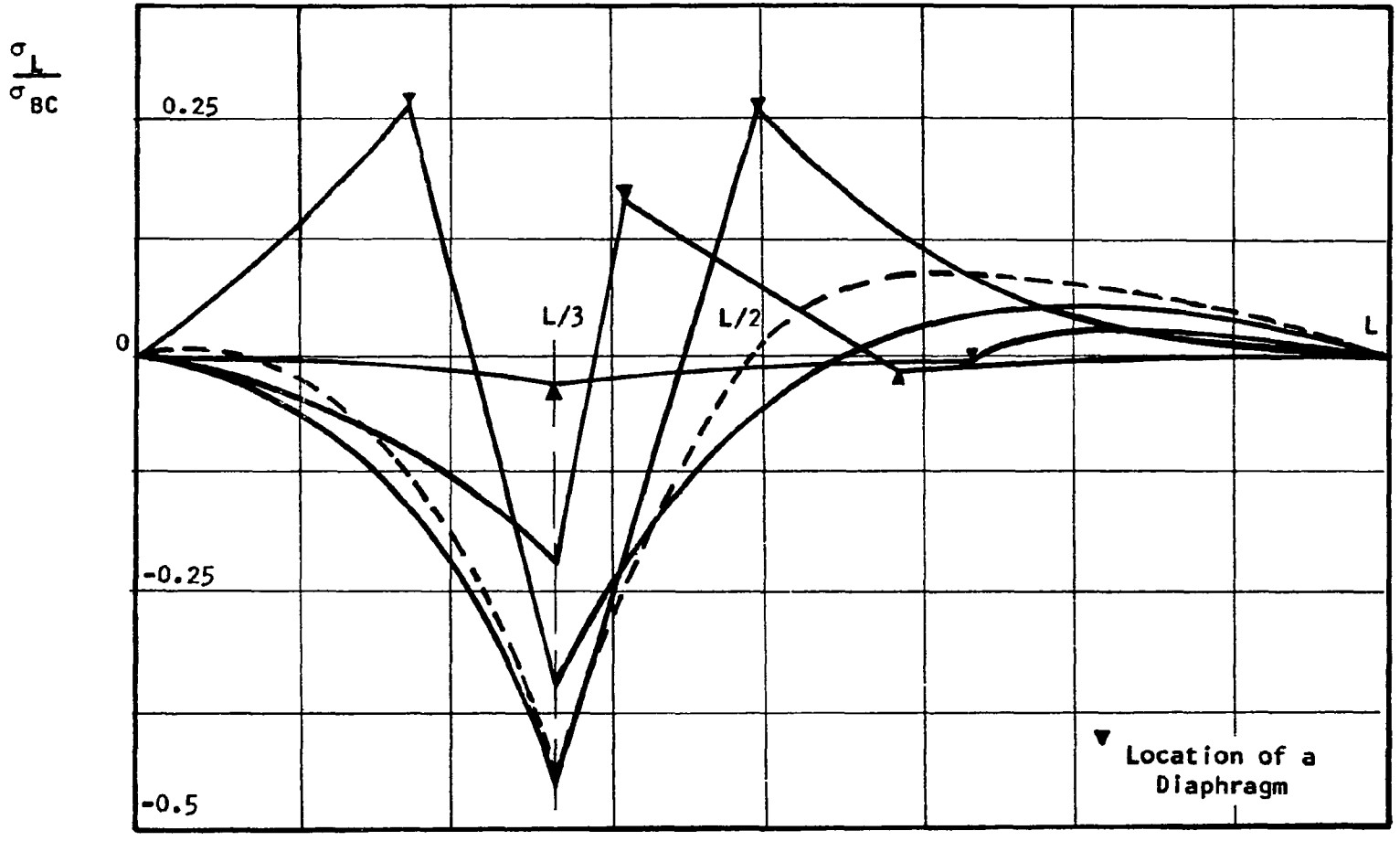

Figure 22. Variation of σ_L along Girder IRC. Simply Supported Ends. Concentrated Torsional Load at L/3.

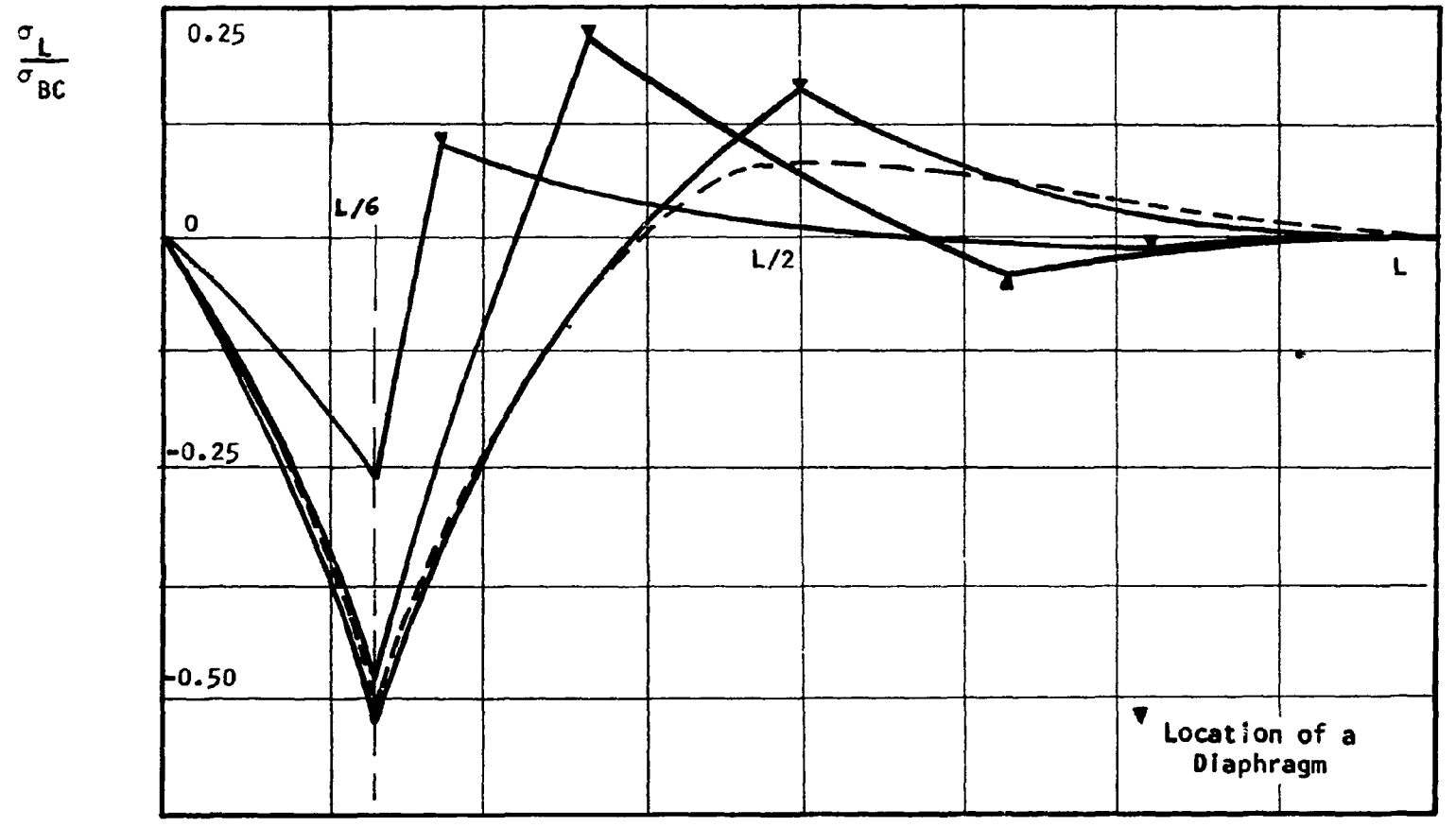

Figure 23. Variation of σ_L Along Girder IRC. Simply Supported Ends. Concentrated Torsional Load at L/6.

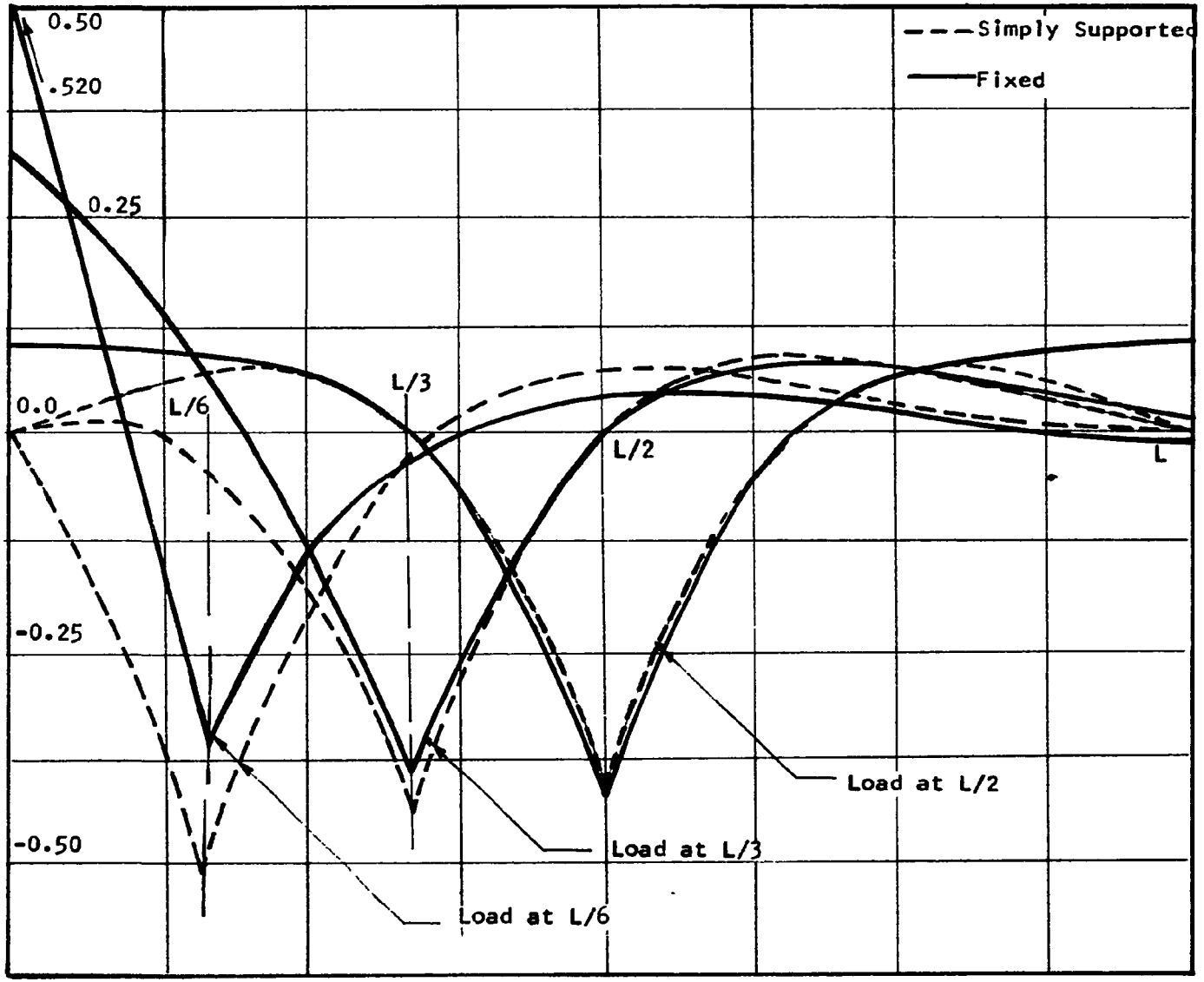

Figure 24. Effect of End Fixity on σ_L. Girder IRC under Concentrated Torsional Loads (End Diaphragms Only).

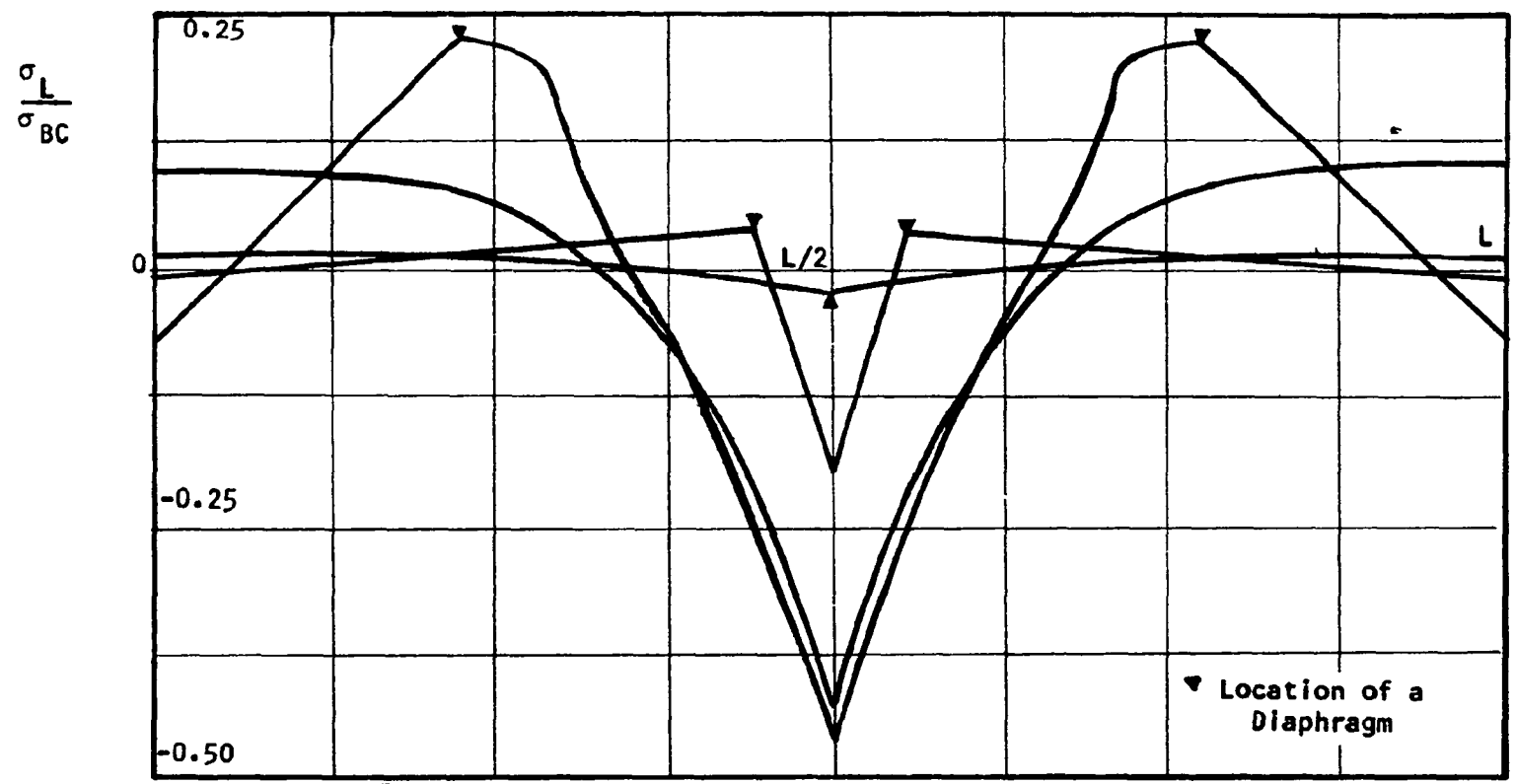

Figure 25. Variation of σ_L Along Girder 1RC. Fixed Ends. Concentrated Torsional Load at L/2.

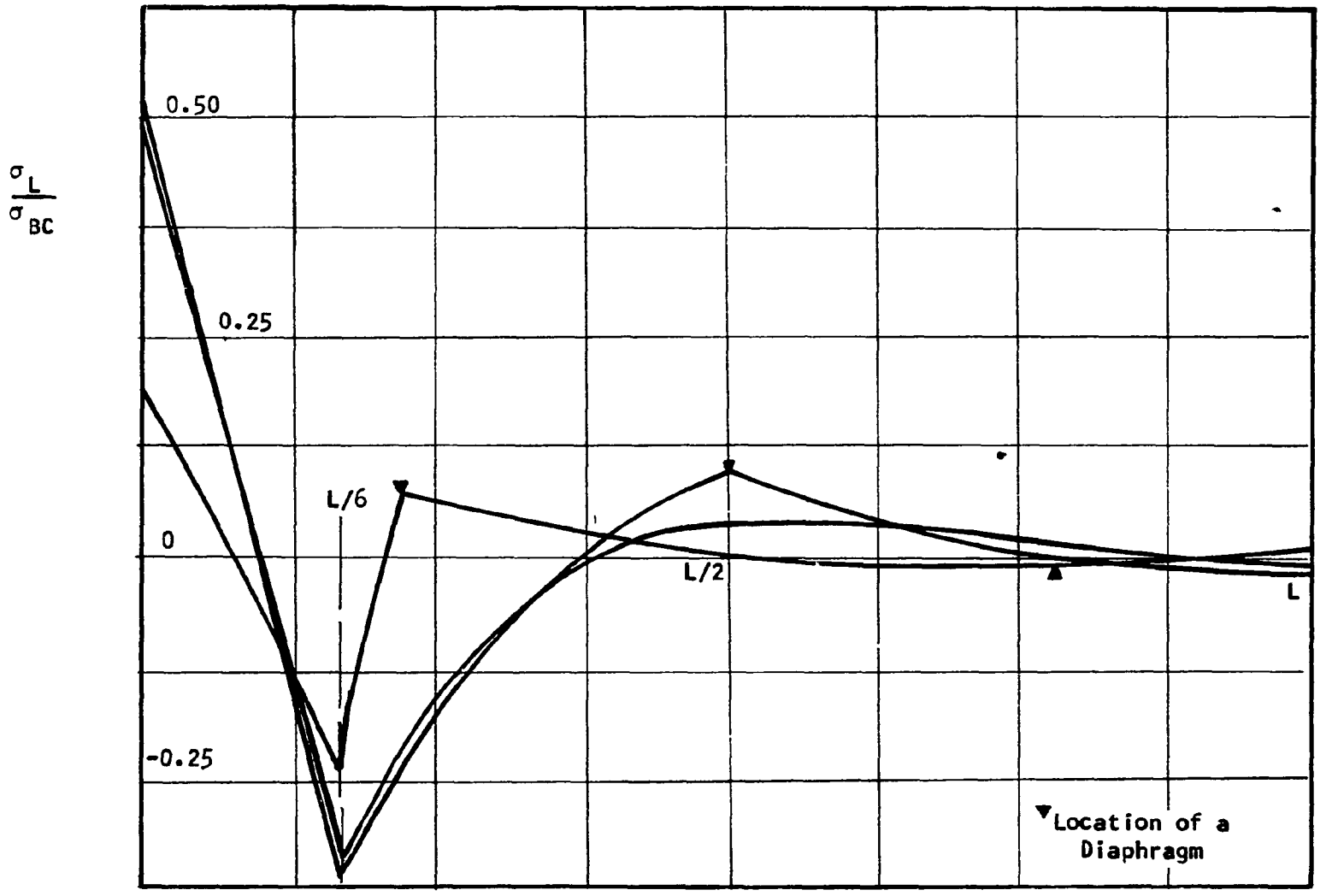

Figure 26. Variation of σ_L Along Girder IRC. Fixed Ends. Concentrated Torsional Load at L/6.

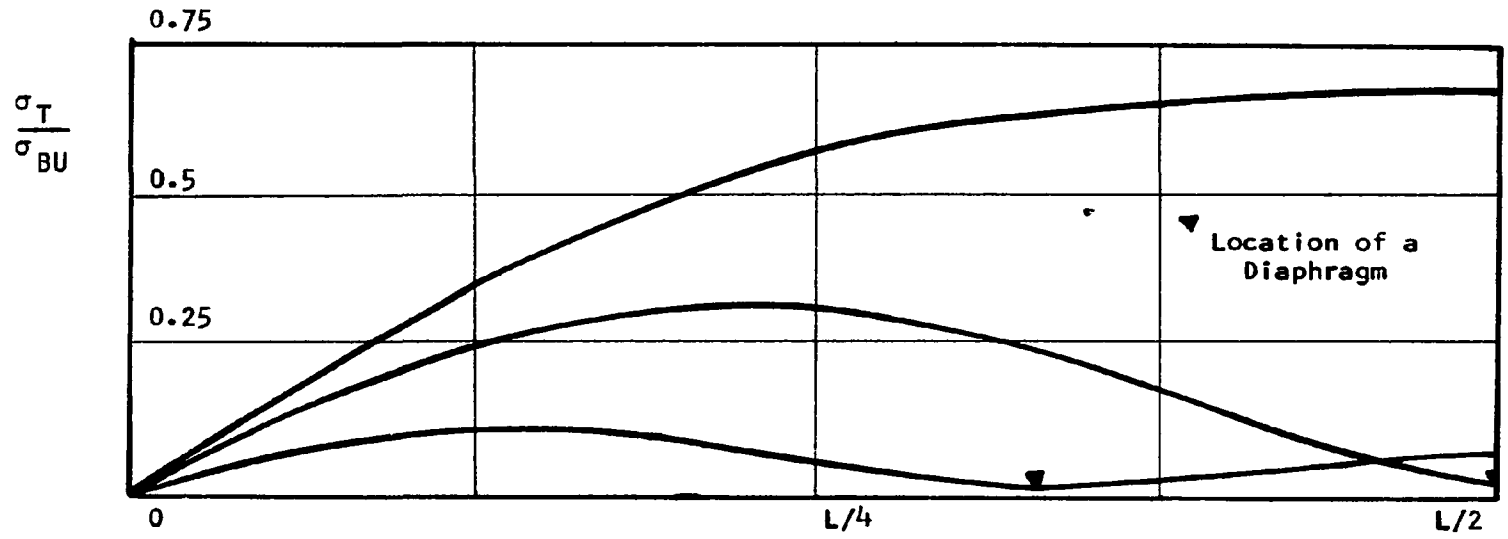

Figure 27. Variation of σ_T Along Girder IRC. Simply Supported Ends. Uniform Torsional Load.

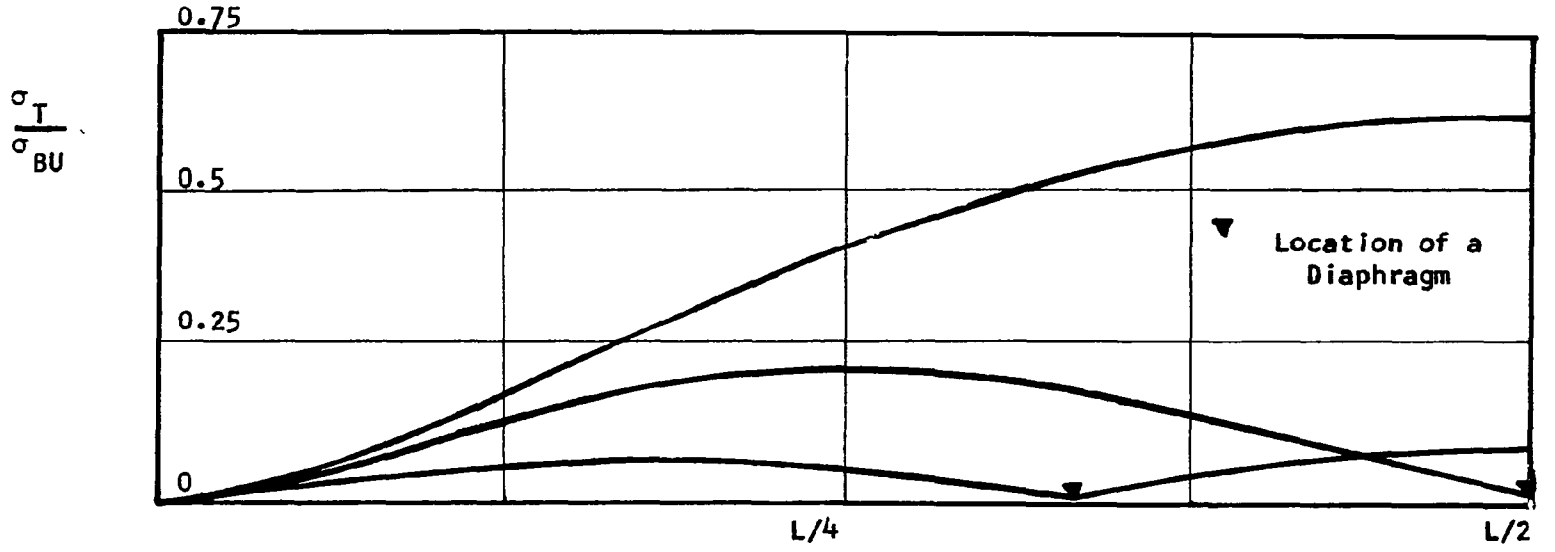

Figure 28. Variation of σ_T Along Girder 1RC. Fixed Ends. Uniform Torsional Load.

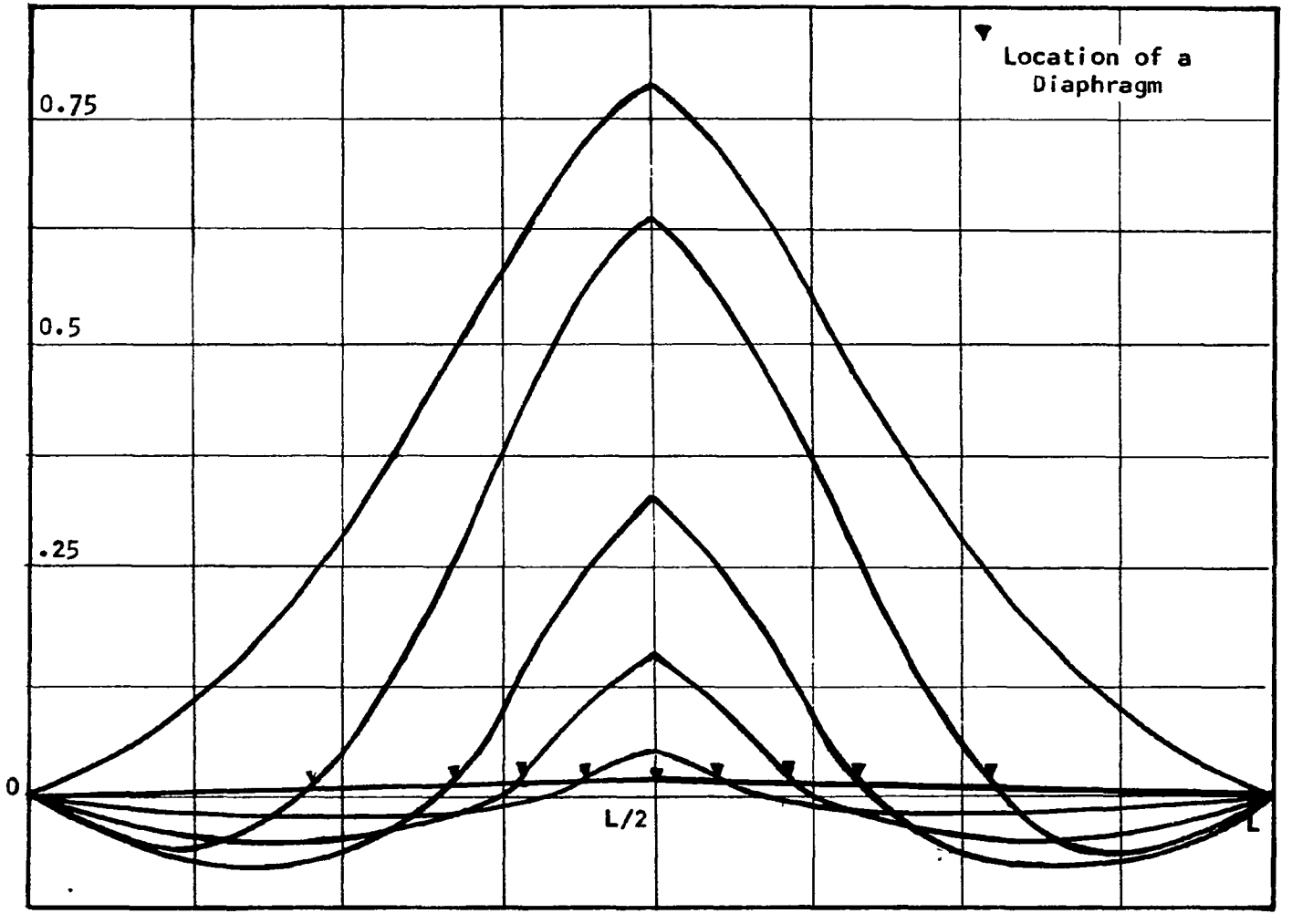

Figure 29. Variation of σ_T Along Girder 1RC. Simply Supported Ends. Concentrated Torsional Load at L/2.

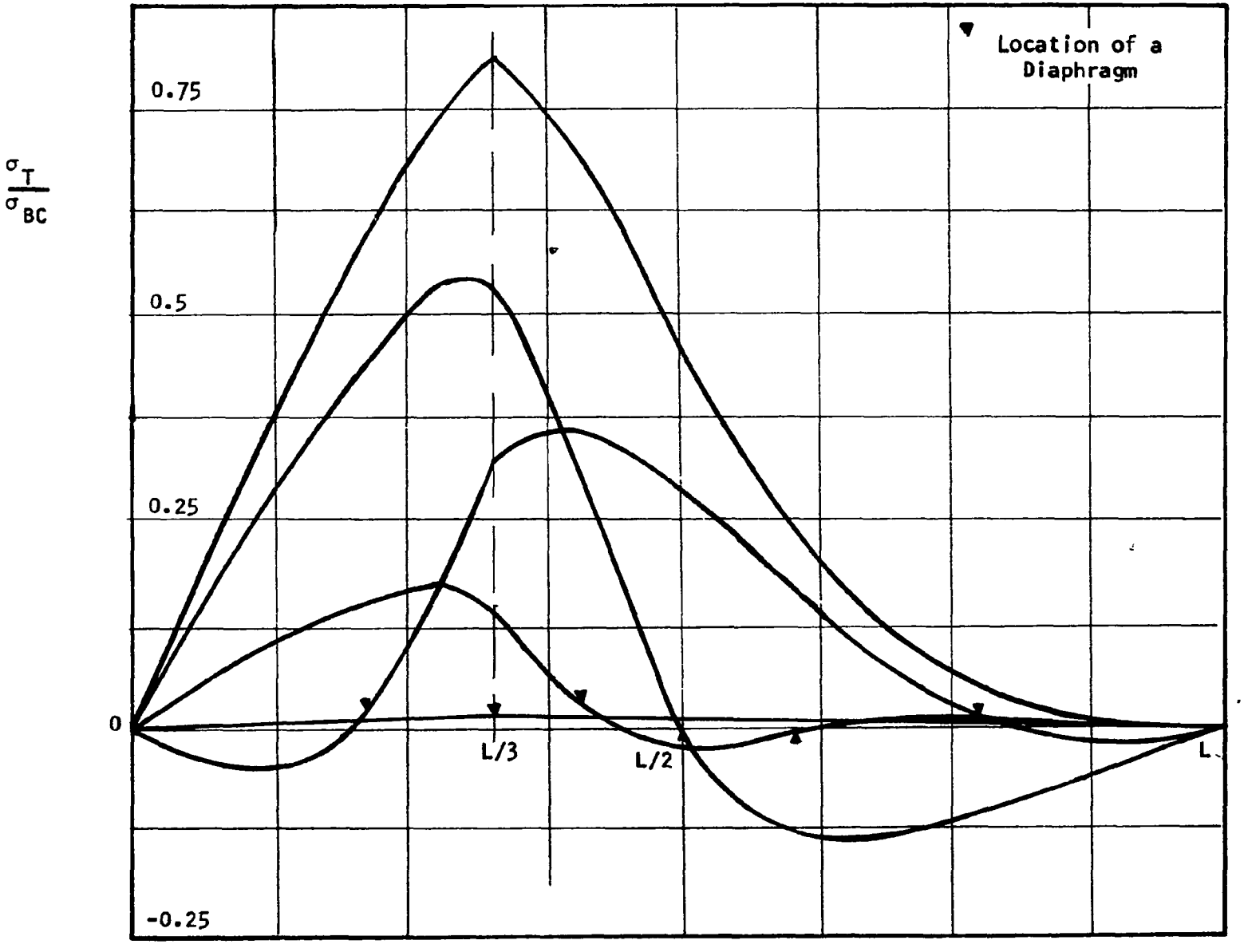

Figure 30. Variation of σ_T Along Girder IRC. Simply Supported Ends. Concentrated Torsional Load at L/3.

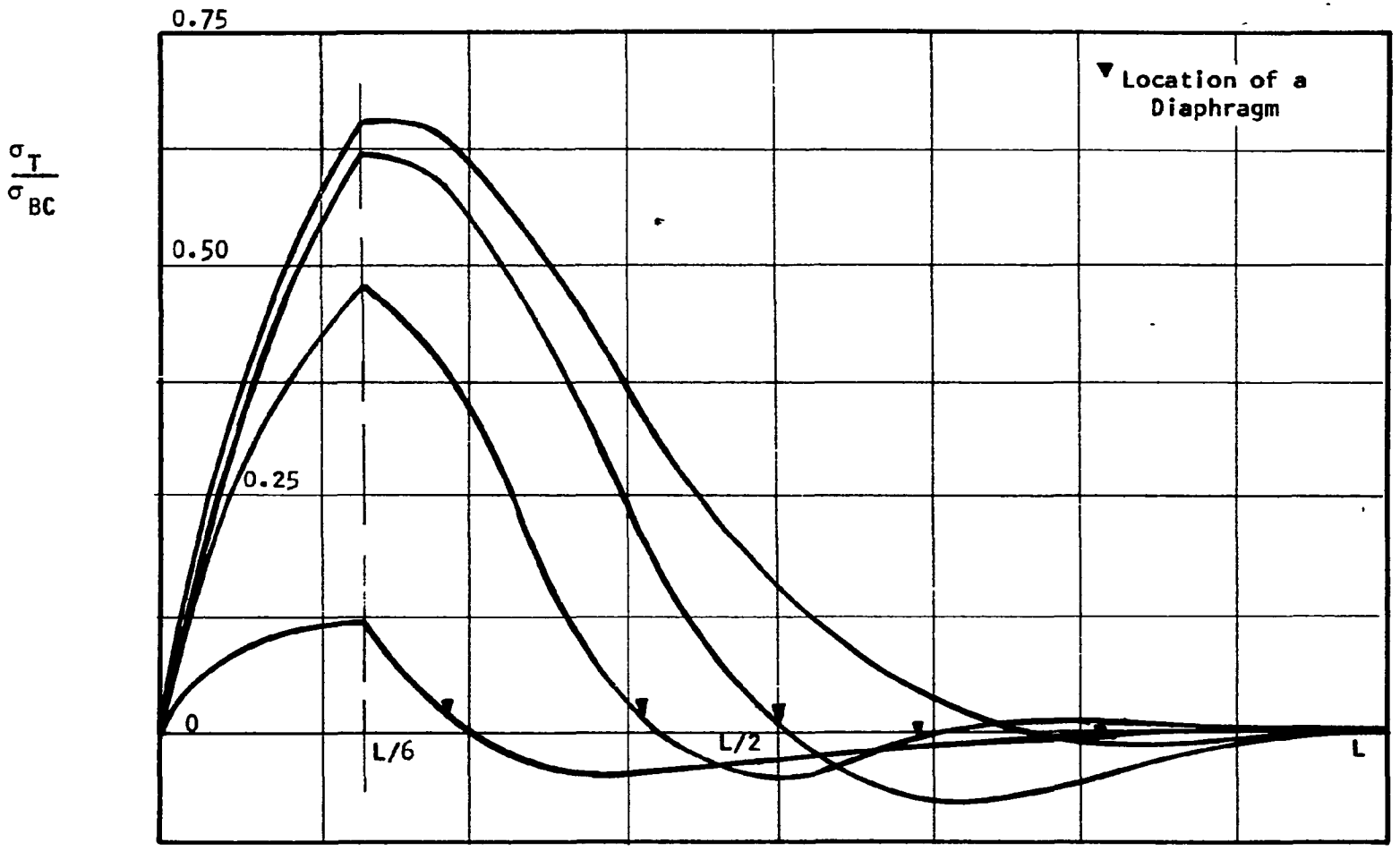

Figure 31. Variation of σ_T Along Girder 1RC. Simply Supported Ends. Concentrated Torsional Load at L/6.

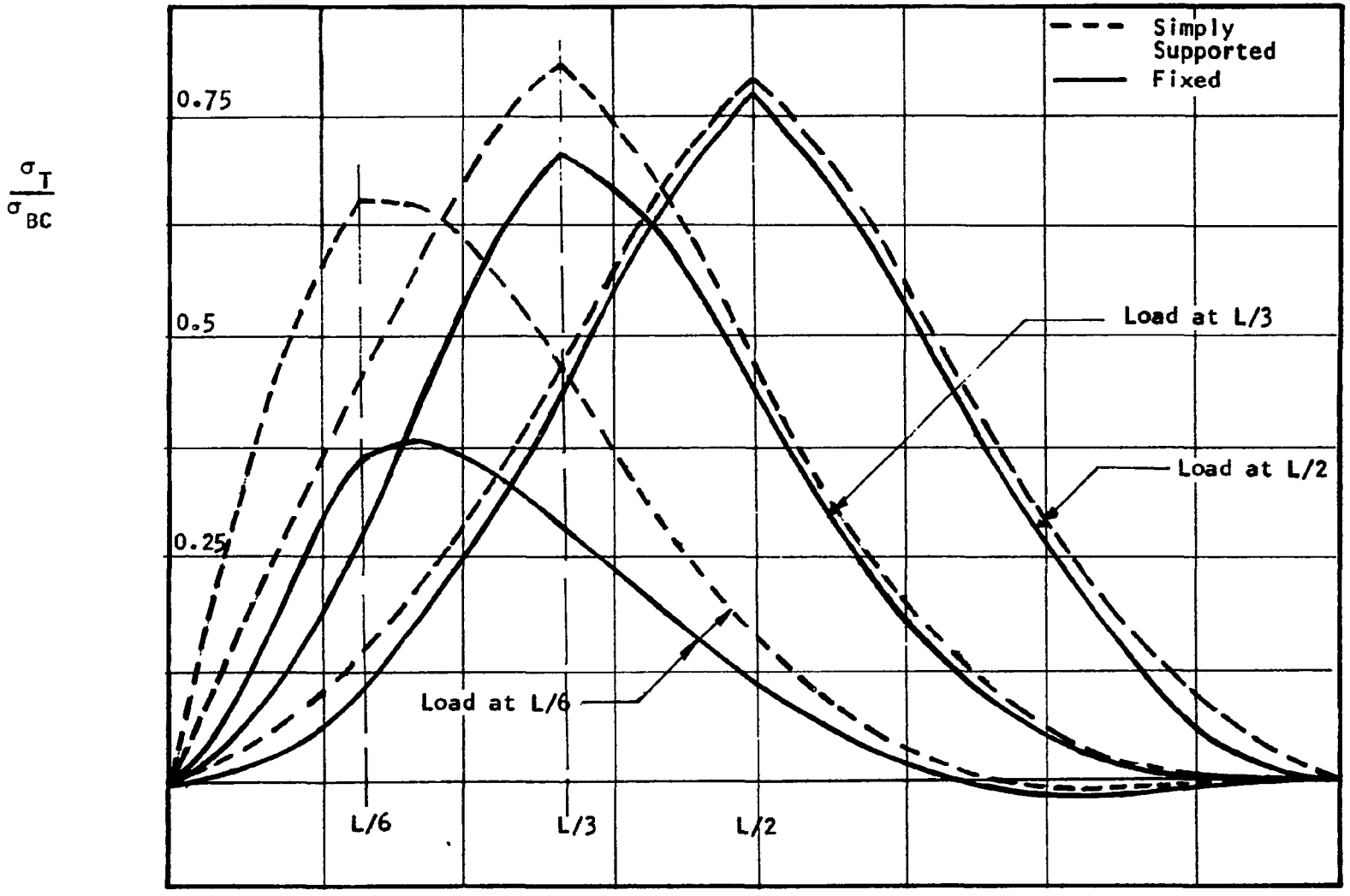

Figure 32. Effect of End Fixity on σ_T. Girder IRC under Concentrated Torsional Loads (End Diaphragms Only).

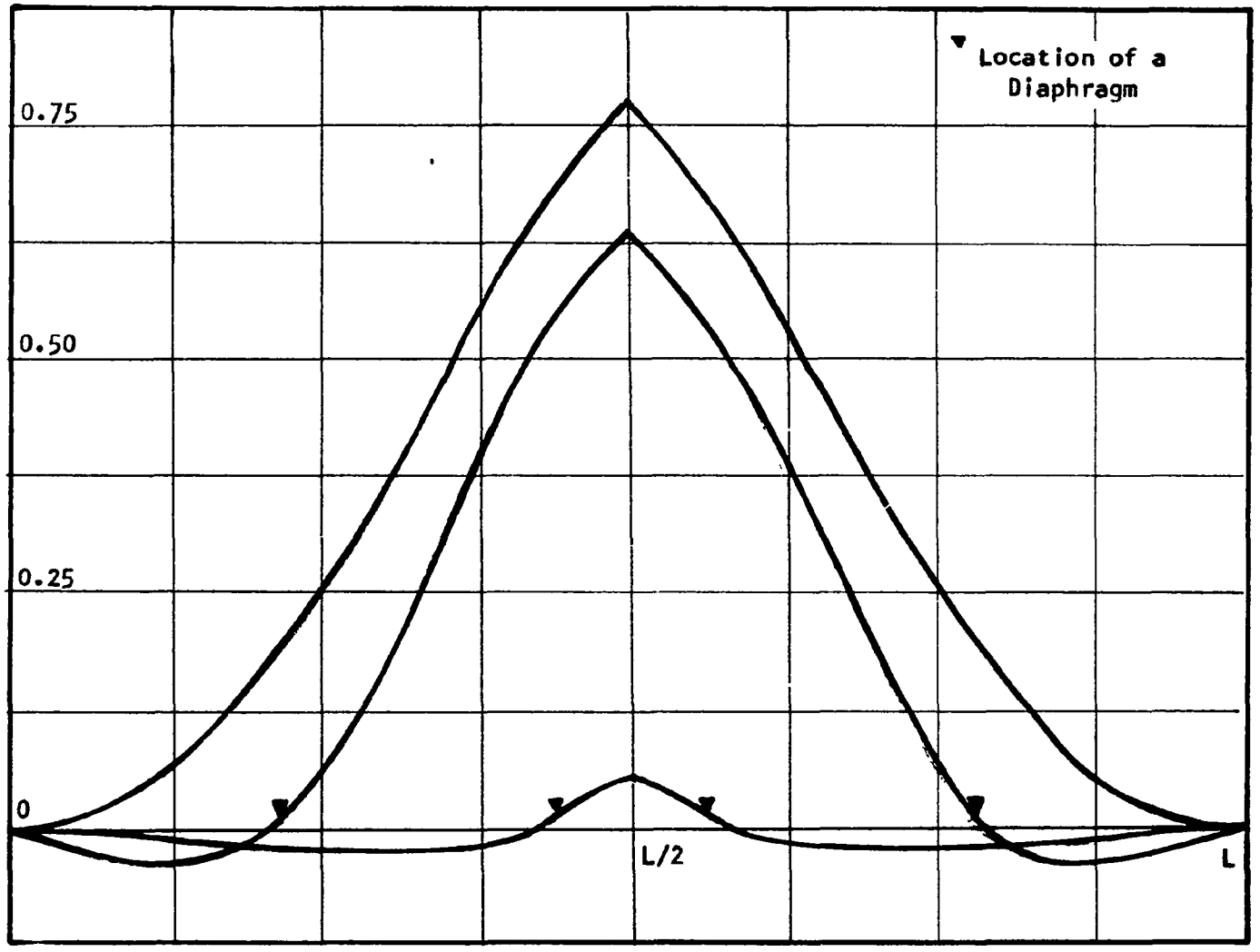

Figure 33. Variation of σ_T Along Girder 1RC. Fixed Ends. Concentrated Torsional Load at L/2.

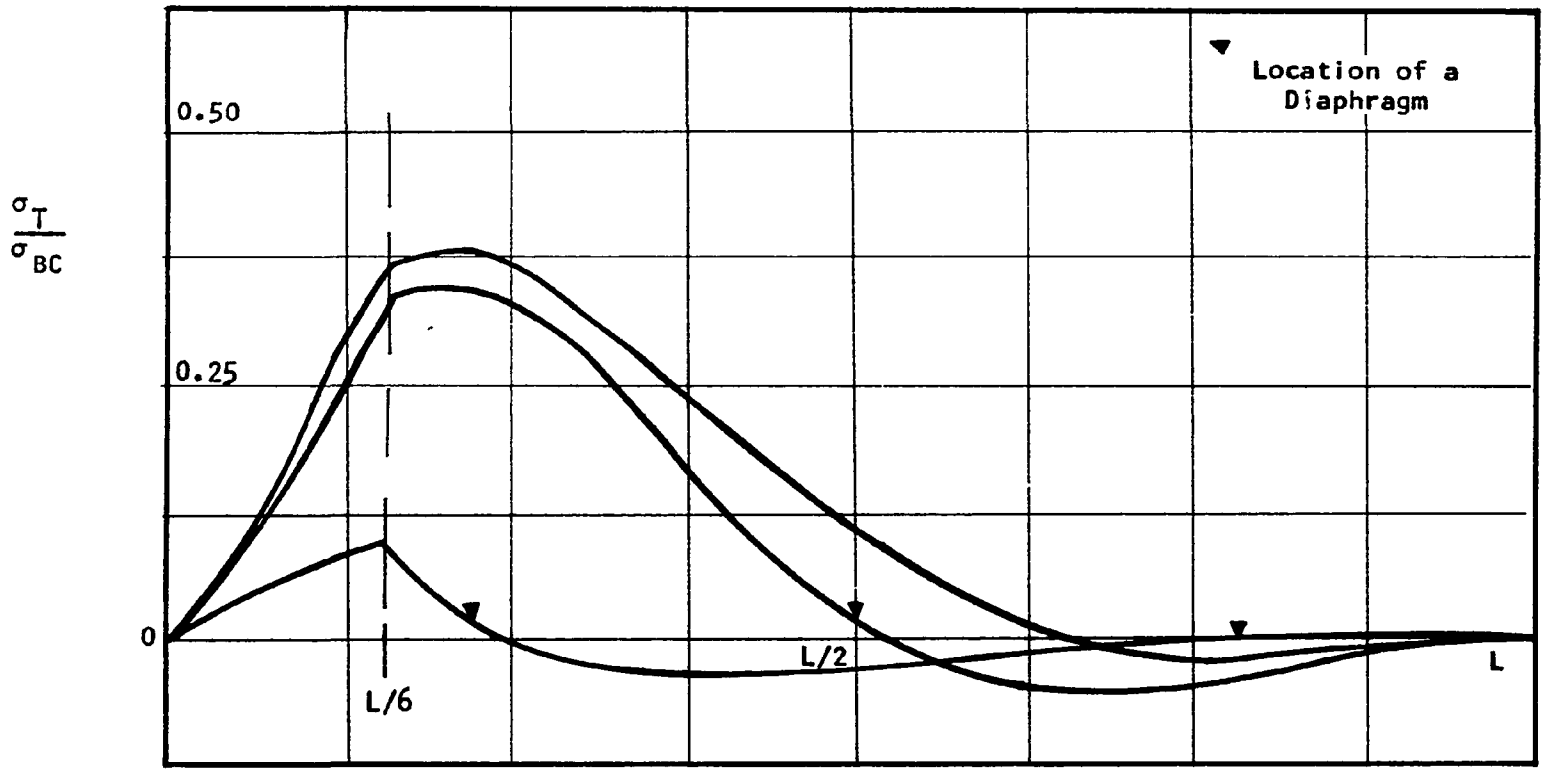

Figure 34. Variation of σ_T Along Girder IRC. Fixed Ends. Concentrated Torsional Load at L/6.

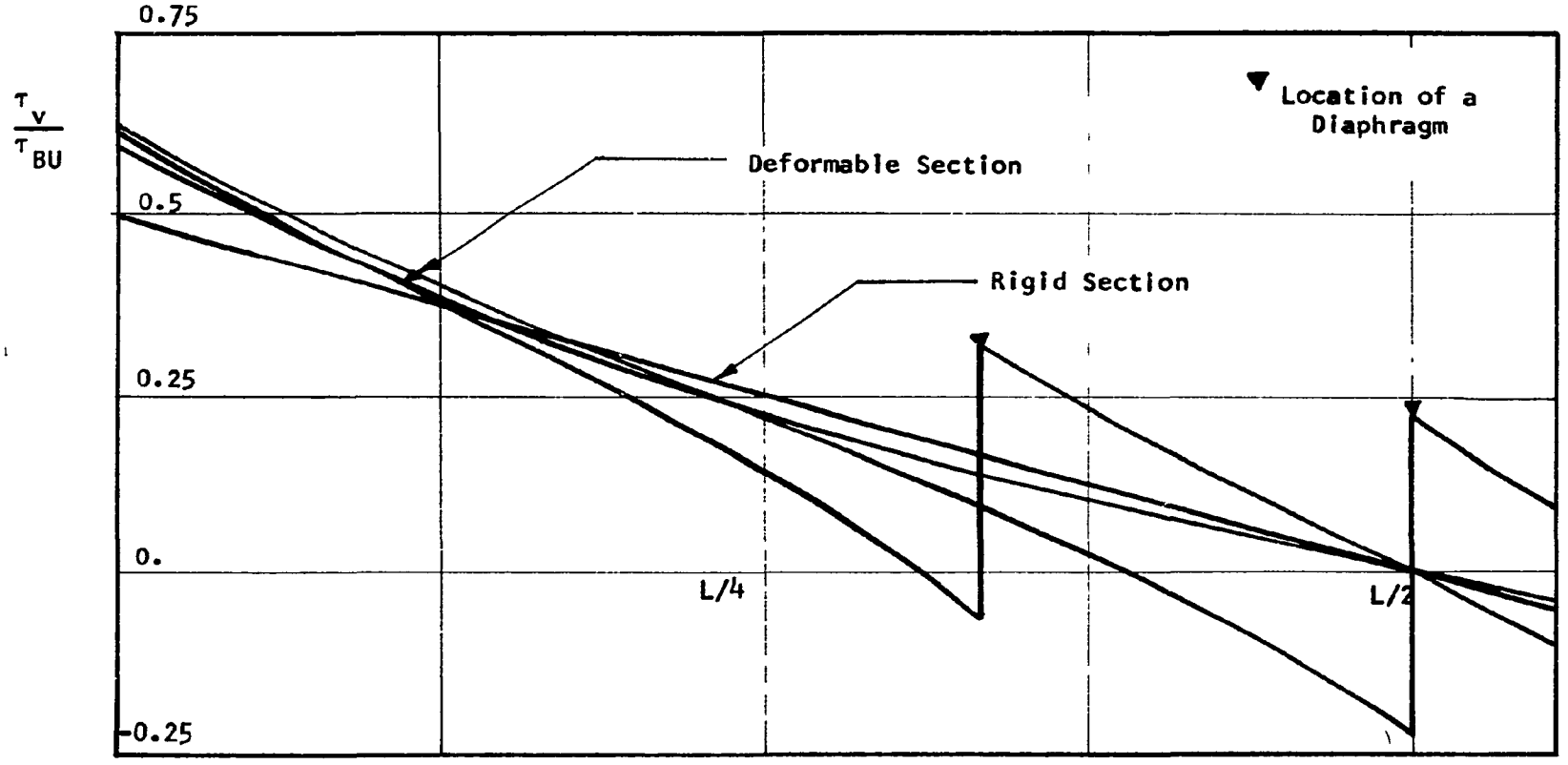

Figure 35. Variation of τ_v Along Girder 1RC. Simply Supported Ends. Uniform Torsional Load.

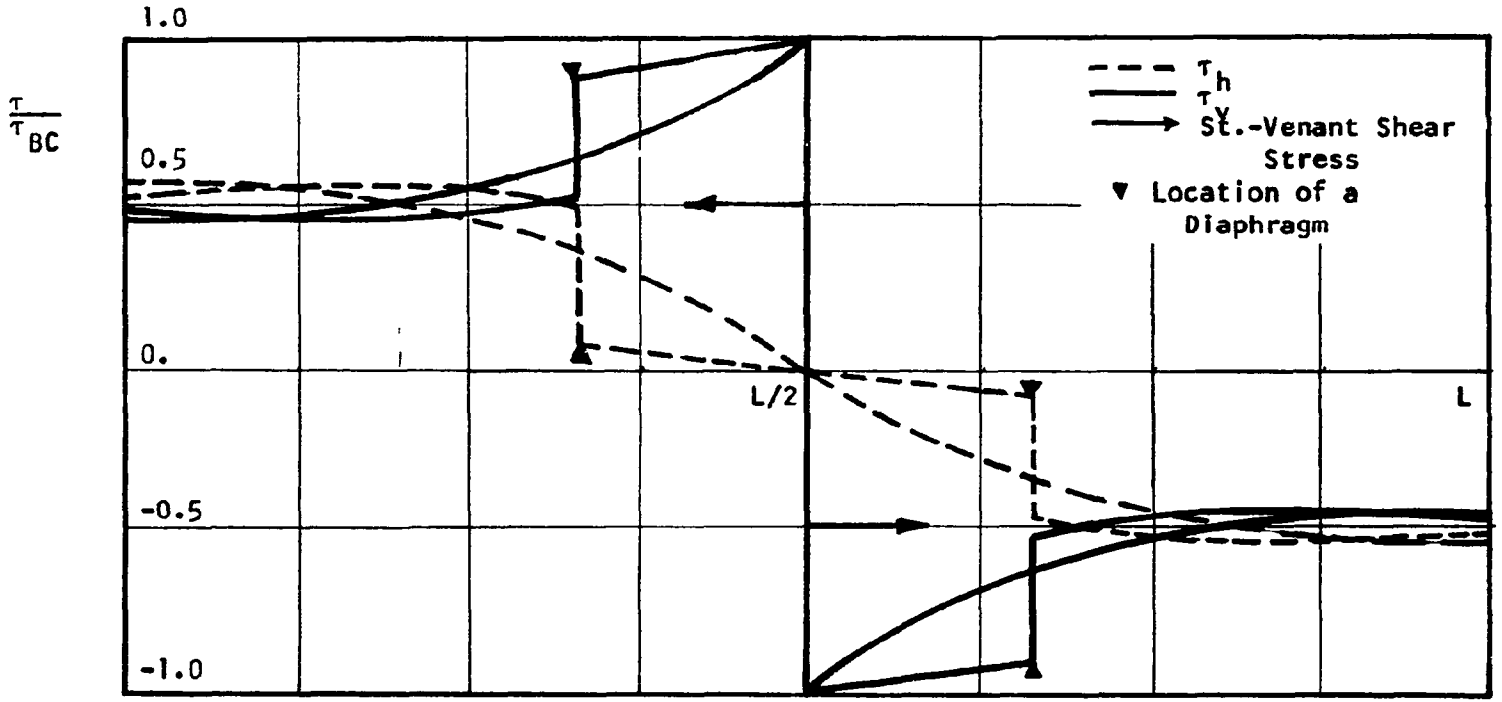

Figure 36. Variation of τ_v and τ_h Along Girder 1RC.
Simply Supported Ends. Concentrated Torsional Load at L/2.

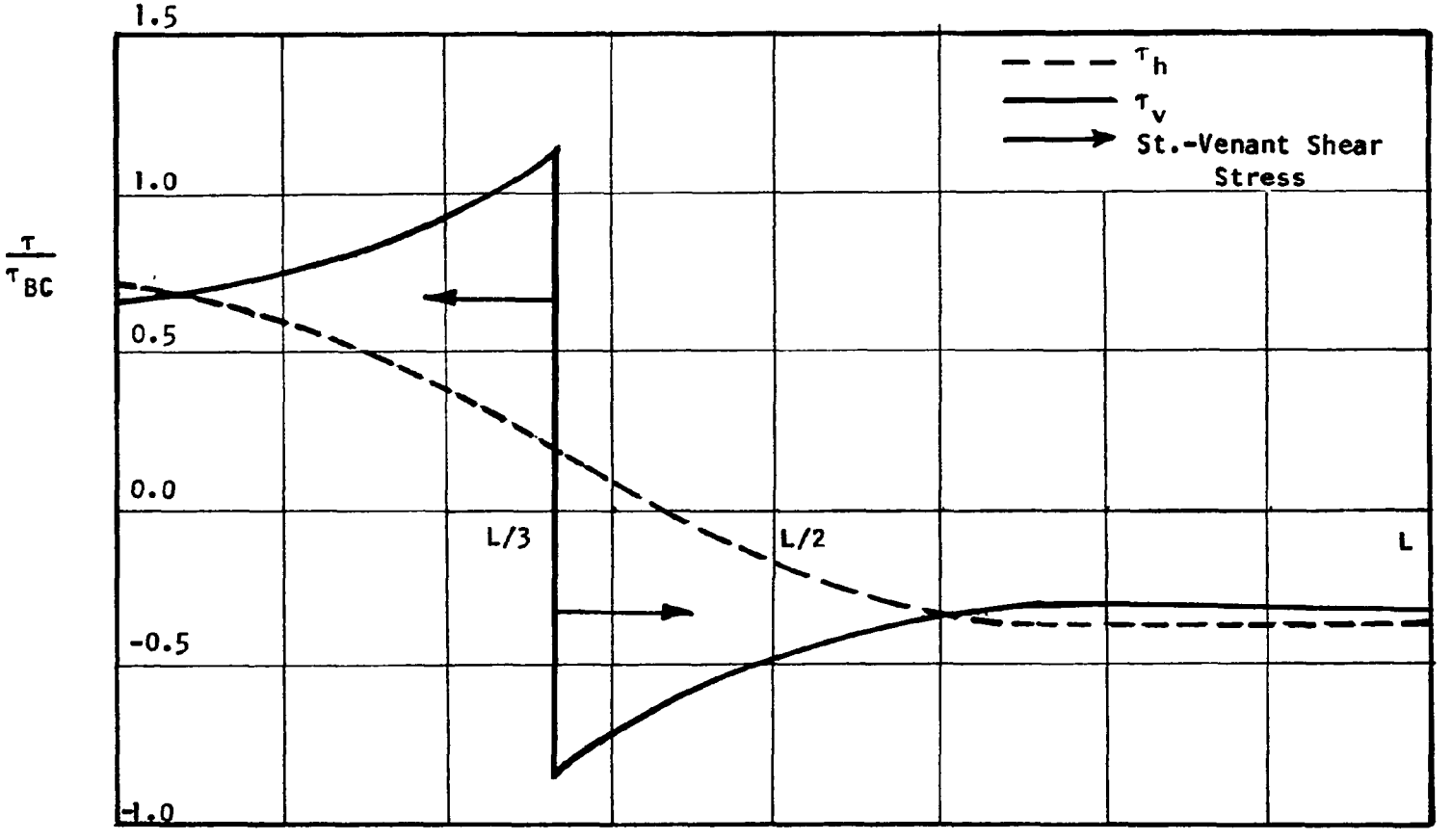

Figure 37. Variation of τ_v and τ_h Along Girder 1RC.
Simply Supported Ends. Concentrated Torsional Load at L/3.

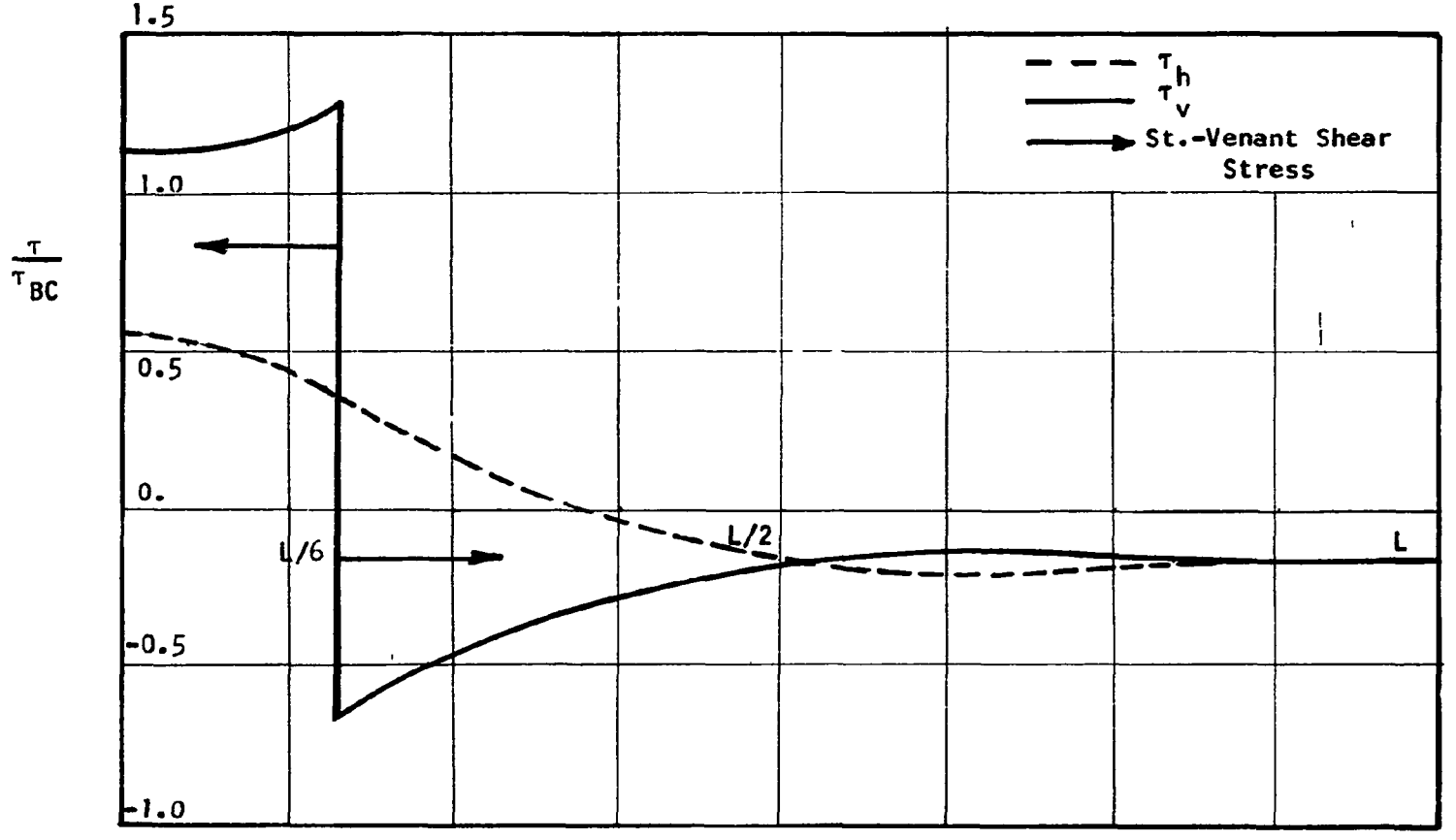

Figure 38a. Variation of τ_v and τ_h Along Girder 1RC. Simply Supported Ends. Concentrated Torsional Load at L/6 (End Diaphragms Only).

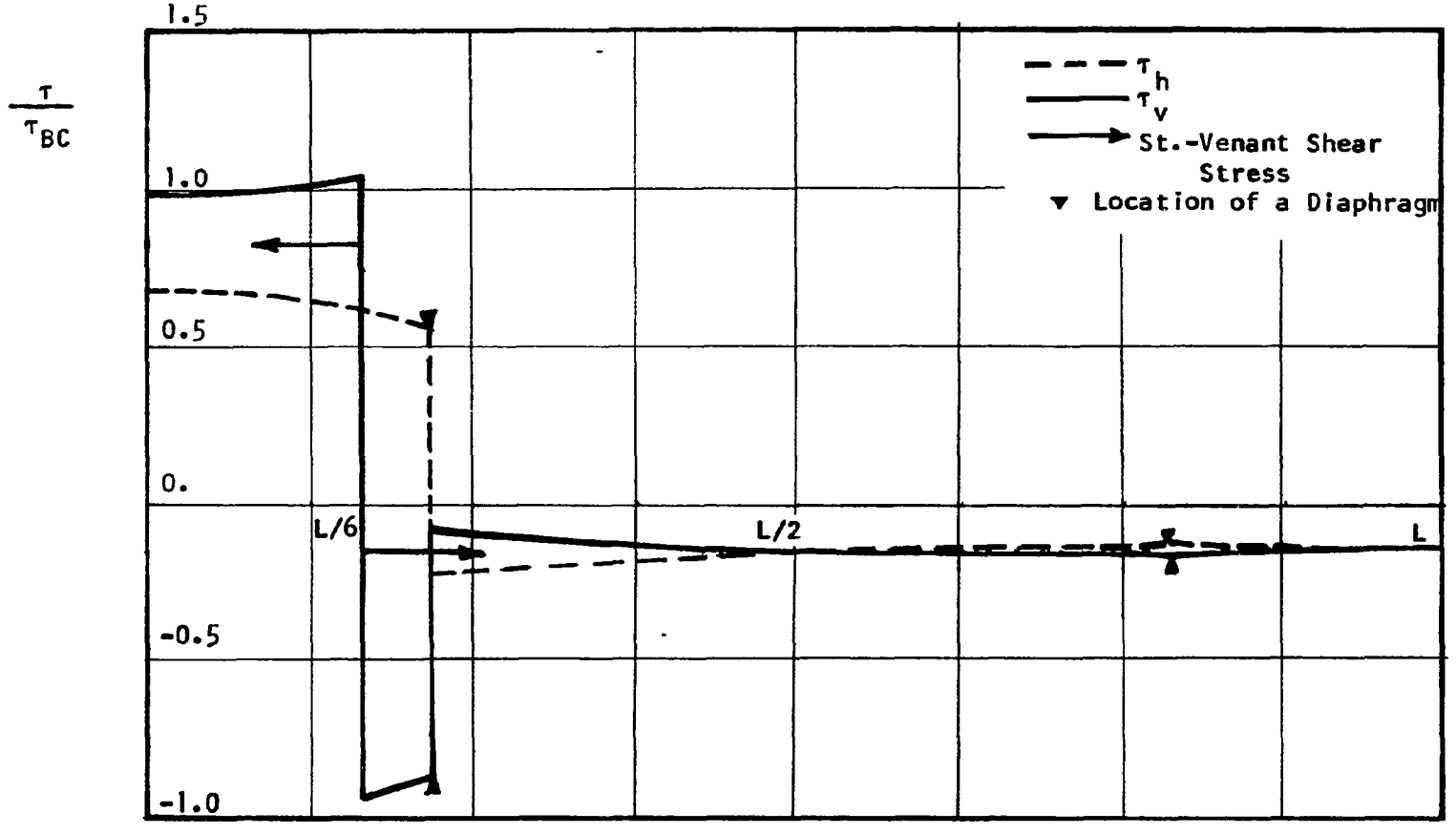

Figure 38b. Variation of τ_v and τ_h Along Girder 1RC. Simply Supported Ends. Concentrated Torsional Load at L/6 (End and Two Intermediate Diaphragms).

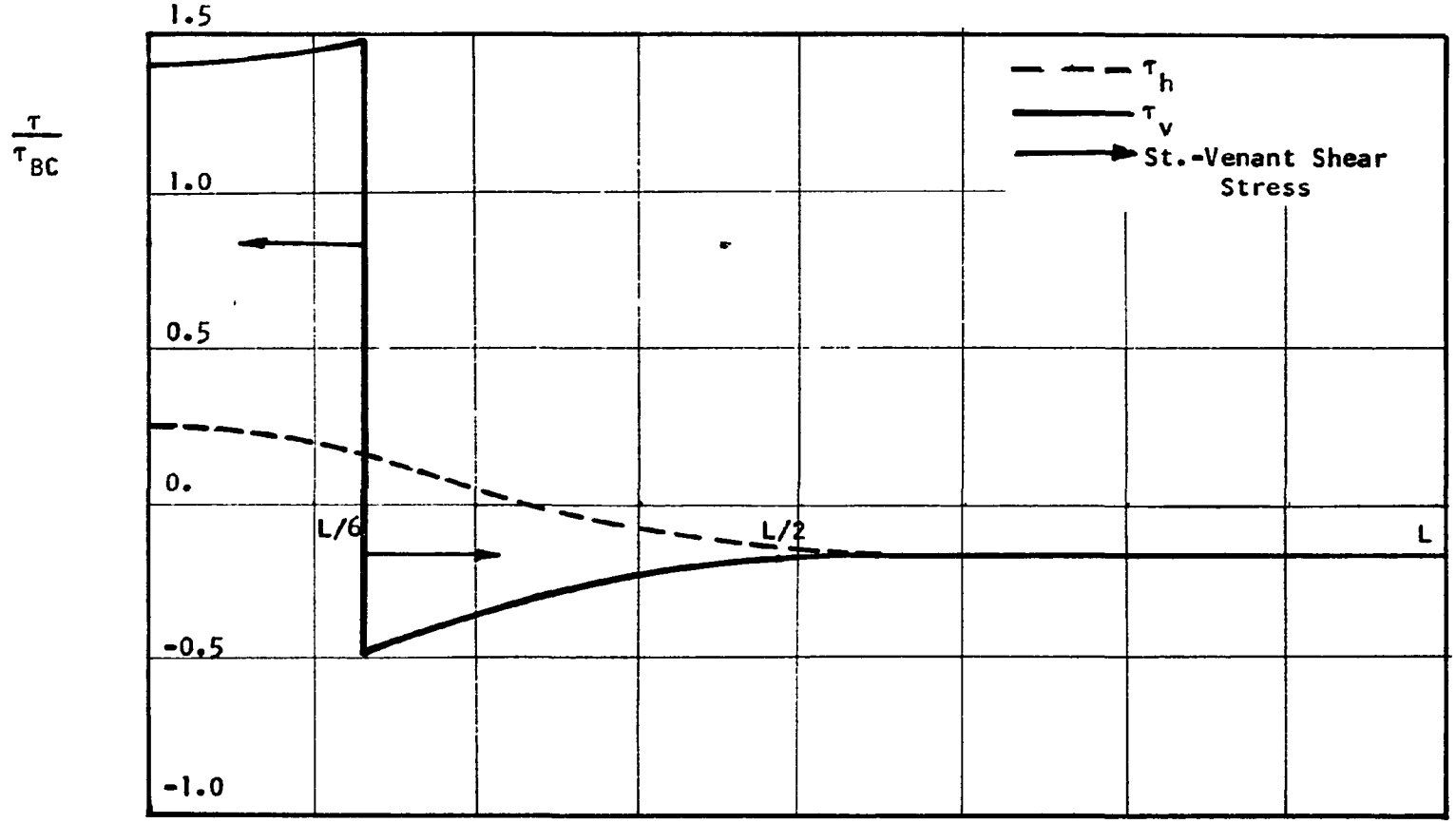

Figure 39. Variation of τ_v and τ_h along Girder IRC. Fixed Ends. Concentrated Torsional Load at L/6.

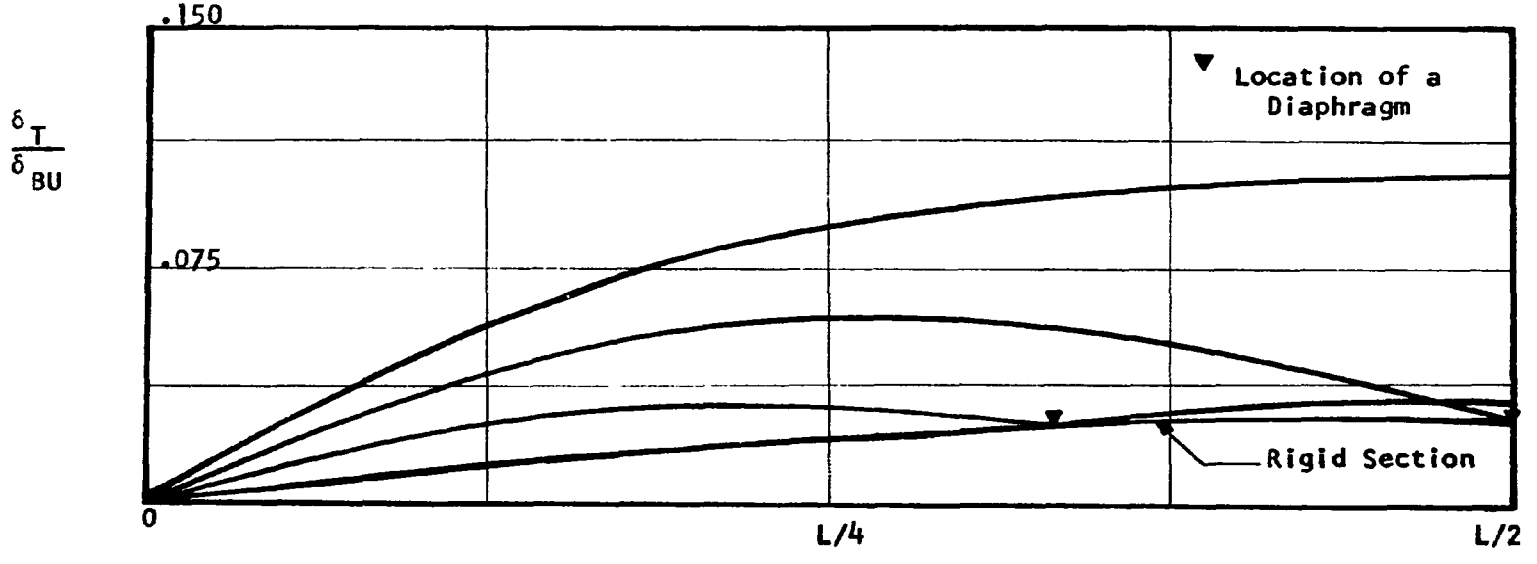

Figure 40. Variation of δ_T Along Girder IRC. Simply Supported Ends. Uniform Torsional Load.

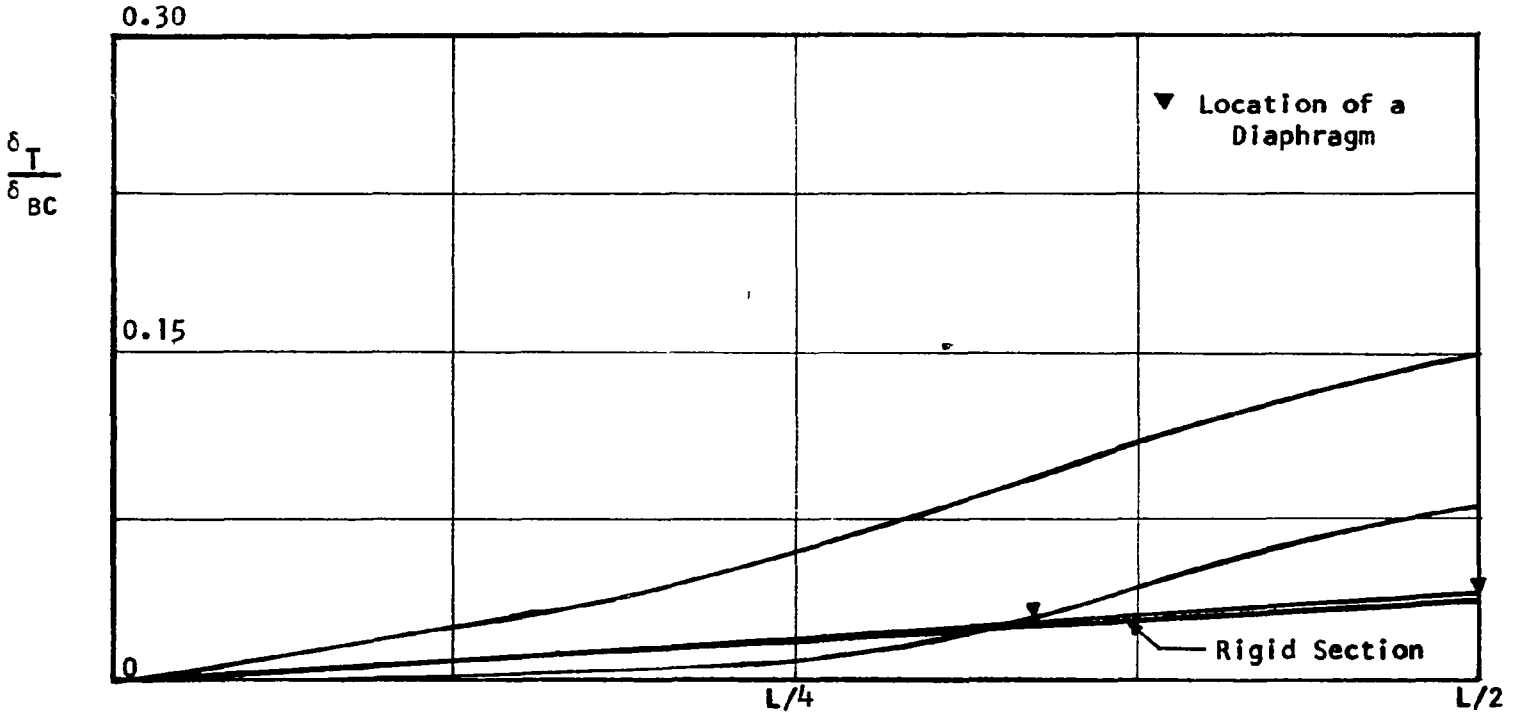

Figure 41. Variation of δ_T Along Girder 1RC. Simply Supported Ends. Concentrated Torsional Load at L/2.

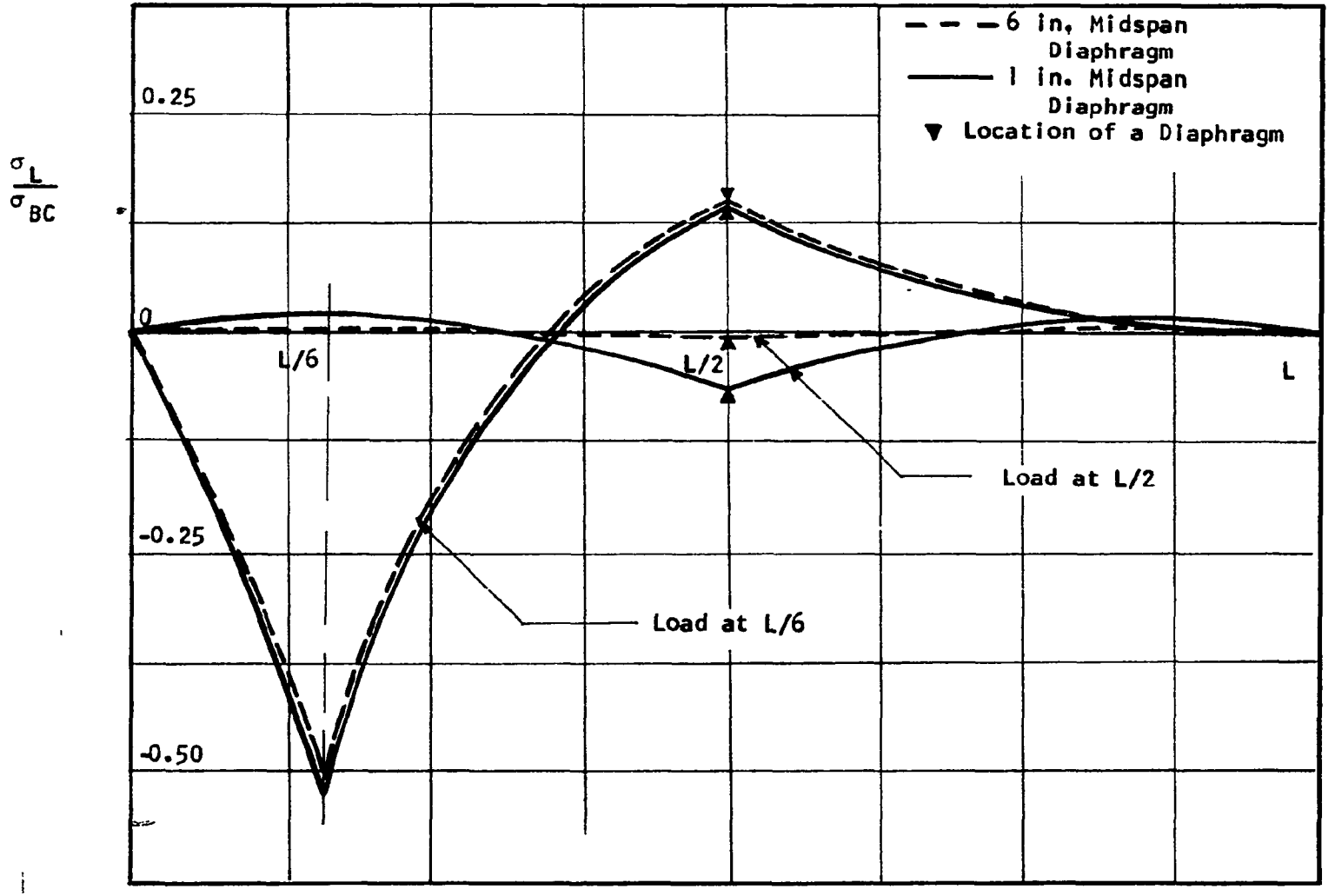

Figure 42. Effect of Midspan Diaphragm Stiffness on the Variation of σ_L Along Girder IRC. Concentrated Torsional Loads.

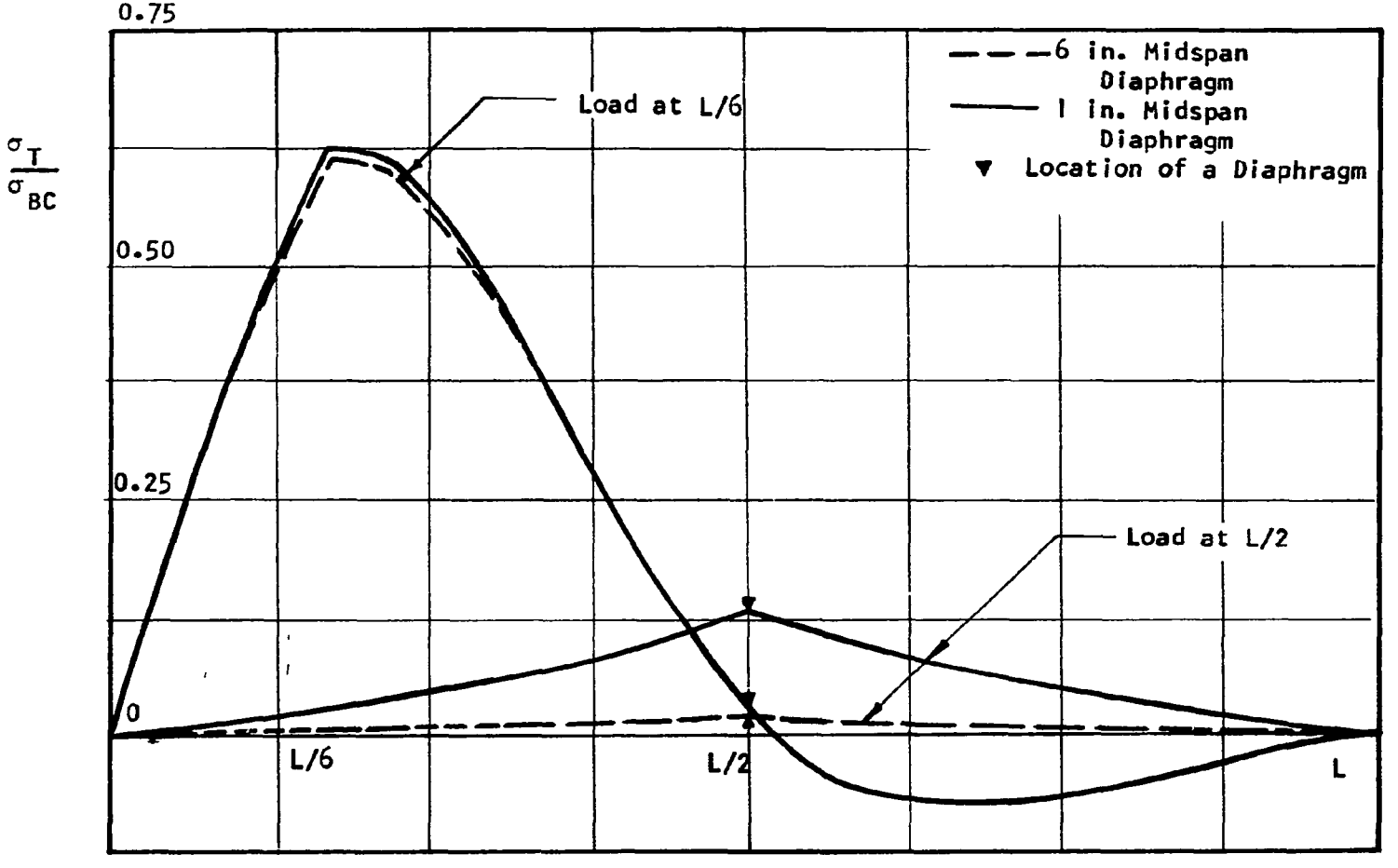

Figure 43. Effect of Midspan Diaphragm Stiffness on the Variation of σ_T Along Girder 1RC. Concentrated Torsional Loads.

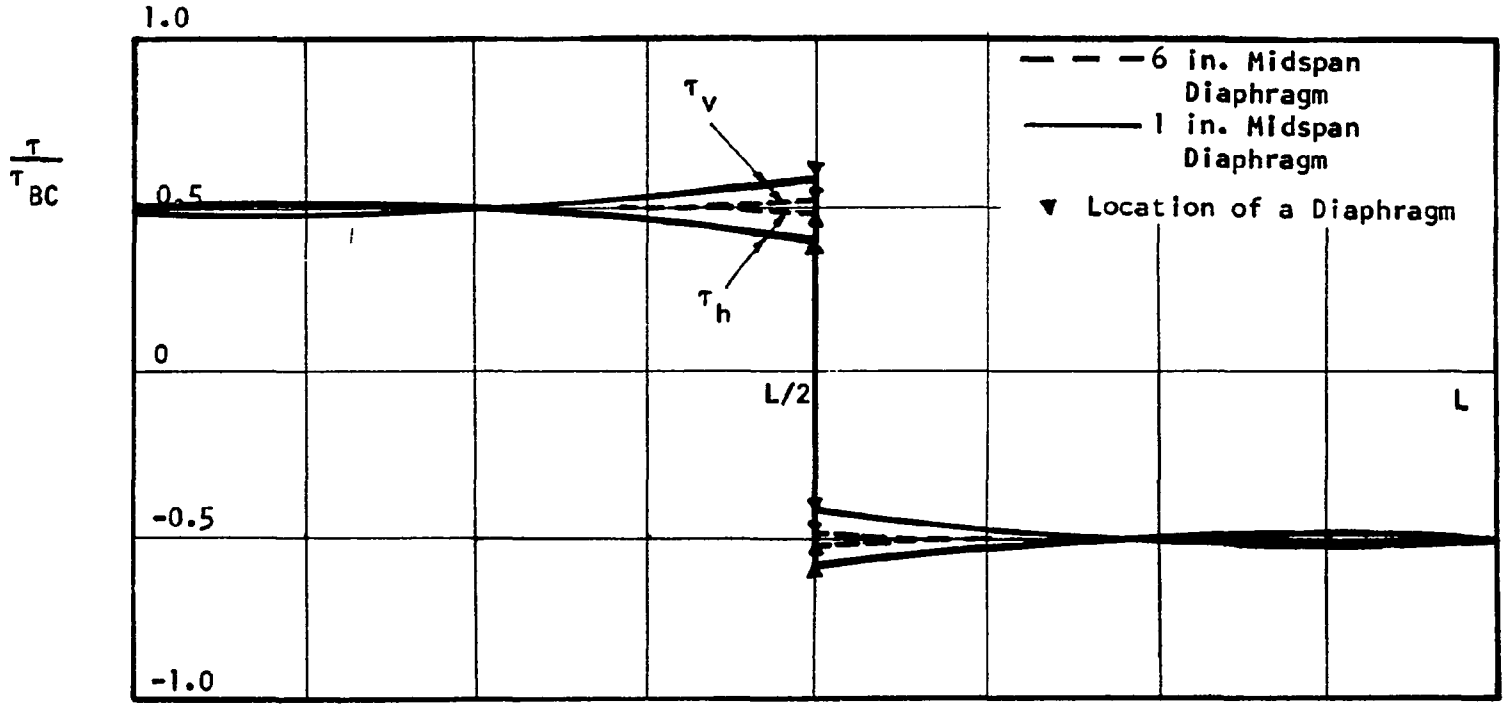

Figure 44. Effect of Midspan Diaphragm Stiffness on the Variation of τ_v and τ_h Along Girder 1RC. Concentrated Torsional Load at L/2.

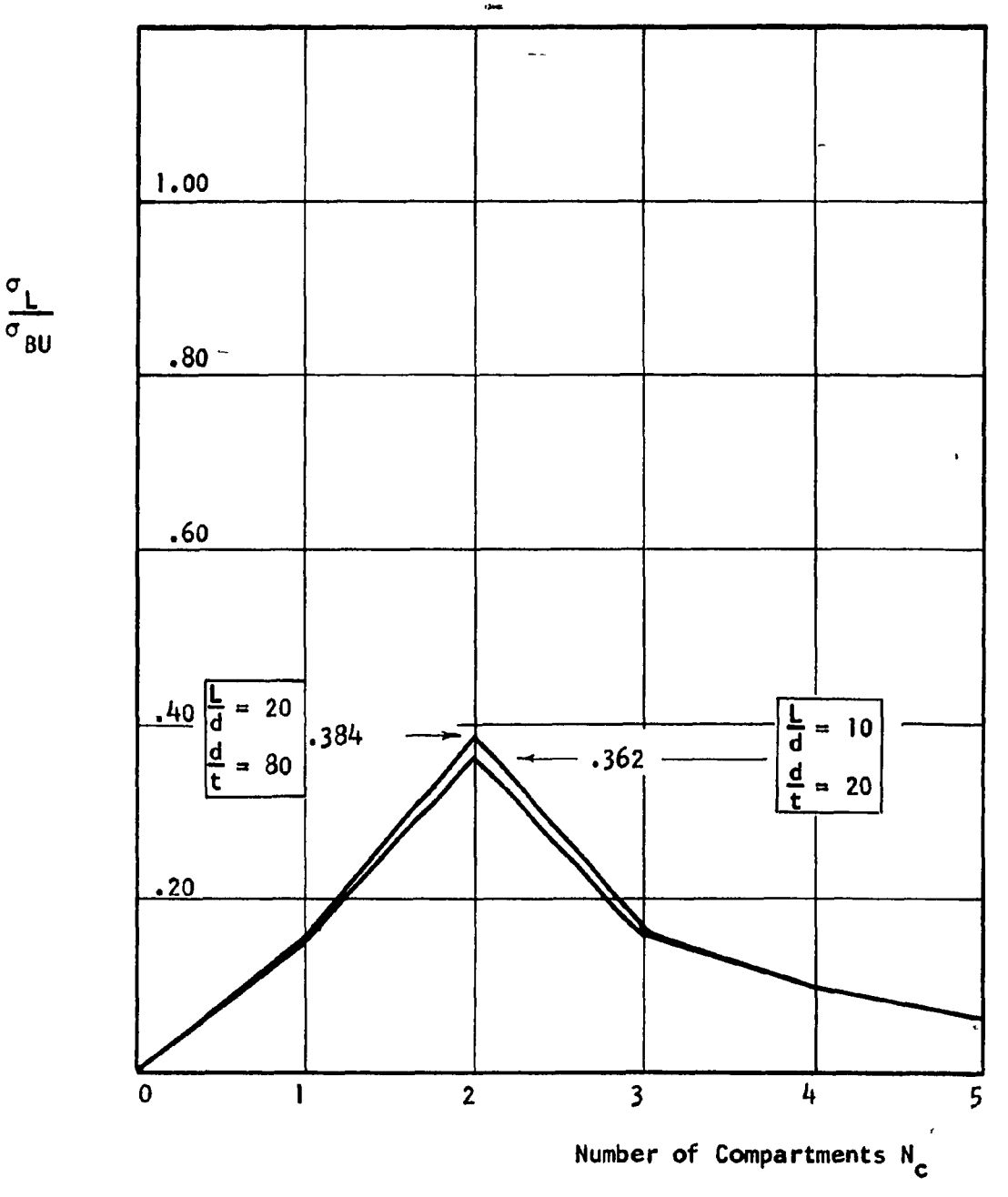

Figure 45. Variation of σ_L with H_c = .200.
Square Box Girder. Uniform Torsional Load.

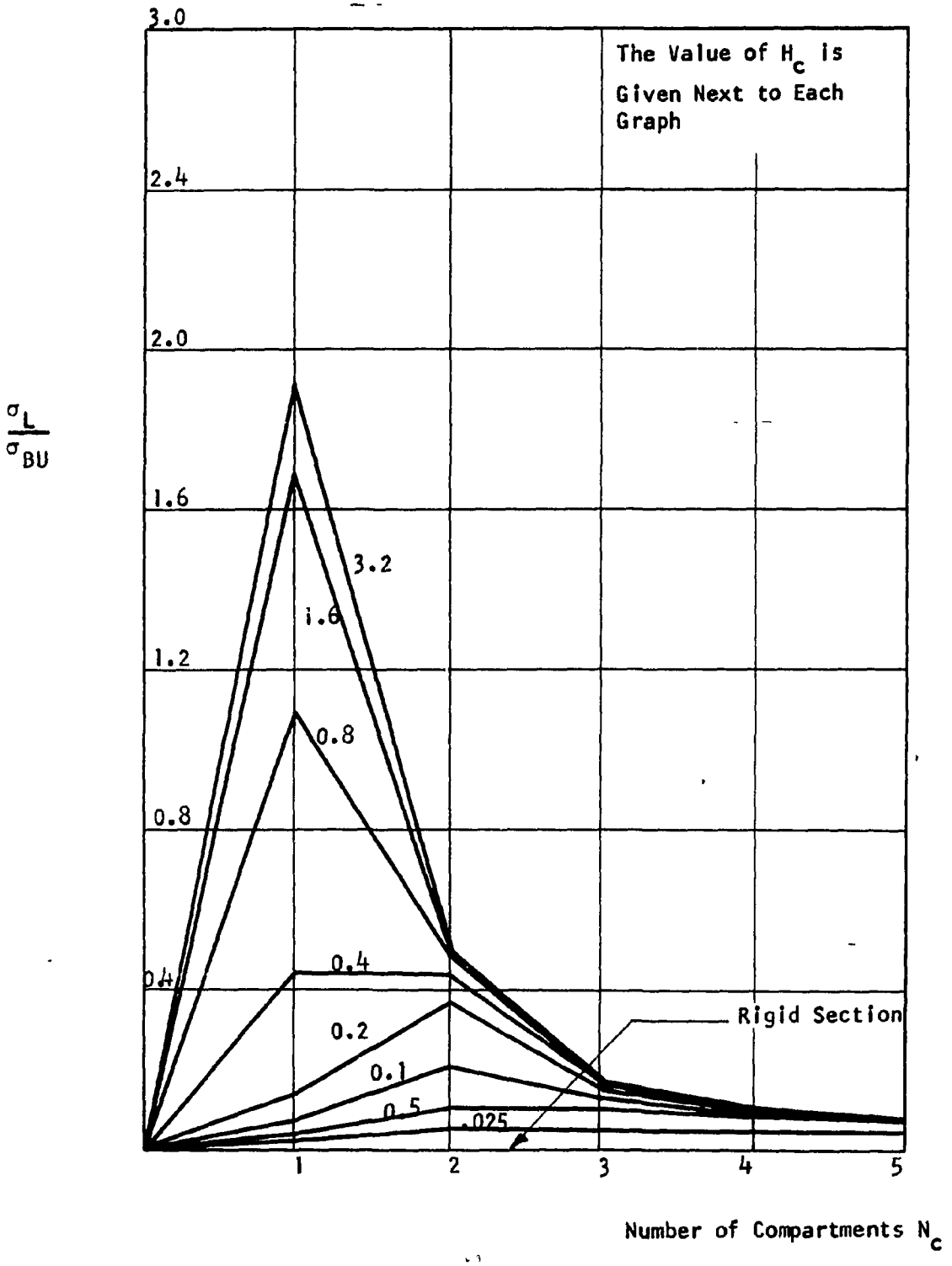

Figure 46. Variation of Maximum σ_L with Number of Compartments for Different Values of H_c. Square Box Girder. Uniform Torsional Load.

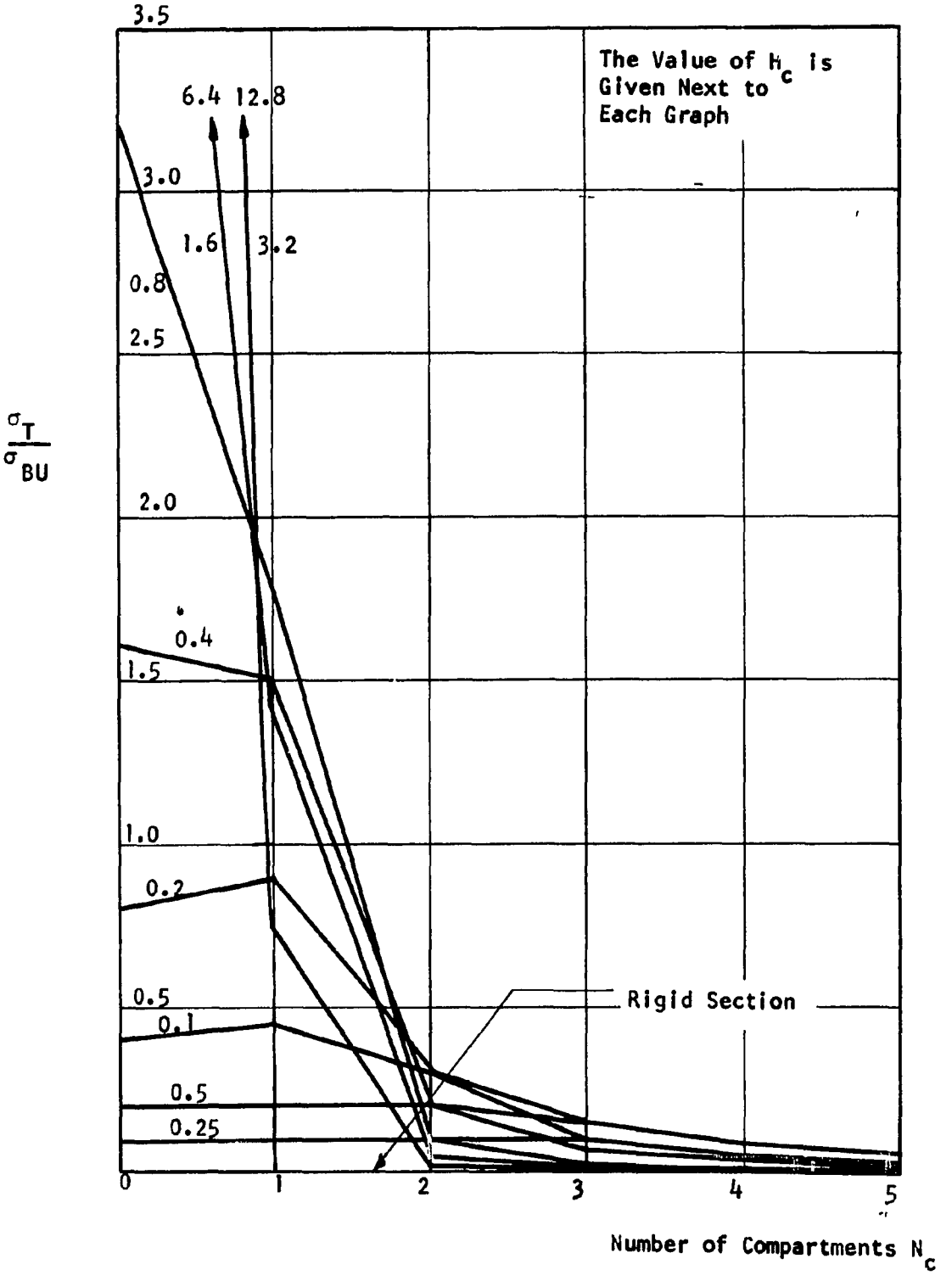

Figure 47. Variation of Maximum σ_T with Number of Compartments for Different Values of H_c. Square Box Girder. Uniform Torsional Load.

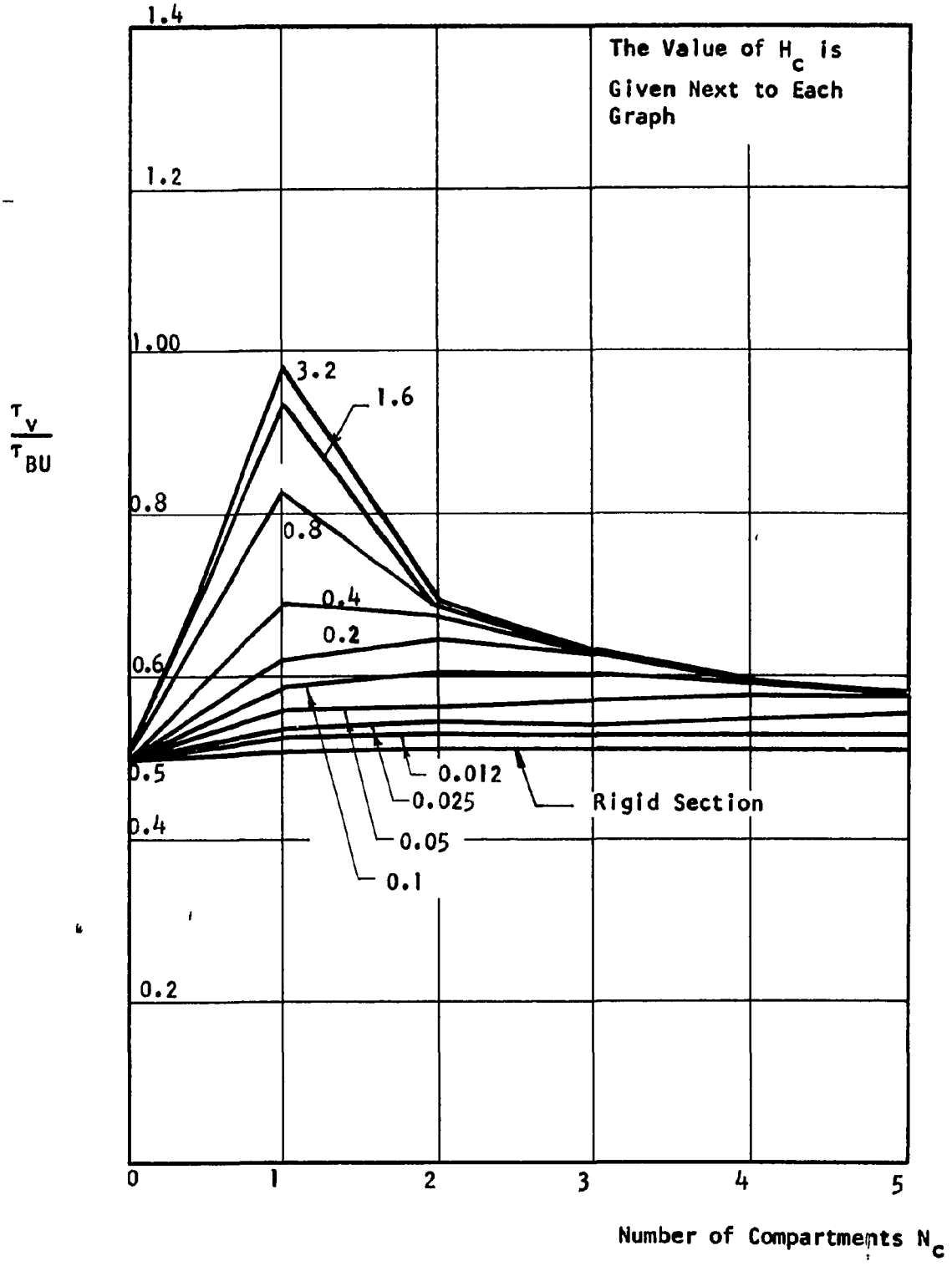

Figure 48. Variation of Maximum τ_v with Number of Compartments for Different Values of H_c. Square Box Girder. Uniform Torsional Load.

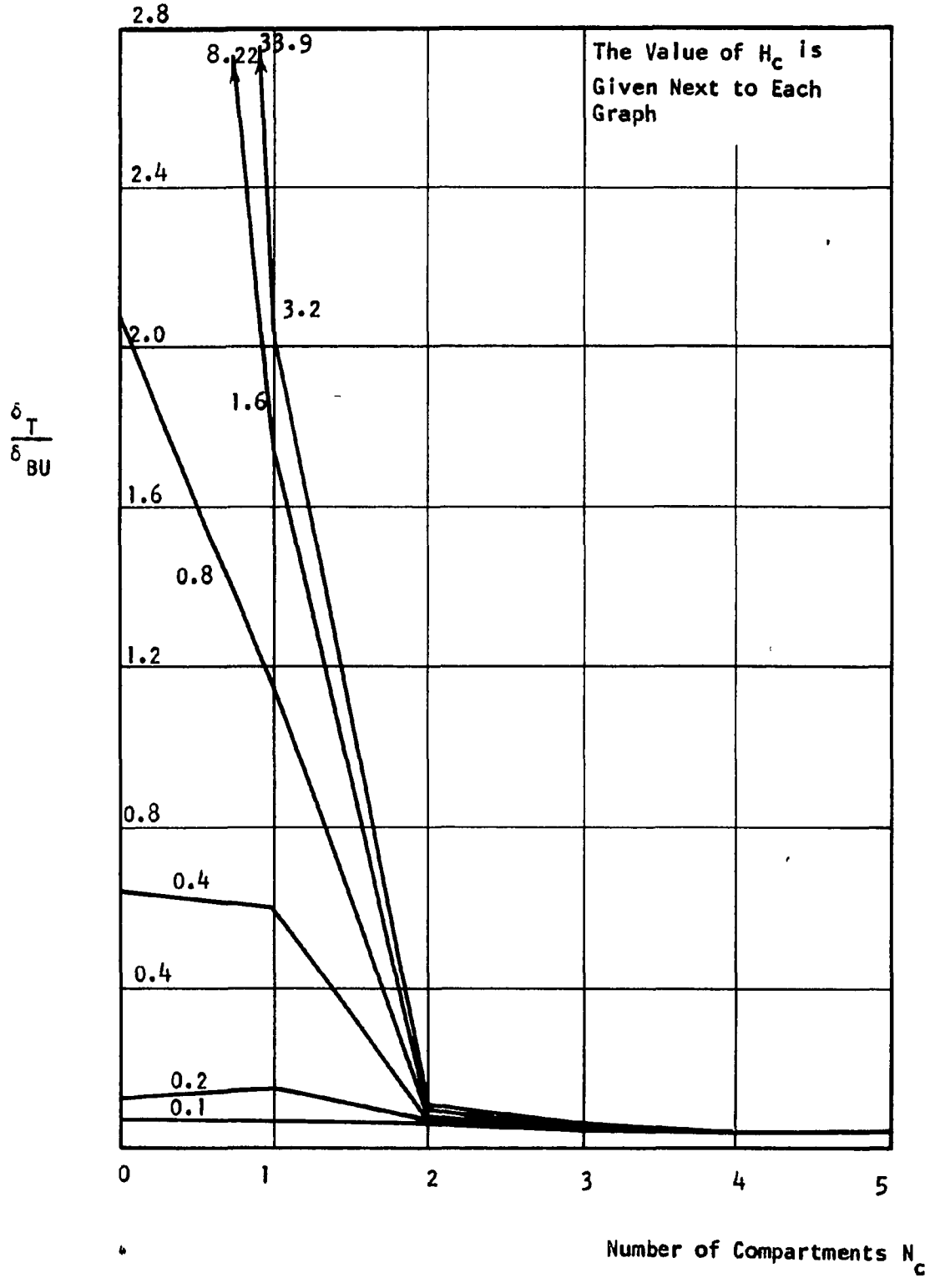

Figure 49. Variation of Maximum δ_T with Number of Compartments for Different Values of H_c. Square Box Girder. Uniform Torsional Load.

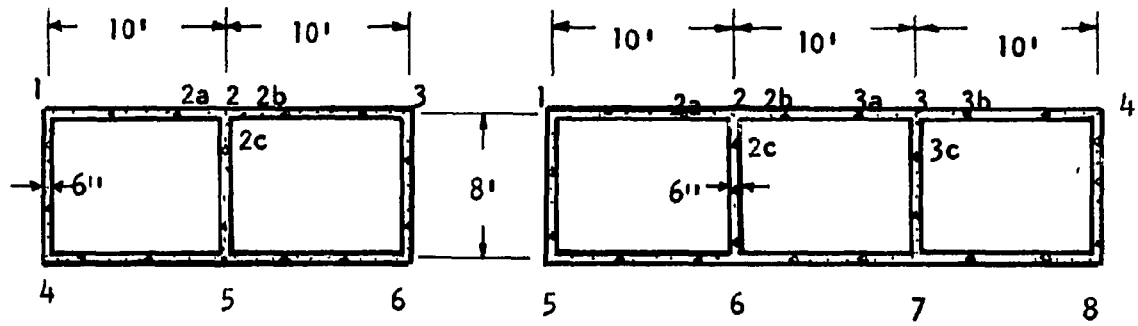

(a) 2RC

(b) 3RC

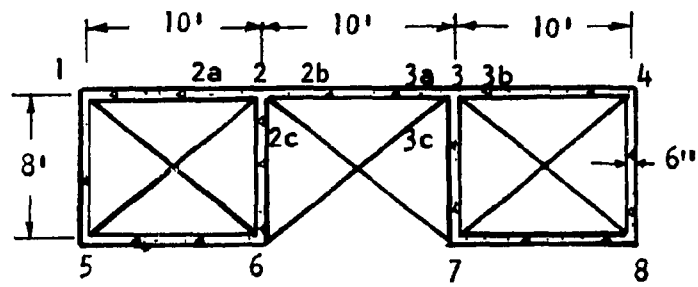

(c) 2RPC

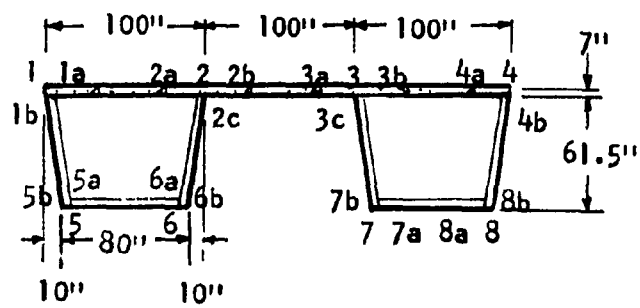

(d) 2TPCS

Figure 50. Cross-Sections of Multicell Box Girders

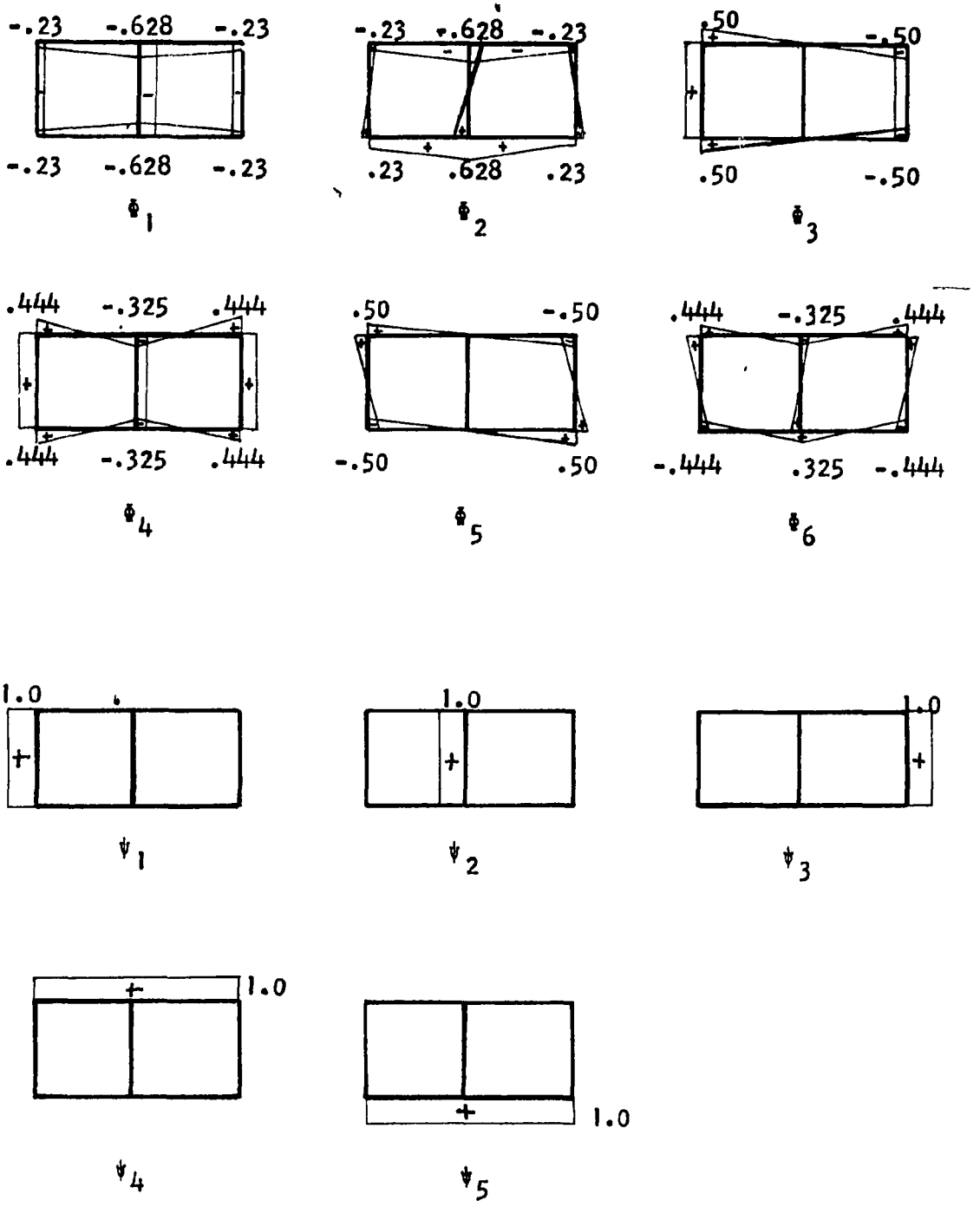

Figure 51. Orthogonal Generalized Coordinates for Girder 2RC.

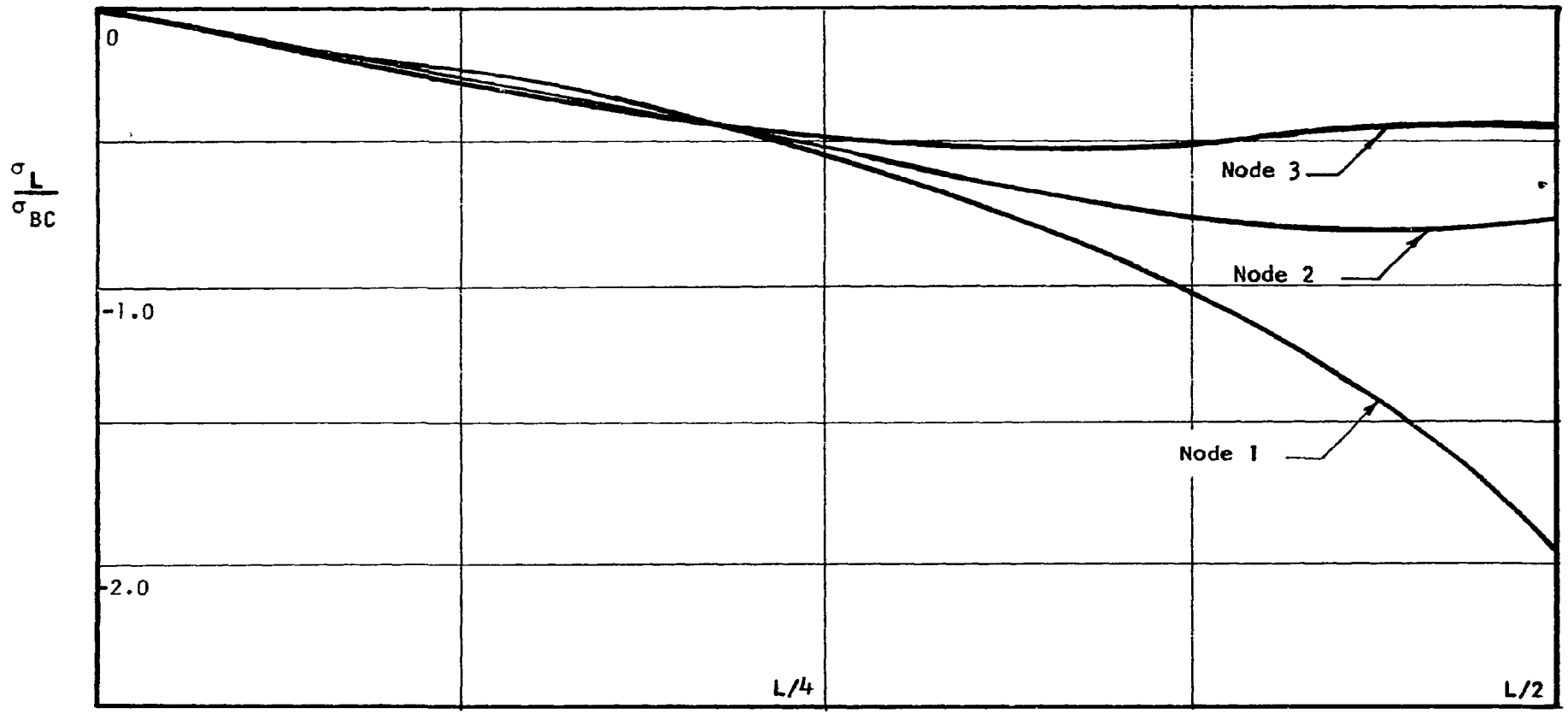

Figure 52. Variation of σ_L at the Nodes. Girder 2RC Loaded by a Concentrated Load at Node 1 and Midspan.

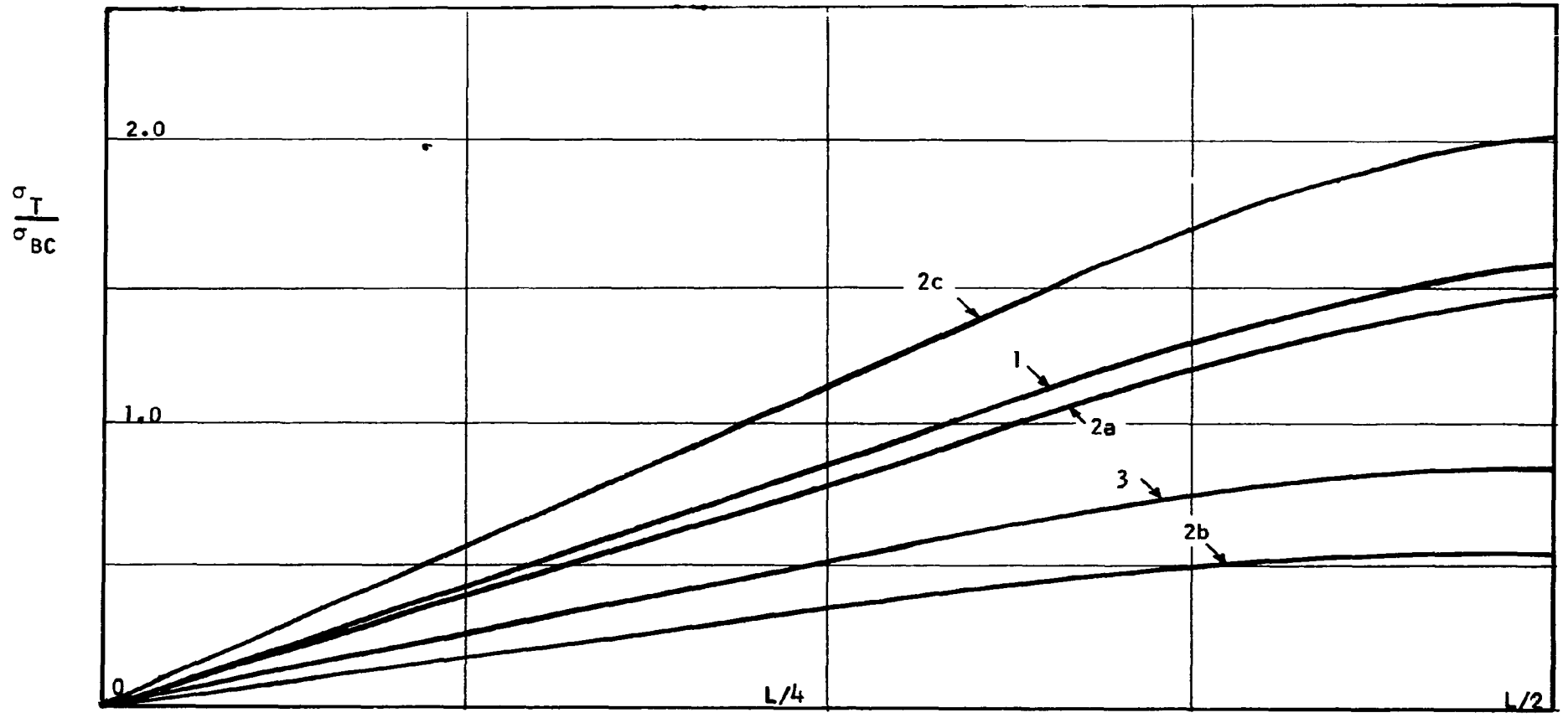

Figure 53. Variation of σ_T at Ends of Elements. Girder 2RC Loaded by a Concentrated Load at Node 1 and Midspan.

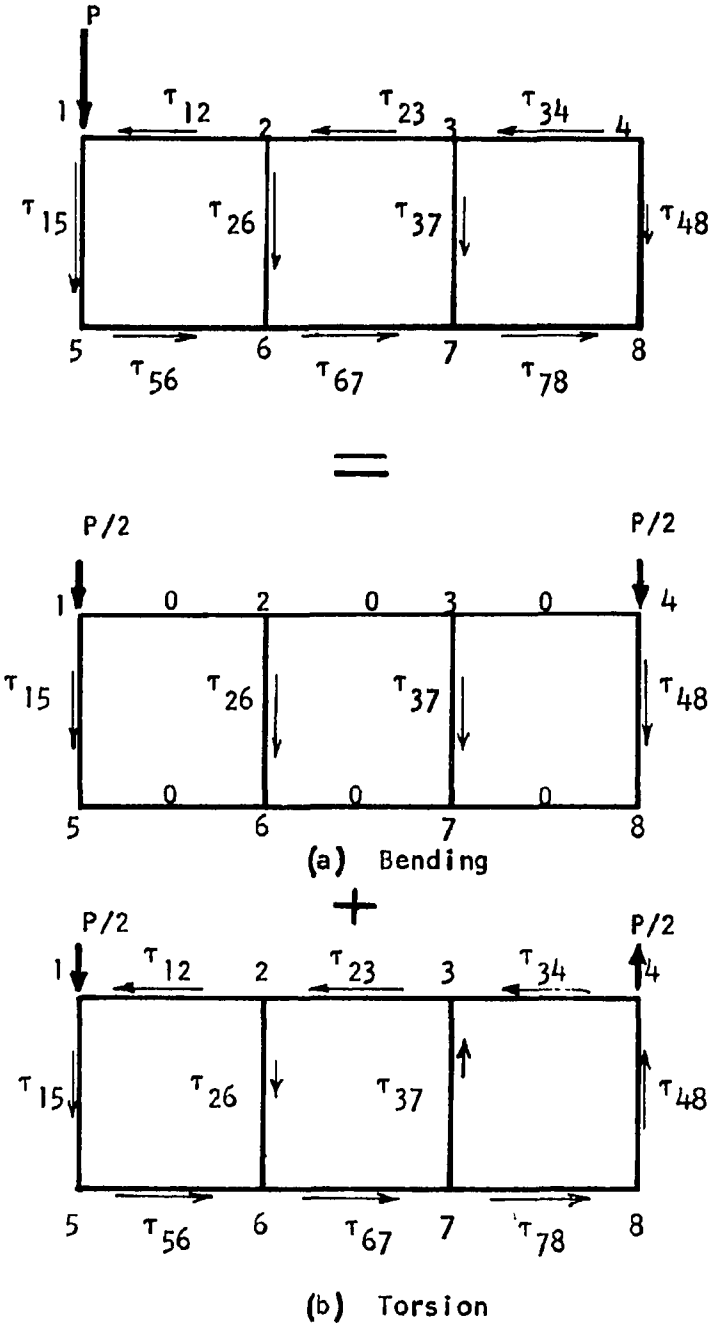

Figure 54. Resolution of Concentrated Load at Node 1 of Girder 3RC. Shear Stress Nomenclature.

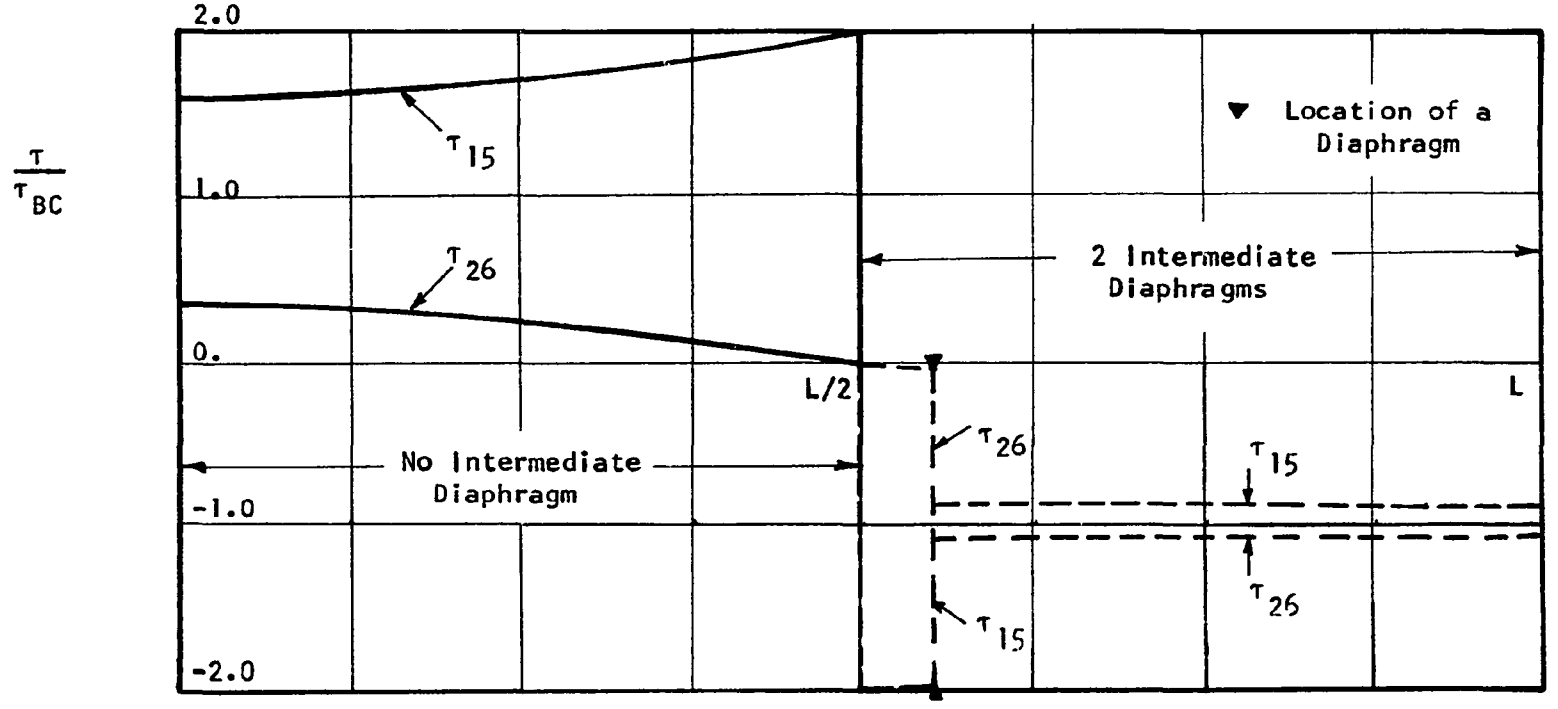

Figure 55. Variation of the Shear Stresses. Girder 3RC Under Load of Figure 54a.

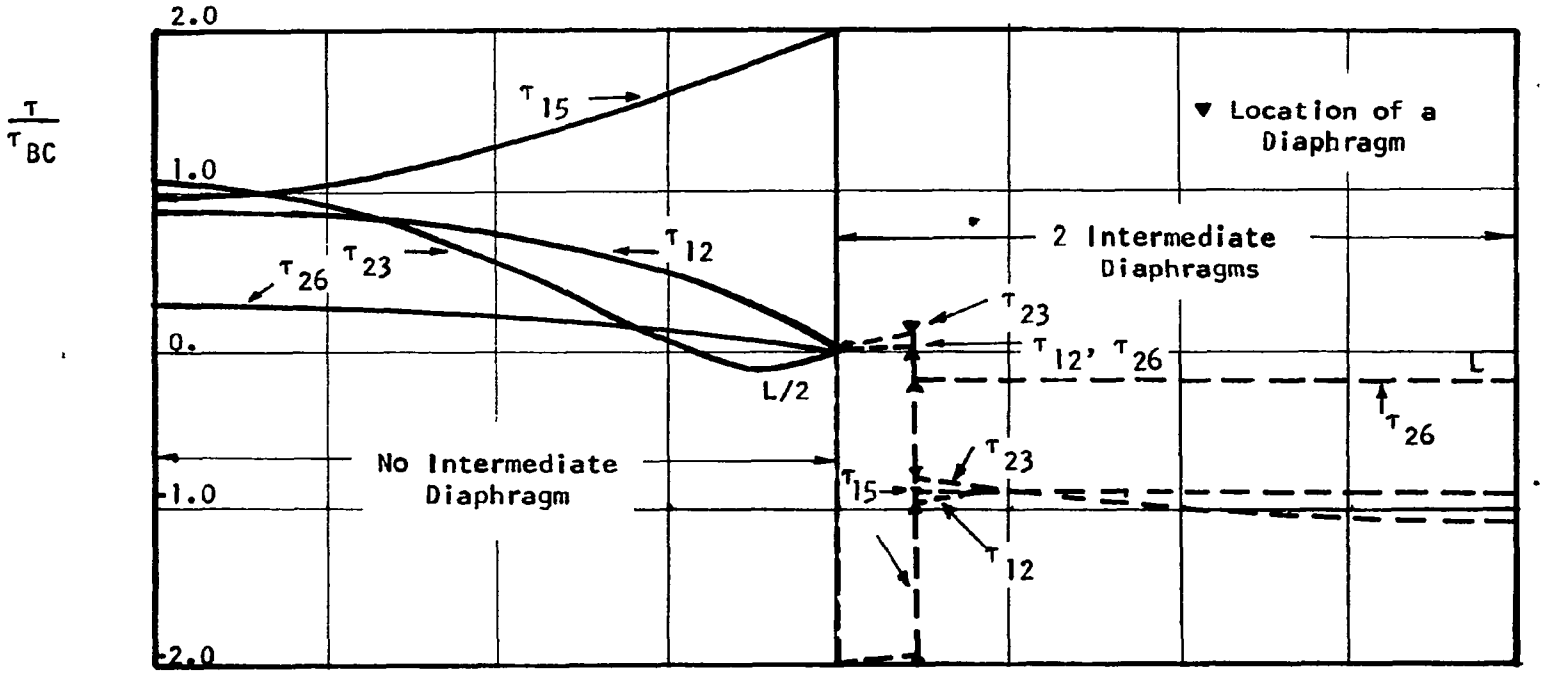

Figure 56. Variation of the shear Stresses. Girder 3RC Under Load of Figure 54b.

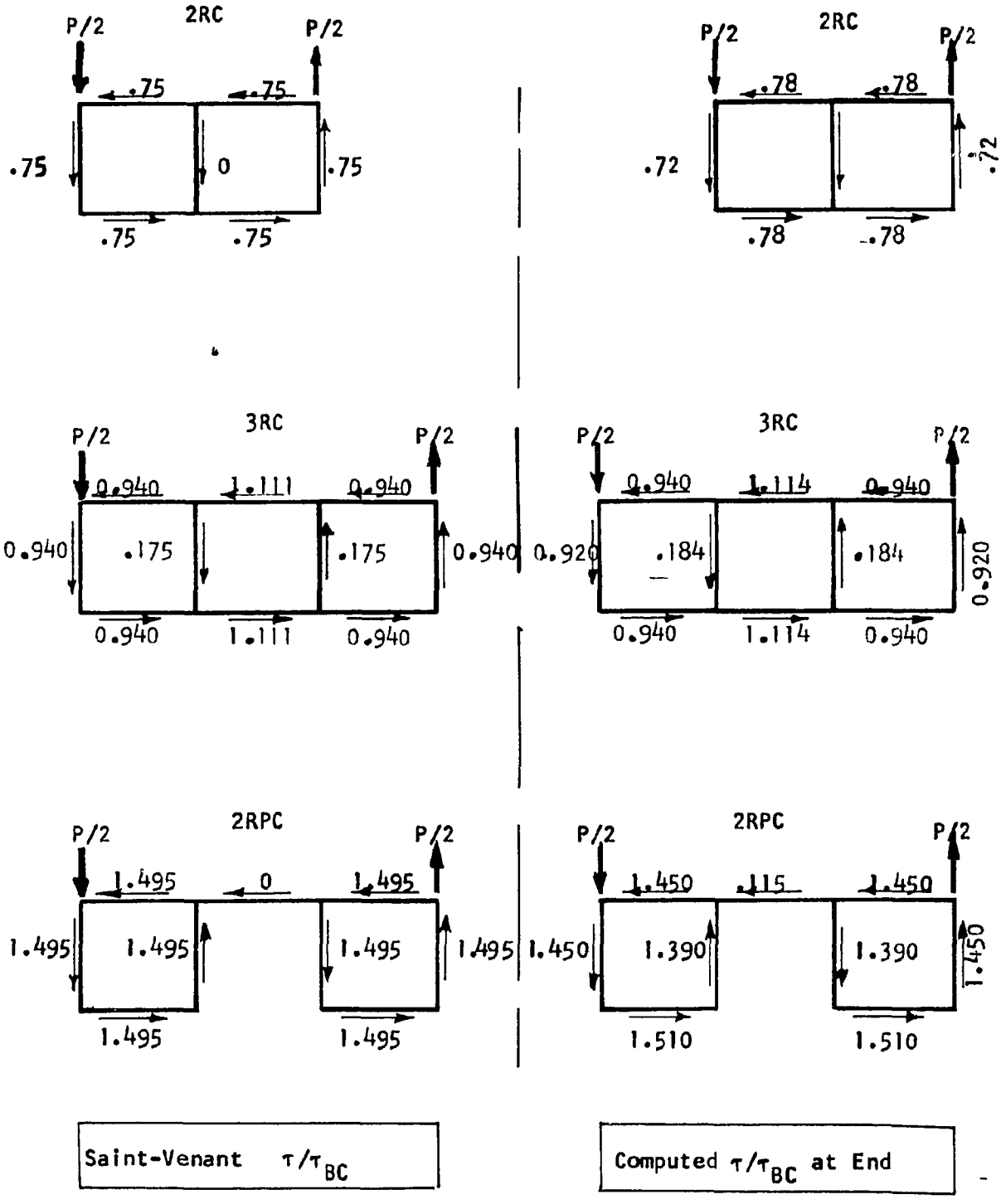

Figure 57. Comparison between Saint-Venant Shear Stresses and Computed Shear Stresses at the Ends of Girders 2RC, 3RC and 2RPC. Two Intermediate Diaphragms at 7L/18 and 11L/18. Midspan Concentrated Torsional Load.

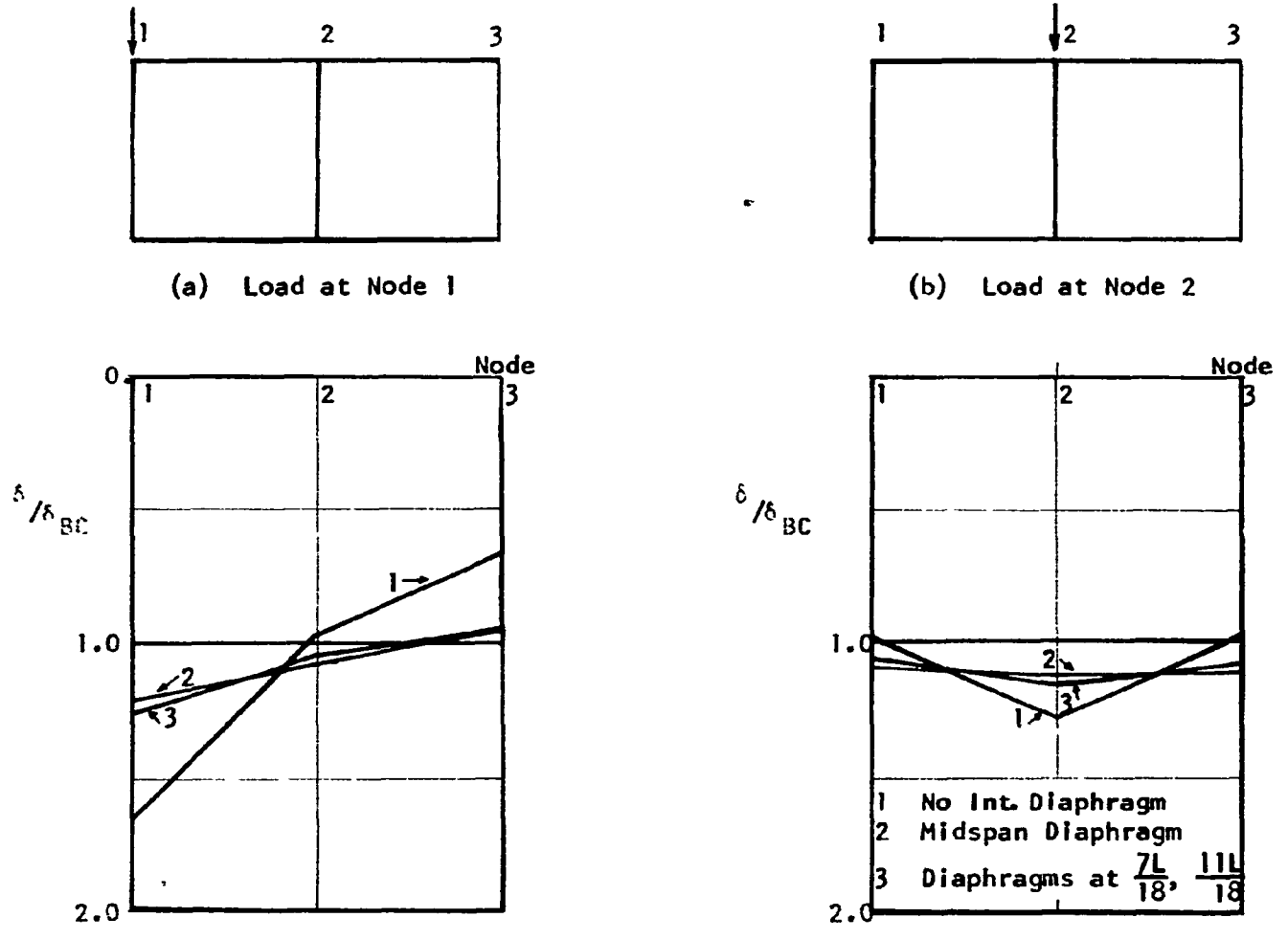

Figure 58. Deflections of Girder 2RC at Midspan. Concentrated Load at Midspan.

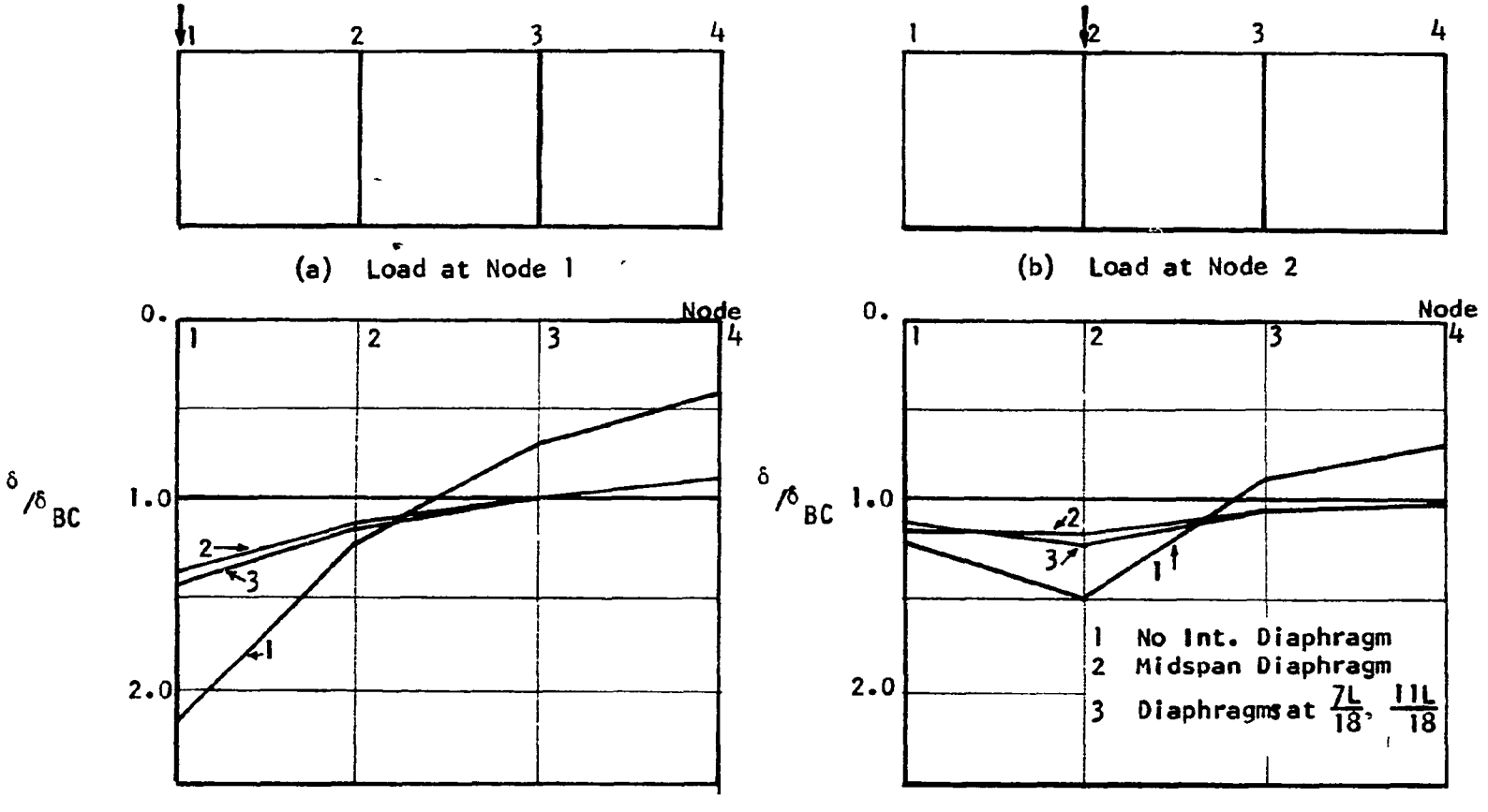

Figure 59. Deflections of Girder 3RC at Midspan. Concentrated Load at Midspan.

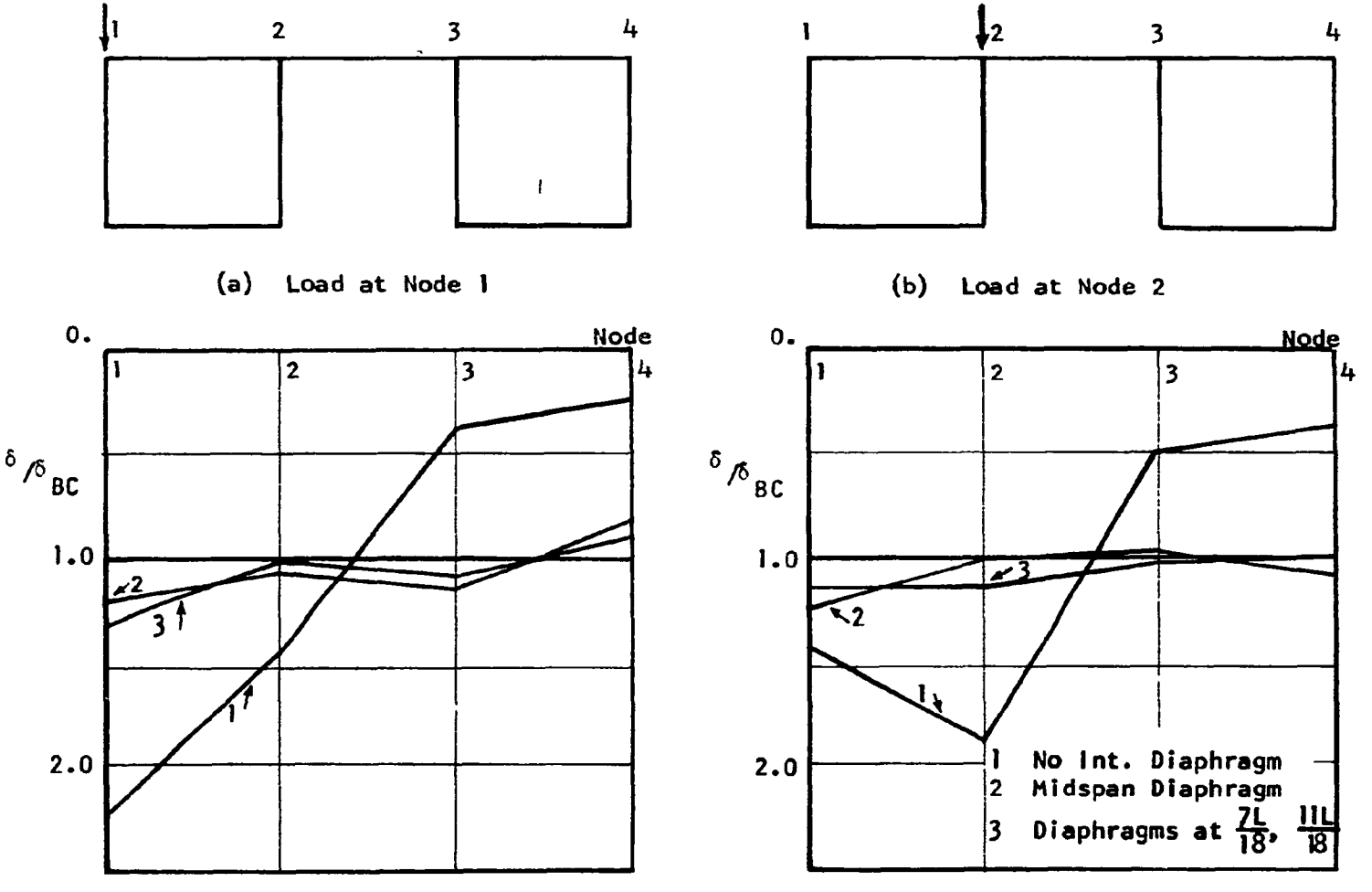

Figure 60. Deflections of Girder 2RPC at Midspan. Concentrated Load at Midspan.

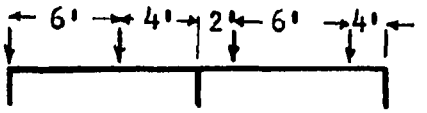

(a) Two Lanes, Left Beam

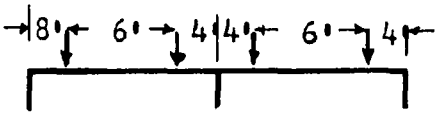

(b) Two Lanes, Interior Beam

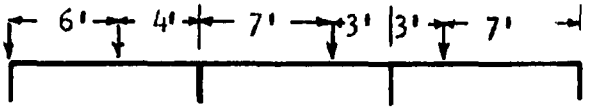

(c) Three Lanes, Left Beam

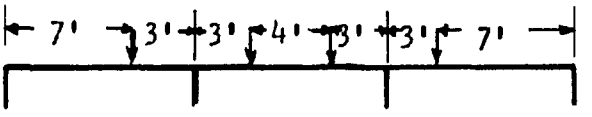

(d) Two Lanes, Interior Beam

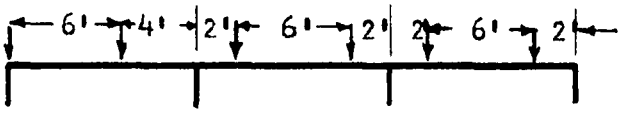

(e) Three Lanes, Left Beam

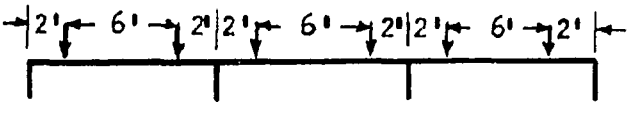

(f) Three Lanes, Leftmost Interior Beam.

Figure 61. Wheel Load Configuration for Maximum Moments in Beam Elements.

APPENDIX A

EFFECTIVE PLATE WIDTH ACTING WITH A TRANSVERSE STIFFENER

The analysis procedure permits consideration of transversely stiffened plate elements if an effective plate width that acts with each stiffener is determined. The following development of effective plate width is based on information given in Reference (31).

A study of Chart 1 of Reference (31) shows that the effective plate width a_o for equally loaded stiffeners is given by:

$$a_o = \frac{a \tanh (2.8\ a/S_1)}{2.8(1-\nu^2)a/S_1} \qquad (A.1)$$

where a is the stiffener spacing, S_1 the effective stiffener span which is the length of the stiffener subjected to moment of the same sign, and ν is Poisson's ratio for plate and stiffeners.

For loads applied at the nodes the stiffeners are almost equally loaded. The effective stiffener span can be best approximated by 0.5S, the term S being the stiffener span and the plate width. Therefore the effective plate width is obtained from Equation (A.1) by replacing S_1 by its value of 0.5 S:

$$a_o = \frac{a \tanh (5.6\ a/S)}{5.6(1-\nu^2)\ a/S} \qquad (A.2)$$

APPENDIX B

OUTLINE OF THE COMPUTER PROGRAM

The computer program developed for the study of multicell box girders is discussed here. It is written in FORTRAN language for use on the IBM-7094 of the University of Illinois. The use of sequential programming is necessary because of limitations on storage capacity. The program consists of two core loads.

The first core load starts by reading in the properties of the structure and the boundary conditions. It then finds the equivalent longitudinal thickness and transverse stiffness of stiffened plate elements. It also reads in the output point locations and the parameters of the numerical integration.

It then proceeds to the determination of the generalized coordinates. The set of orthogonal transverse generalized coordinates is read in directly. The orthogonal set of longitudinal generalized coordinates is obtained from a set of non-orthogonal longitudinal generalized coordinates by using the orthogonalization procedure of Section 3.1 and the library subroutine EIGI. This subroutine fails to give results for repeated eigenvalues which occur for a single cell square box with uniform thickness. In this trivial case, the program provides the orthogonal longitudinal coordinates of Figure 6b directly. The program then proceeds to find the coefficients of the system of differential equations a_{ji}, b_{ji}, c_{jk}, d_{hl} and r_{hk}.

The program proceeds to read in matrices s_{hk} and μ_h at both ends of each plate element. Both matrices are obtained from a separate program written in the "STRESS" language.

Beam elements properties are read in and computed. Plate diaphragms properties are read in and the forces exerted by the diaphragms on the box girder are determined for all unit generalized displacements and stored. The same is done for the cross-bracing and the program calls the second core load.

The second core load is repeated for each loading case applied on the structure. It starts by reading the first loading. It goes on to integrate the system of differential equations for each initial-value problem after setting the initial values of the displacement functions. The integration is done by an iteration process until convergence, as explained in Section 3.4. If the number of iterations exceeds 10, the length of the interval is divided by two and the process is repeated. The initial interval length is taken as 1/180 of the span and the generalized displacements and their derivatives are stored at several equally spaced output points along the span. In most cases analyzed here convergence occurred before the sixth iteration using 360 equal intervals. The effects of concentrated loads and diaphragms is introduced if loads and diaphragms are located at the end of the interval.

If the values for the generalized displacements or their derivatives are large the numerical integration is stopped for all the initial-value problems at the same point and the suppression discussed in Section 3.6 is applied. A new set of initial-value problems is obtained containing very little of the growing solutions. The previously stored values of the generalized displacements and their derivatives at

the output points are modified accordingly. The integration then proceeds for all the new initial-value problems from the point of suppression onward with a new set of initial values. This process is repeated until the far end. Suppressions are made wherever necessary. In all the problems solved the number of suppressions never exceeded 6 for a permitted magnification factor of 16.

When the integration reaches the far end, the initial-value problems are linearly combined to satisfy the far end boundary conditions. The unique solution for the generalized displacements and first derivatives is obtained using a Gauss elimination procedure. The stresses and deflections are found and written out for the first loading. The second core load reads in the remaining loadingsand treats them seccessively as explained for the first loading. Then core load two transfers control to core load one which starts reading in the next problem.

The problem is solved separately for each loading case because of limitations on the storage capacity. A more efficient scheme is possible by considering all the loading cases at the same time. This would require the use of tape operations.

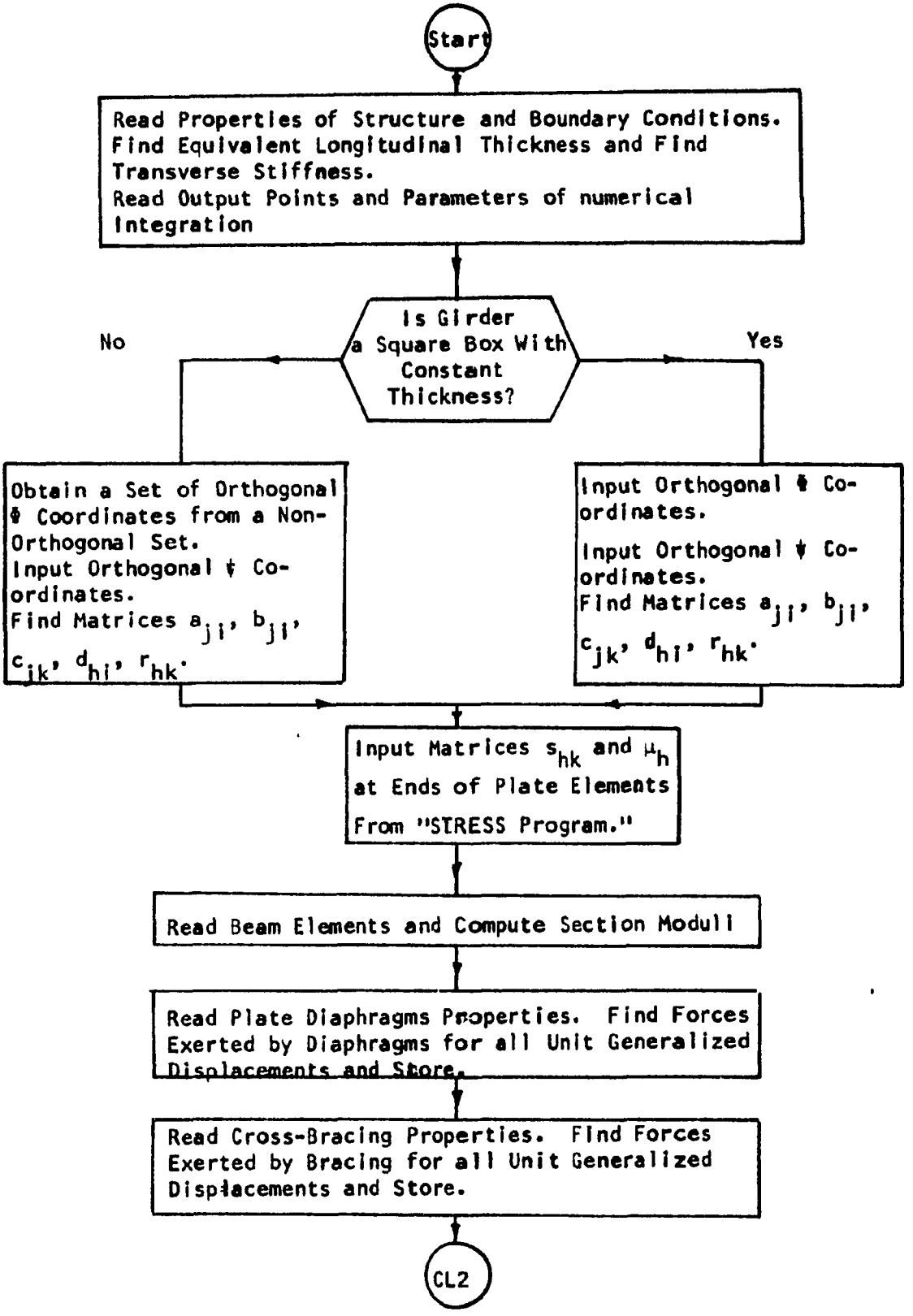

Figure A.1. Core Load 1

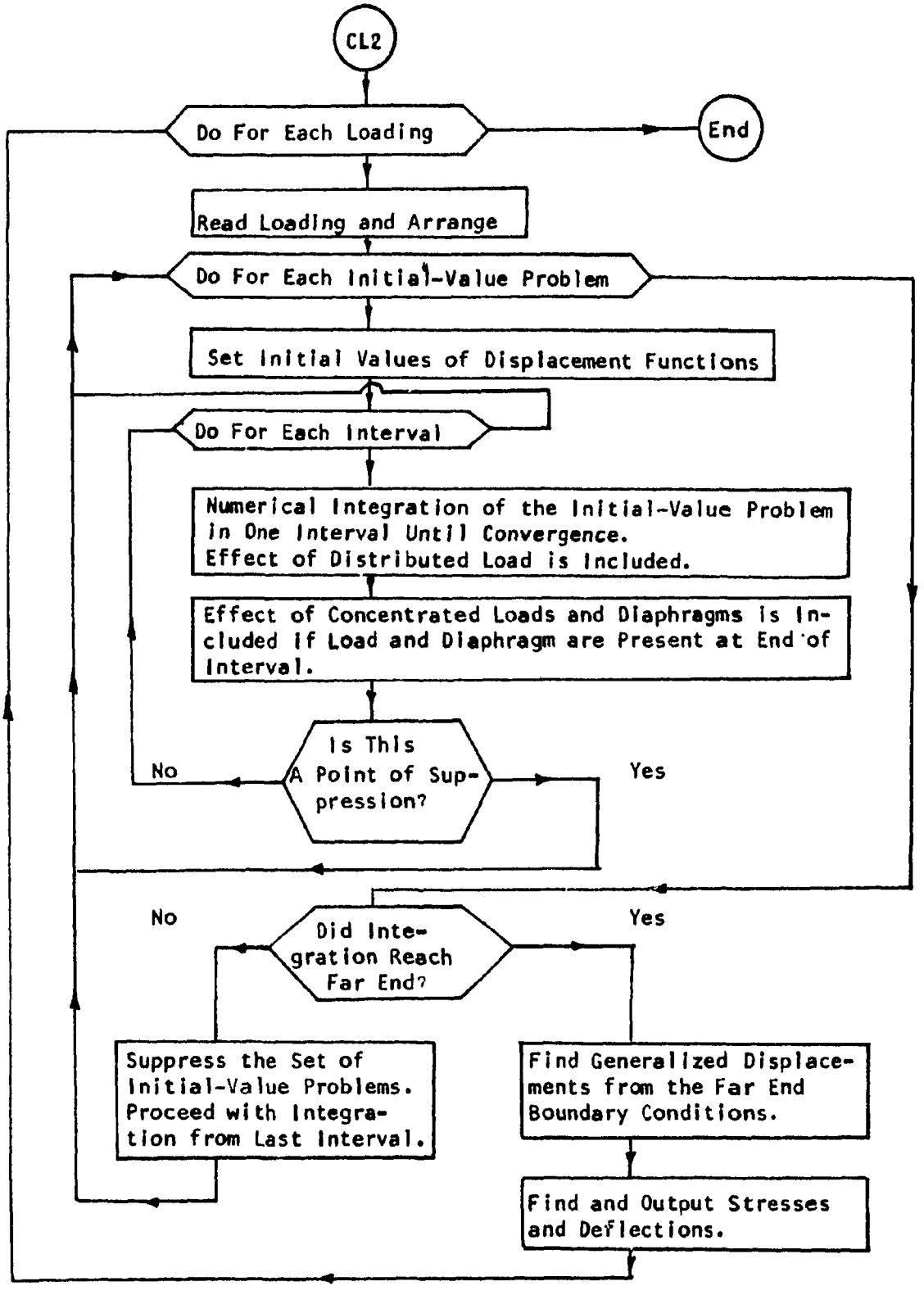

Figure A.2. Core Load 2

REFERENCES

1. Vlasov, V. Z., Thin-Walled Elastic Beams, First Edition, 1940 (in Russian). Translation available from U. S. Department of Commerce, Washington, D.C., 1961.

2. Timoshenko, S., and Goodier, J., Theory of Elasticity, McGraw-Hill Publishing Company, Second Edition, 1951.

3. von Karman, T., and Chien, W. Z., "Torsion with Variable Twist," Journal of the Aeronautical Sciences, Vol. 13, No. 10, October 1946.

4. von Karman, T. and Christensen, N. B., "Methods of Analysis for Torsion with Variable Twist," Journal of the Aeronautical Sciences, Vol. 11, No. 4, April 1944.

5. Benscoter, S. U., "A Theory of Torsion Bending for Multicell Beams," Journal of Applied Mechanics, Vol. 21, No. 1, March 1954.

6. Dabrowsky, R., Skrecanie Mostowych i Hydrotechnicznych Konstrukcji Cienkosciennyh o Przekroju Zamknietym, Politechnika Gdanska, Danzig 1958 (in Polish).

7. Pool, R., Arya, A., Robinson, A., and Kachaturian, N., "Analysis of Multibeam Bridges with Beam Elements of Slab and Box Section," University of Illinois, Engineering Experiment Station, Bulletin 483, Urbana.

8. Gruber, E., "Berechnung Prismatisher Scheibenwerke," International Association of Bridge and Structural Engineering, Publications, Vol. 1, 1932, p. 225.

9. Gruber, E., "Hohlträger als Faltwerke," International Association of Bridge and Structural Engineering, Publications, Vol. 7, 1943-44, p. 139.

10. Vlasov, V. Z., General Theory of Shells and its Applications in Engineering, 1949 (in Russian). NASA Technical Translation, NASA TT F-99, April 1964.

11. Girkmann, K., Flächentragwerke, Springer-Verlag, Vienna, 4th Edition, 1956.

12. Gaafar, I., "Hipped Plate Analysis Considering Joint Displacements," ASCE, Transactions, Vol. 119, 1954.

13. Grüning, G., "Die Nebenspannungen der Prismatisher Faltenwerke," Ingenieur - Archiv, Vol. 3, No. 4, 1932.

14. Yitzhaki, D., Prismatic and Cylindrical Shell Roofs, Haifa Science Publishers, Haifa, Israel, 1958.

15. Goldberg, J., and Leve, H., "Theory of Prismatic Folded Plate Structures," International Association of Bridge and Structural Engineering, Publications, Vol. 17, 1957.

16. Scordelis, A., and DeFries-Skene, A., "Direct Stiffness Solution for Folded Plates," ASCE, Journal of the Structural Division, August 1964.

17. Wright, R. N., Private Communications.

18. Rowe, R. E., Concrete Bridge Design, J. Wiley and Sons, 1962.

19. Davis, R., Kozak, T., and Scheffey, C., "Structural Behavior of a Concrete Box Girder Bridge," Highway Research Record, No. 76, 1965.

20. Sparkes, S. R., Chapman, J. C., and Pippard, A. J. S., "Experiments on the Flexure of Rectangular Box Girders of Thin Steel Plating," Colston Papers, V. 2, Engineering Structures, Butterworths Scientific Publications, London, 1949.

21. American Association of State Highway Officials, Standard Specifications for Highway Bridges, 1961.

22. Portland Cement Association, Continuous Hollow Girder Concrete Bridges.

23. Newmark, N. M., "A Distribution Procedure for the Analysis of Slabs Continuous Over Flexible Beams," University of Illinois, Engineering Experiment Station, Bulletin 304, Urbana.

24. Gustafson, W. C., "Analysis of Eccentrically Stiffened Skewed Plate Structures," Ph.D. Thesis, University of Illinois, 1966.

25. Hall, A. S., and Woodhead, R. W., Frame Analysis, J. Wiley and Sons, 1961.

26. Hildebrand, F. B., Methods of Applied Mathematics, Prentice-Hall, 8th Printing, 1961.

27. Fenves, S., Logcher, R., Mauch, S., and Reinschmidt, K., STRESS: A User's Manual, M. I. T. Press, 1964.

28. Newmark, N. M., "A Method of Computation for Structural Dynamics," ASCE, Journal of the Engineering Mechanics Division, July 1959.

29. Zarghamee, M., and Robinson, A., "Free and Forced Vibrations of a Spherical Shell," University of Illinois, Structural Research Series No. 293, June 1965.

30. Siess, C. P., and Veletsos, A. S., "Distribution of Loads to Girders in Slab-and-Girder Bridges: Theoretical Analysis and Their Relation to Field Tests," Highway Research Board, Research Reports 14-B, 1953.

31. American Institute of Steel Construction, Design Manual for Orthotropic Steel Plate Deck Bridges, 1963.

VITA

Sana Rachrach Abdel-Samad was born in Beirut, Lebanon, January 28, 1939.

He attended the Lycée Français in Beirut from which he was graduated with the "Baccalauréat 2ème partie" in 1957. He then attended the American University of Beirut from 1957-1961 and received the degree of Bachelor of Engineering, major civil, with distinction.

He worked as a road engineer in the "Conseil Executif des Grands Projets" of Lebanon 1961-1962.

He attended the Massachusetts Institute of Technology from 1962-1963 and received an M.S. degree in Civil Engineering in 1963. He was awarded a fellowship at the University of Illinois, 1963-64, and since 1964 has been a Research Assistant while pursuing his graduate studies.

He is Member of the Lebanese Order of Architects and Engineers, Associate Member of the American Society of Civil Engineers, Student Member of the American Concrete Institute and Associate Member of the Sigma Xi scholastic honorary society.